

Dissertation
submitted to the
Combined Faculties for the Natural Sciences and for Mathematics
of the Ruperto-Carola University of Heidelberg, Germany
for the degree of
Doctor of Natural Sciences

presented by
Michele Oliva, M.Sc. in Molecular Biology
Born in Venice (Italy)
Oral examination:

Identification and functional characterization
of novel genes contributing to iron
homeostasis of *Arabidopsis thaliana*

Referees: Prof. Dr. Ute Krämer
Prof. Dr. Karin Schumacher

SUMMARY

Because of its ability to catalyse oxidation/reduction reactions, iron (Fe) is an essential microelement in living beings. However, high levels of Fe in the cell can lead to detrimental effects, as this metal can also catalyse the production of harmful reactive oxygen species. Therefore, tight regulation of cellular Fe concentration is required. In this thesis, two independent genes with a putative role in Fe homeostasis were characterized in the model organism *Arabidopsis thaliana*.

AtRAI1 is homolog to the yeast Rai1p (Rat1 Interacting protein 1), an activator of 5'-to-3' exoribonucleases, enzymes that degrade decapped RNAs. In *Arabidopsis* protoplasts, *AtRAI1* co-localized with the decapping enzyme DCP2 (Decapping 2) in processing bodies, which are structures where mRNAs are processed for degradation. DK9, a loss-of-function mutant for *AtRAI1*, had phenotypic traits attributable to impaired Fe homeostasis (chlorosis, reduced size) and to homeostasis of the phytohormone auxin (curly leaves and low fertility). Assessment of the activity of the Fe-dependent anti-oxidant enzymes catalase and SOD (SuperOxide Dismutase), multi-element analysis and determination of transcript levels of genes involved in Fe homeostasis showed that *AtRAI1* is an upstream regulator of Fe uptake and transport in *A. thaliana*. The studied protein probably activates the cytosolic exoribonuclease XRN4, which is a component of the ethylene signalling pathway that is known to control Fe uptake in roots. Since homozygous knockout alleles of the analysed gene were not viable, it is concluded that *AtRAI* plays an essential role for Fe acquisition and proper growth of *A. thaliana*.

The second gene studied in this thesis is *BTS2* (*BRUTUS2*). It encodes a protein that shares similarity with BTS, an E3 ubiquitin ligase with putative roles in Fe regulation. A loss-of-function allele was more tolerant to excess Zn, a condition that leads to physiological Fe deficiency in *A. thaliana*. Under this condition, the mutant accumulated less Fe in the root than wild-type plants, indicating that the protein probably induces Fe uptake under Fe deficiency conditions. Furthermore, low Zn concentrations and reduced transcript levels of marker genes for excess Zn in shoots suggest an additional function in Zn translocation to the shoot. Therefore, *BTS2* may play a critical role in positively regulating Fe deficiency response in roots and Zn translocation to the shoot by targeting negative regulators for degradation.

ZUSAMMENFASSUNG

Wegen seiner Fähigkeit Redoxreaktionen zu katalysieren ist Eisen ein für alle Lebewesen essentielles Spurenelement. Da dieses Metall aber auch die Produktion von gefährlichen reaktiven Sauerstoffspezies katalysiert, können hohe Konzentrationen von Eisen in der Zelle schädlich sein. Daher benötigt die Zelle eine strenge Regulation der Fe-Konzentration. In dieser Arbeit wurden zwei unabhängige Gene mit einer mutmaßlichen Rolle in der Eisen-Homöostase in dem Modellorganismus *Arabidopsis thaliana* charakterisiert.

AtRAI1 ist ein Homolog von Hefe Rat1p (Rat1 Interacting protein 1), einem Aktivator von 5'-3' Exoribonukleasen, welche RNAs ohne 5'-Cap-Struktur abbauen. In *Arabidopsis* Protoplasten kolokalisiert *AtRAI1* mit dem Enzym *AtDCP2* (*Decapping Enzyme 2*) in *processing bodies*, in denen mRNAs abgebaut werden. DK9, eine *Arabidopsis* Mutante mit einem Funktionsverlust von *AtRAI1*, wies phänotypische Merkmale einer beeinträchtigten Homöostase von Fe (Chlorose, verringerte Größe) und dem Phytohormon Auxin (gewellte Blätter, geringe Fruchtbarkeit) auf. Die Analyse der Aktivität der Fe-abhängigen antioxidativen Enzyme Katalase und SOD (Superoxid-Dismutase), die Elementanalyse von Spurenelementen und die Bestimmung der Transkriptmengen von Genen, die eine Rolle in der Fe-Homöostase spielen, zeigten, dass *AtRAI1* ein übergeordneter Regulator von Fe-Aufnahme und -Transport in *A. thaliana* ist. Das Protein aktiviert wahrscheinlich die cytosolische Exoribonuklease *AtXRN4*, die eine Komponente des Ethylen-Signalweges ist, welcher die Fe-Aufnahme in Wurzeln kontrolliert. Da homozygote Knockout-Allele von *AtRAI1* nicht lebensfähig waren, scheint *AtRAI1* essentiell für die Fe-Aufnahme und das korrekte Wachstum von *A. thaliana* zu sein.

Das zweite Gen, das in dieser Arbeit untersucht wurde, ist *BTS2* (*BRUTUS2*). Das kodierte Protein weist Ähnlichkeit zu der E3 Ubiquitin-Ligase BTS auf, die vermutlich eine Rolle in der Fe-Homöostase spielt. Die Expression von *BTS2* war ubiquitär, zeigte aber einen starken Anstieg unter Fe-defizienten Bedingungen. Funktionsverlust von *BTS2* führte zu einer erhöhten Toleranz gegenüber Anzucht unter Zn-Überschuss, eine Bedingung die zu einer physiologischen Fe-Defizienz in *A. thaliana* führt. Unter diesen Bedingungen akkumulierte die Mutante weniger Eisen in den Wurzeln als der Wildtyp. Dies zeigt, dass *BTS2* wahrscheinlich die Fe-Aufnahme unter Fe-defizienten

Bedingungen induziert. Die niedrige Zn-Konzentrationen und die verringerten Transkript-Level von Markergenen für Zn-Überschuss im Spross lassen auf eine zusätzliche Rolle von BTS2 in der Zn-Translokation im Spross schließen. Daher scheint BTS2 eine kritische Rolle in der positiven Regulation der Fe-Defizienz-Antwort in Wurzeln und der Zn-Translokation im Spross zu spielen, indem es negative Regulatoren für den Abbau markiert.

INDEX

1.	INTRODUCTION	1
1.1	IRON	1
1.1.1	Abundance and chemical properties of iron	1
1.1.2	Roles of iron in biochemistry	2
1.1.3	Iron as an essential element for humans	3
1.1.4	Iron homeostasis in plants	4
1.1.5	Iron homeostasis and Ubiquitin/proteasome - mediated protein degradation	7
1.2	EUKARYOTIC mRNA	8
1.2.1	Modifications and processing of eukaryotic mRNA in the nucleus	8
1.2.2	Translation of mRNA	9
1.2.3	mRNA stability and degradation	10
1.3	SCOPE OF THE THESIS	12
2.	MATERIAL	13
2.1	Plant material	13
2.2	Bacteria and localisation vectors	14
2.3	Chemicals and reagents	14

2.4	Equipment	15
2.5	Media and soils for plant growth	16
2.6	Medium for bacterial growth	17
3.	METHODS	19
3.1	PLANT GROWTH METHODS	19
3.1.1	Sterilisation and plating of <i>Arabidopsis thaliana</i> seeds	19
3.1.2	Plant growth conditions	19
3.1.3	Preparation of chelator-washed agar	20
3.2	MOLECULAR BIOLOGY METHODS IN <i>Arabidopsis thaliana</i>	20
3.2.1	Polymerase Chain Reaction (PCR) and agarose gel preparation	20
3.2.2	Purification of genomic DNA from tissues	21
3.2.3	Purification of total RNA from tissues	22
3.2.4	cDNA synthesis	22
3.2.5	Quantitative real-time PCR	23
3.2.6	Preparation of nuclei-enriched genomic DNA	24
3.2.7	Preparation and transformation of protoplasts	26
3.3	MOLECULAR BIOLOGY METHODS IN <i>Escherichia coli</i>	28
3.3.1	Transformation of <i>E. coli</i> cells by heat-shock	28
3.3.2	Plasmid DNA isolation from large <i>E. coli</i> culture volumes	29

3.3.3	Plasmid DNA isolation from small <i>E. coli</i> culture volumes	29
3.3.4	Cloning strategy	30
3.4	GENETIC METHODS	30
3.4.1	Map-based cloning	30
3.4.2	High Resolution Melting	32
3.5	BIOCHEMICAL AND ANALYTICAL METHODS	34
3.5.1	Protein extraction	34
3.5.2	Catalase activity	34
3.5.3	Superoxide dismutase activity	34
3.5.4	Root-surface ferric-chelate reductase activity	36
3.5.5	Chlorophyll quantification	36
3.5.6	Multi-element analysis	37
3.6	HISTOCHEMICAL METHODS	37
3.6.1	Perls' stain	37
3.6.2	Histochemical β -glucuronidase (GUS) stain	38
3.6.3	Alexander's stain	39
4.1	RESULTS	41
4.1	CHARACTERIZATION OF <i>rail-1</i>	41

4.1.1	The phenotype of the DK9 (<i>rail-1</i>) mutant is partly rescued by the administration of exogenous Fe	41
4.1.2	Mapping of the mutation in DK9	44
4.1.3	At4g17620 transcript in <i>rail-1</i> lacks an exon	45
4.1.4	The At4g17620 gene encodes a putative activator of 5'-to-3' exoribonucleases	46
4.1.5	<i>RAII</i> is expressed in all organs of <i>A. thaliana</i>	48
4.1.6	Root-shoot partitioning of metals is altered in <i>rail-1</i>	49
4.1.7	The reduction in shoot Fe concentration is associated with a physiological Fe deficiency in <i>rail-1</i>	51
4.1.8	Fe(III) accumulates in the outer cell layers of the root of the <i>rail-1</i> mutant	53
4.1.9	Root Fe deficiency responses are dampened in the <i>rail-1</i> mutant	54
4.1.10	FRO2 activity is reduced in the <i>rail-1</i> mutant	56
4.1.11	<i>rail-1</i> mutant has low fertility	57
4.1.12	Male sterility of <i>rail-1</i> is temperature-dependent and linked to an altered distribution of IAA in the mutant	58
4.1.13	The <i>rail-1</i> mutant displays an alteration in free IAA release	60
4.1.14	<i>LCR</i> transcript levels in <i>rail-1</i> are lower than in wild type	62
4.1.15	miRNA accumulation is aberrant in the <i>rail-1</i> mutant	63
4.1.16	A chimeric <i>AtRAI1</i> -GFP fusion protein localizes in the cytosol of <i>A. thaliana</i> mesophyll protoplasts	65
4.1.17	<i>rail-1</i> seedlings are ethylene-insensitive	66
4.1.18	The <i>xrn4/ein5-1</i> mutant does not show iron-dependent defects	67

4.1.19	Recapitulation of the <i>rail-1</i> phenotype in a <i>AtRAII</i> -RNAi line	68
4.1.20	The homozygous knockout mutant <i>rail-2</i> is not viable	70
4.2	CHARACTERIZATION OF <i>bts2-1</i>	73
4.2.1	The amino acid sequence of the BTS2 protein exhibits two hemerythrin motifs and two zinc finger domains	73
4.2.2	<i>BTS2</i> is highly expressed in seedlings and siliques, and transcript levels increase under Fe deficiency conditions	75
4.2.3	The <i>bts2-1</i> knockout mutant is more tolerant to high Zn concentrations than the wild type	76
4.2.4	<i>bts2-1</i> exhibits an altered distribution of metals under excess Zn conditions	79
4.2.5	Zn excess- and Fe deficiency- responsive genes in the shoot of <i>bts2-1</i> are repressed under stress Zn conditions	80
4.2.6	<i>BTS2</i> -RNAi lines exhibit tolerance to high Zn concentrations	81
5.	DISCUSSION	83
5.1	CHARACTERIZATION OF <i>rail-1</i>	83
5.1.1	Disruption of a gene encoding a putative activator of 5'-to-3' exoribonucleases causes pleiotropic phenotypes	83
5.1.2	Impairment of Fe homeostasis in the <i>rail-1</i> mutant	85
5.1.3	Impairment of IAA-conjugation in the <i>rail-1</i> mutant	87
5.1.4	Curly leaves and low fertility are associated with defects in auxin signalling and conjugation, respectively	88

5.1.5	RAI1 is likely to impact the ethylene response, a pathway known to regulate transcripts of genes involved in Fe homeostasis	89
5.1.6	Rationale for the phenotypes of <i>rail-1</i> , <i>rail-2</i> and <i>AtRAI1</i> -RNAi	92
5.1.7	Towards a model explaining <i>AtRAI1</i> function	92
5.1.8	Outlook	95
5.2	CHARACTERIZATION OF <i>bts2-1</i>	96
5.2.1	The predicted BTS2 domain structure is reminiscent of mammalian E3 ligases involved in Fe-dependent regulation	96
5.2.2	BTS2 modulates Fe deficiency responses	97
5.2.3	Outlook	99
6. SUPPLEMENTAL DATA		
6.1	SUPPLEMENTAL FIGURES	100
6.2	SUPPLEMENTAL TABLES	105
6.3	LIST OF ABBREVIATIONS	111
7. LITERATURE		113
8. ACKNOWLEDGEMENTS		127

1. INTRODUCTION

1.1 IRON

1.1.1 Abundance and chemical properties of iron

Iron (Fe) is a transition metal included in the group VIII of the periodic table (atomic number 26). Fe has seven oxidation states. Among them, Fe(II) and Fe(III) are the most common forms in nature. Elemental Fe is known to oxidize in moist air and can be dissolved in diluted acid and in hot sodium hydroxide solution. Among the 16 different Fe oxides, FeO and Fe₃O₄ are widely used as pigments, while Fe₂O₃ is the main source of Fe in the steel industry. Metallic, elemental Fe is rather rare and found, for example, in meteorites.

Fe is the most abundant element of the Earth (by mass, 34.6%), and it is the major component of the inner core of the planet, where it is likely to form an alloy with nickel. In the external crust, Fe is mainly distributed among the ores hematite (Fe₂O₃), magnetite (Fe₃O₄) and siderite (FeCO₃). Fe represents *ca.* 5% of the crust (Marshak, 2007).

Due to its unique properties (malleability, ductility, high strength), Fe is used in a broad range of applications, including the production of objects of everyday life. World resources are estimated around 800 billion tons of ore containing more than 230 billion tons of iron (U.S. Geological Survey, 2003). Fe is obtained from the oxide ores hematite, magnetite, goethite, lepidocrocite and siderite via a complex process termed “beneficiation”. Several forms of Fe with differing degrees of purity can be produced during this process, but the commercially relevant ones are the “Cast Iron”, extensively used to make machine parts and stoves, and the “Wrought Iron”, ideal for making rivets, pipes and ornamental craft. Fe ores are prevalently extracted from mines in China, USA, Brazil, Australia, Russia and Ukraine (Campbell, 2008).

1.1.2 Roles of iron in biochemistry

Fe is among the 25 mineral elements that are indispensable for human health (Graham et al., 2007; Stein, 2010). As the oxidation state of Fe can reversibly change depending on the physiological environment, this metal can act as electron donor/acceptor in living organisms and is required as co-factor in many biological processes. Fe-containing proteins can be clustered into three major groups: heme proteins, Fe-S cluster-containing proteins and proteins in which Fe is directly bound to amino acid residues.

In the human body, *ca.* 2/3 of the total Fe is found in hemoglobin, a protein that carries oxygen from the respiratory organs to the rest of the body through the bloodstream. Hemoglobin consists of four polypeptide subunits, each of them containing a heme group, i.e. a porphyrin ring bound to Fe²⁺. A molecule of oxygen can reversibly bind the Fe²⁺ cation, converting it in Fe³⁺ (Campbell, 1999). In addition to hemoglobin, other heme-containing proteins are known to bind Fe, for example myoglobin and cytochromes. The former takes oxygen from hemoglobin and moves it throughout the muscle cells, while the latter group of proteins contributes to electron transport in mitochondria. For example, cytochrome *c* is a mobile electron carrier able to diffuse through the mitochondrial intermembrane space. This protein receives an electron from cytochrome *c*₁ in complex III and gives it to the Cu_A site in complex IV of the respiratory electron transport chain.

Non-heme Fe proteins are also involved in vital processes, such as DNA synthesis and cell division (Solomon et al., 2003). In the first group of these proteins, Fe atoms bind to sulphides to form 2Fe-2S, 4Fe-4S or 3Fe-4S clusters (Johnson et al., 2005). In the second group, Fe directly binds to amino acid residues of the protein. For example, mammalian transferrins are known to bind Fe³⁺ in the blood. This binding makes iron soluble under physiological conditions, it prevents iron-mediated free radical toxicity, and it ensures transport into cells (Anderson and Vulpe, 2009). A carbonate ion serves as a bridging ligand between metal and amino acid residues (two tyrosines, one histidine and one aspartic acid) (Harris and Aisen, 1989).

It is worth noting that free Fe also plays a role as catalyst in the formation of harmful free radicals from reactive oxygen in the Fenton reaction (Fenton, 1894). Therefore, organisms require a tight regulation of tissue concentrations and compartmentalization of this metal and its binding forms.

1.1.3 Iron as an essential element for humans

In the human body, Fe concentration ranges between 380 and 450 ppm in blood, 20-1400 ppm in tissues and 3-380 units in bones. With the human diet, a man needs at least 7 mg of Fe per day, whereas a woman needs 11 mg (Trumbo et al., 2001). The World Health Organization (WHO) estimates that *ca.* 1.2 billion people suffer from Fe deficiency, a condition that is termed iron deficiency anemia (Beard and Connor, 2003). For several reasons, a plant-based diet can lead to Fe malnutrition. First, the human body absorbs non-heme Fe from plant tissues to a lesser extent than heme-Fe from animal products. In plants, the negatively charged molecule phytate binds to the positively charged Fe, thus inhibiting its assimilation in the human body (Zhou and Erdman, 1995). Recent studies suggest that Fe bioavailability is around 10% of total Fe intake *via* plant-based diets (FAO/WHO, 2002). In addition, plants grown in soils with low Fe availability (i.e. calcareous or alkaline soils) can contain low concentrations of this mineral. Furthermore, loss of Fe during post-harvest processes (i.e. polishing, cooking and storage) was reported (United States Department of Agriculture, 2003). To address the Fe deficiency problem in human populations, plant scientists employ two different strategies. The “agronomic” one consists in increasing Fe availability and/or concentrations in the soil by applying fertilizers. Since the 1950s, several chelates have been studied and successfully used to overcome Fe deficiency in soil (among them EDTA and DCHA). However, non-chelated fertilizers have recently been shown to be more efficient in maintaining Fe available in soil for prolonged time periods (Lopez-Rayó et al., 2010; Carrasco et al., 2012).

The second strategy to alleviate Fe malnutrition is termed “biofortification”, and it consists in obtaining plants with increased concentrations of Fe by breeding or cultivating GMOs (Genetically Modified Organisms). In a selective breeding process, plants with high Fe content are searched among existing varieties of crops (whose seeds are stored in banks). This characteristic is then bred into cultivated varieties by crossing, and individual plants with high Fe content are selected. Approaches to obtain transgenic Fe-biofortified plants have also recently been successful, but no biofortified GM crops have been commercialised so far (Haas et al., 2005; Johnson et al., 2011).

1.1.4 Iron homeostasis in plants

In addition to C, H and Cl, plants need 12 elements for their survival (N, P, K, Ca, Mg, S, Fe, Mn, Zn, B, Cu, Mo) (White and Brown, 2010). Among them, Fe plays a central role in numerous physiological and biochemical processes. Fe concentrations between 10^{-9} M and 10^{-8} M are required to complete the life cycle (Guerinot and Yi, 1994). As component of the photosynthetic apparatus, Fe is required in the electron transport chain in chloroplasts (Govindjee et al., 2010). Fe is also a component of the complexes responsible for the respiratory electron transport in the inner mitochondrial membrane. As cofactor of many enzymes, Fe is required for the biosynthesis of important molecules, such as chlorophyll and auxin.

Because of the low solubility in aerobic, alkaline and neutral soils, Fe availability for plants is limited. Typical symptoms of Fe deficiency in plants are reduced growth and leaf chlorosis (Bienfait and Van Der Mark, 1983). Fe toxicity in plants is a less studied condition, as it occurs very rarely in nature. Symptoms related to high levels of Fe in tissues are bronzing of leaves and appearance of tiny brown spots on the leaf surface (Kampfenkel et al., 1995). To control the internal Fe concentration, a complex machinery (Fe homeostasis) has evolved in plants, with regulation operating at several different levels.

The first step is Fe uptake from the soil/medium: non-grasses, such as the model organism *Arabidopsis thaliana*, use an iron reduction strategy (“strategy I”) consisting in mobilizing Fe from the medium by releasing protons from the root. In *A. thaliana*, the H⁺-ATPase AHA2 is the main protein responsible for the acidification of the rhizosphere (Santi and Schmidt, 2008). Once in solution, Fe(III) chelates are converted into Fe²⁺ by a reductase that is located in the plasma membrane. Members of the FERRIC REDUCTASE-OXIDASE (FRO) family have been shown to carry out this reaction in *A. thaliana* (FRO2) (Connolly et al., 2003) and in pea (Waters et al., 2002). In *A. thaliana*, Fe²⁺ is then transported into the root by IRON-REGULATED TRANSPORTER 1 (IRT1), a plasma membrane protein belonging to the ZRT and IRT-LIKE PROTEIN (ZIP) family (Eide et al., 1996; Varotto et al., 2002). Differently from dicotyledonous plants, grasses extrude enhanced quantities of phytosiderophores (PS), which act to chelate Fe³⁺, under Fe deficiency conditions (“strategy II”). Recent studies found that *OsTOM1* and *HvTOM1* (TRANSPORTER OF MUGINEIC ACID) may be the major PS

efflux transporters in rice and barley, respectively (Nozoye et al., 2011). The uptake of the Fe³⁺-Phytosiderophore complex into the root occurs through YELLOW STRIPE (YS)/YELLOW STRIPE-LIKE (YSL) transporters. The central roles for YS1 in maize and *OsYSL15* in rice in this process have been studied in depth (Curie et al., 2001; Lee et al., 2009).

In the cell, the Fe taken up from the rhizosphere binds to high-affinity chelators or proteins. The micronutrient can be transferred in a symplastic way to the pericycle layer and, subsequently, to the shoot via the xylem. In *A. thaliana*, FERRIC REDUCTASE DEFECTIVE 3 (FRD3) maintains the root-to-shoot mobility of Fe by exporting citrate from pericycle cells into the apoplastic xylem. Citrate chelates Fe(II) in xylem, thus permitting its efficient translocation to the aerial part of the plant (Durrett et al., 2007). Nicotianamine (NA), a precursor of phytosiderophores, can form complexes with Fe(II), as well (von Wiren et al., 2009). Recent studies suggested that this chelator is likely to facilitate the transport of Fe from the phloem to sink organs (Schuler et al., 2012). Interestingly, the extent of vacuolar accumulation of NA affects Fe homeostasis. Overexpression of ZINC-INDUCED FACILITATOR (ZIF1), a tonoplast protein mediating the transport of NA into the vacuole (Haydon and Cobbett, 2007), leads to Zn and NA accumulation in the root vacuoles, and reduced root-to-shoot translocation of Zn. However, enhanced root-to-shoot transport was observed for Fe, suggesting a role for ZIF1 in balancing the transport of Fe and Zn (Haydon et al., 2012). IREG (IRON REGULATED FROM GUT) proteins are orthologs of mammal transporters mediating the basolateral efflux of iron from epithelial cells to the portal vein circulation (McKie et al., 2000). Although experimental confirmation is still lacking, in plants IREG1 is likely to have a role loading Fe (and other transition metals) in the vasculature (Morrissey et al., 2009). Other studies proposed that the transporter OLIGO-PEPTIDE TRANSPORTER 3 (OPT3) may have a role in the post-phloem movement of Fe to seeds (Stacey, 2008).

Another important process in Fe homeostasis is the transport of this micronutrient into subcellular compartments. *AtPIC1* (PERMEASE IN CHLOROPLAST1) was referred to as the major transporter of Fe into the chloroplast (Duy et al., 2007). Inside chloroplasts, Fe is mainly bound to ferritins, hollow spheres that can store up to 4500 Fe(III) atoms per assembled ferritin molecule. Lines of evidence showed that *FER1*, the most abundant ferritin transcript in the shoot, accumulates under Fe-excess conditions (Petit et al., 2001). Interestingly, the intracellular Fe status has an impact on the half-life of *FER1* transcript,

too. In its 3'-untranslated region, the *FER1* transcript contains the DownStream (DST) motif, a 40 nt long region conferring instability to mRNAs (Newman et al., 1993). Indeed, Arabidopsis cells treated with high levels of H₂O₂ or Fe showed a DST-dependent reduction in the stability of *FER1* mRNA in comparison to untreated cells (Ravet et al., 2012). It has been hypothesised that Fe is likely to trigger the oxDST-mediated degradation of the transcript *via* the formation of H₂O₂ and other ROS through the Fenton reaction.

Vacuolar compartmentalization plays also an important role in Fe homeostasis. During seedling establishment under Fe-limited conditions, proteins of the NRAMP family (NATURAL RESISTANCE-ASSOCIATED MACROPHAGE PROTEINS), namely *AtNRAMP3* and *AtNRAMP4*, were shown to mediate the export of Fe from vacuoles (Lanquar et al., 2005). In contrast, at least in embryo development, VACUOLAR IRON TRANSPORTER 1 (*VIT1*) mediates the transport of Fe into vacuoles (Kim et al., 2006).

Two main regulatory networks were shown to affect Fe deficiency responses in *A. thaliana*: the most studied so far involves the basic HELIX-LOOP-HELIX (bHLH) transcription factor *FIT1* (FER-LIKE IRON-DEFICIENCY-INDUCED TRANSCRIPTION FACTOR). Under Fe deficiency, this protein is required for the activation of *FRO2* transcription and affects *IRT1* expression both transcriptionally and post-transcriptionally (Colangelo and Guerinot, 2004; Jakoby et al., 2004). Recent work showed that *FIT1* may orchestrate these Fe deficiency responses by forming heterodimers with bHLH38 or bHLH39 (Yuan et al., 2008). In addition, stabilisation of *FIT1* was proposed to occur via direct interaction with ETHYLENE INSENSITIVE 3 and ETHYLENE INSENSITIVE 3-LIKE 1 (*EIN3/EIL1*), two transcription factors that are up-regulated under Fe deficiency (Lingam et al., 2011). The second network effects a repression of the Fe deficiency-responsive genes *NAS4* (NICOTIANAMINE SYNTHASE 4), *ZIF1* (ZINC-INDUCED-FACILITATOR) and *FRO6* in dependence of the bHLH transcription factor POPEYE (*PYE*) under Fe deficiency (Long et al., 2010). However, another process acting in parallel must act to overcompensate this, because net transcript levels of *NAS4* and *ZIF1* increase under Fe deficiency. According to yeast-two-hybrid studies, bHLH115 and IAA-LEUCINE-RESISTANT 3 (*ILR3*) are potential interaction partners of *PYE*. Additional information about these pathways will be given in the paragraph 1.1.5.

The regulation of Strategy II has mainly been studied in rice. Under Fe deficiency, the bHLH transcription factor *OsIRO2* (IRON-RELATED TRANSCRIPTION FACTOR 2) activates the transcription of genes involved in PS-mediated Fe uptake (Ogo et al., 2006). At least on the onset of Fe starvation, up-regulation of *OsIRO2* was proposed to be driven by *OsIDEF1* (IDE BINDING FACTOR), a member of the ABI3/VP1 transcription family (Kobayashi et al., 2007). Interestingly, *OsIRO3*, the rice ortholog of PYE, is likely to negatively regulate the Fe deficiency response. *OsIRO3* overexpressing plants have lowered transcript levels of *OsIRO2* and of other genes that are usually up-regulated under Fe-deficiency (Zheng et al., 2011b).

1.1.5 Iron homeostasis and ubiquitin/proteasome - mediated protein degradation

Fine-tuned regulation of protein degradation is required to control all aspects of biology in eukaryotes. In plants, this regulation is mainly exerted by the ubiquitin/26S proteasome pathway, a process leading to the ubiquitination and subsequent degradation of target proteins (Smalle and Vierstra, 2004). In a first step, the activating enzyme E1 is linked to the ubiquitin (Ub) protein *via* a thioester bond. The activated Ub is then transferred to the conjugating enzyme E2. E3 ubiquitin ligases are the enzymes responsible for the transfer of ubiquitin to the target protein and the substrate specificity of this transfer, as they can bridge E2 and the substrate. Some classes of E3s are able to conjugate the Ub moiety and directly transfer it to a lysine residue of the target protein, whereas others just help the passage of Ub from E2 to the target protein (Moon et al., 2004). In plants, this process is usually repeated several times, leading to poly-ubiquitination, rather than mono-ubiquitination, of the target protein. The ubiquitinated protein can finally bind the 26S proteasome, a protein complex consisting of a cylindrical core (20S) and 2 regulatory particles (19S). Once the protein is attached to the 19S part, ubiquitin is removed and the protein is unfolded. The protein is then degraded by proteases in the 20S component (Smalle and Vierstra, 2004)

Due to their importance in conferring substrate specificity to the pathway, E3s are the most numerous and diverse proteins amongst all the components of the Ub/26S proteasome machinery. In the genome of *A. thaliana*, more than 1500 genes are predicted to encode E3s. Amongst the better characterised ubiquitin protein ligases, the RING E3 CONSTITUTIVE PHOTOMORPHOGENESIS1 (COP1) has been implicated in

controlling light response and flowering signalling pathways (Yi and Deng, 2005; Jang et al., 2008).

Even though progress has been made in identifying the major players in Fe uptake, storage and transport, little is known about their regulation, especially at the post-translational level. Several lines of evidence suggest that the stability of the major component proteins of the Fe uptake machinery in *A. thaliana* roots is regulated in response to Fe (Connolly et al., 2002). Analyses of point mutants revealed that two lysine residues are required for the turnover of the protein (Kerkeb et al., 2008). Although the details of this regulation are still unclear, FIT1 was suggested to negatively regulate IRT1 degradation under Fe deficiency conditions (Colangelo and Guerinot, 2004). Regulation of FIT1 stability *via* the proteasome pathway, in turn, was reported to contribute to the regulation of iron deficiency responses (Sivitz et al., 2011). Intriguingly, published work also showed that the stabilisation of FIT1 under Fe deficiency conditions requires its physical interaction with EIN3/EIL1 (Lingam et al., 2011).

To date, BTS is the only E3 ligase that has been implicated in the response to Fe deficiency of *A. thaliana*. The protein was shown to interact with ILR3, the bHLH transcription factor that in turn can bind to PYE (Long et al., 2010). Even though further characterization of BTS is still required to determine a precise function for this E3 ligase, it was hypothesized that BTS may be a downstream target of PYE or that BTS may act as a negative regulator of the activity of PYE by competing with its interacting partners under Fe-limited conditions (Long et al., 2010).

1.2. EUKARYOTIC mRNA

1.2.1 Modifications and processing of eukaryotic mRNA in the nucleus

During and after its synthesis, eukaryotic mRNA undergoes a series of modifications leading to the formation of the mature mRNA, the final molecule that is translated into a protein. The primary transcript, also called pre-mRNA, has the same intron/exon structure as the coding sequence from which it was transcribed, and it contains additional nucleotides at the 5' and 3' ends (Neugebauer, 2002). As example of a well-studied

process in eukaryotes, RNA polymerase II in *Homo sapiens* transcribes past the site corresponding to the last codon, and a specific sequence in the 3'-untranslated region (UTR) is recognized as target by a protein complex able to cut and polyadenylate the 3' end. This consensus of this sequence is supposed to be the hexamer AAUAAA, conserved in almost all eukaryotes, in the region between 11 and 30 nucleotides upstream the site where a poly(A) tail polymerization is initiated (Millevoi and Vagner, 2010). At the 5' end, a cap consisting of a guanosine attached to the first base of the transcript *via* a 5'-5' link is generated. The guanosine is then methylated at position 7 to form the so-called "cap 0". Additional methylation may occur on the bases close to the cap (Cowling, 2009). Polyadenylation and capping are supposed to primarily prevent the degradation driven by exoribonucleases, but other functions have also been suggested (Ghosh and Lima, 2010). After these first modifications, mRNA undergoes the splicing process, consisting in the removal of introns and joining of the ends of the exons, carried out by RNA-protein complexes (spliceosomes). After splicing, some proteins of the spliceosome remain attached to the exon-exon junctions and direct the RNA to the nuclear pore. In *Homo sapiens*, REF (RNA AND EXPORT FACTOR) proteins assemble at the splicing junctions on the RNA and directly interact with TIP ASSOCIATED PROTEIN (TAP), an export factor which binds the nuclear pore and facilitates the passage of the RNA through it (Okada and Ye, 2009). Similar mechanisms were reported for yeast (Brown et al., 1995), whereas the nuclear mRNA export in plant cells is still poorly understood (Meier, 2012).

1.2.2 Translation of mRNA

Once in the cytoplasm, mature mRNAs are recognized by ribosomes at the level of the 5' end and translated into a sequence of amino acids. Only the region of mRNA comprising the codons (coding sequence) is actually translated: each nucleotide triplet corresponds to one amino acid. Transfer RNA (tRNA) molecules couple each codon with the corresponding amino acid: one end of the tRNA has an anticodon complementary to the triplet on the mRNA, whereas the other end carries the amino acid corresponding to the codon (Lewin, 2004). A ribonucleoprotein particle known as ribosome allows aminoacyl-tRNAs to bind the codon on the mRNA (Wilson and Doudna Cate, 2012). The ribosome moves along the mRNA starting from the 5' end, scanning the molecule for the start

codon. Aminoacyl-tRNAs pass through the large subunit of the ribosome and the amino acid of the tRNA corresponding to the target codon is transferred to the growing peptide chain, which elongates by one residue for each codon traversed (Lewin, 2004). Several ribosomes (fewer than 10 in plants), can simultaneously bind the same RNA, forming a complex called polysome (Arava, 2009).

1.2.3 mRNA stability and degradation

The amount of an mRNA is governed by its rate of synthesis and its rate of degradation. mRNA stability is often given as the half-life and can thus contribute to regulating the amount of protein that can be synthesized in a specific period of time. As mentioned in the paragraph 1.2.1, capping and polyadenylation are thought to prevent degradation by 5'-to-3' and 3'-to-5' exoribonucleases, respectively. Furthermore, specific sequence motifs in the RNA sequence have been proposed to influence the stability of a given mRNA. In particular, regions rich in A and U nucleotides in the 3'-UTR of some mRNAs in yeast and mammals (AU-rich elements) have been suggested to promote RNA destabilisation, likely by enhancing de-adenylation and subsequent decay (Duttgupta et al., 2003; Vergara et al., 2011).

Degradation of mRNAs is a complex process, which is overall similar, but varies slightly, among eukaryotes. In yeast, two major pathways are known to occur in the cytoplasm (Slomovic and Schuster, 2011). Both of them require an initial step consisting of the deadenylation of the 3'-UTR by PABP (POLY(A)-BINDING PROTEIN). In the first pathway, the cap at the 5' end is then removed by the decapping enzyme Dcp2, and RNA is degraded by the cytoplasmic 5'-to-3' exoribonuclease Xrn1 (Simon et al., 2006). The second pathway does not require the decapping activity at the 5' end and involves the action of a complex of 3'-to-5' exoribonucleases (exosome), which degrades RNA starting from the 3' end (Lykke-Andersen et al., 2009). However, this traditional two-model scenario has recently been challenged, as a third pathway involving mRNA fragmentation by endoribonucleases and subsequent degradation by both 5'-to-3' and 3'-5' exoribonucleases has also been suggested to occur in the cytoplasm (Schoenberg, 2011). It is worth noting that some specific RNAs are also degraded in the nucleus. For example, the exosome can also be found in this compartment, where it degrades unspliced precursors of mRNA (Vanacova and Stefl, 2007). Furthermore, Rat1, a paralog of Xrn1,

has a role in degrading uncapped mRNAs in the nucleus (Bousquet-Antonelli et al., 2000). Interestingly, the protein Rai1p (Rat1 interacting protein 1) has been shown to enhance Rat1 activity by direct interaction and decapping of RNAs. *In vitro* analyses suggested that Rat1p may facilitate Rai1-mediated degradation of RNAs with a stable secondary structure (stem loops) (Xiang et al., 2009).

Likewise, mRNA degradation in *A. thaliana* occurs *via* pathways highly similar to the three pathways known in yeast (Lewin, 2004). However, some differences exist, especially concerning the roles of some RNA degradation-related enzymes. *A. thaliana* has three different 5'-to-3' exoribonucleases, which are orthologous to Xrn1 and Rat1. XRN2 and XRN3 are localised in the nucleus, whereas XRN4 is in the cytosol. Comparable to the role of Rat1 in yeast, XRN2 has been implicated in the 5' processing of pre-ribosomal RNAs (Zakrzewska-Placzec et al., 2010). In addition, both XRN2 and XRN3 play a role in suppressing post-transcriptional gene silencing, a defence response typical of eukaryotes (Gy et al., 2007). However, neither protein directly affects mRNA decay. XRN4 appears to function in several decay pathways, as it can directly degrade uncapped mRNAs, 3'-UTR products and 3' cleavage products generated through microRNA-mediated cleavage (Souret et al., 2004). Intriguingly, XRN4 predominantly affects the transcripts of genes in specific functional categories, such as those expressed in stamen and encoding hydrolases (Rymarquis et al., 2011). In other publications, XRN4 was proposed to directly or indirectly lead to the degradation of *EIN3 BINDING F-BOX PROTEIN1 (EBF1)* transcript, a key player in the ethylene response mechanism (Olmedo et al., 2006; Potuschak et al., 2006). A unique homolog to yeast Rai1 exists in *A. thaliana*, but information about its function is still lacking.

1.3 SCOPE OF THE THESIS

This thesis reports experiments aimed at characterizing two distinct, novel *Arabidopsis thaliana* mutants impaired in Fe homeostasis. In both cases, the affected gene was found to be a putative regulator of Fe deficiency responses. The first section addresses DK9 (*rail-1*), a mutant identified from a population of EMS (ethyl methanesulfonate) mutagenized Col-0 seedlings on the basis of leaf chlorosis as a potentially Fe-deficiency related phenotype. Physiological and biochemical analyses of the mutant were accompanied by map-based cloning studies aimed at localizing the position of the mutation in the *Arabidopsis thaliana* genome for a subsequent functional characterization of the corresponding gene.

The second part of the present work focuses on the characterisation of BTS2, a protein with similarity to the putative E3 ubiquitin ligase BTS (Long et al., 2010). Previously published microarray data showed an up-regulation of *BTS2* transcript levels in response to excess Zn conditions and limited Fe availability (Colangelo and Guerinot, 2004; van de Mortel et al., 2006), suggesting a potential role in metal homeostasis. To gain insight into the possible function of this gene, a knockout mutant disrupted in the *BTS2* locus and the corresponding wild type were compared with respect to phenotypic, elemental and transcriptomic parameters. The molecular identification and functional characterization of novel components of Fe deficiency responses provides valuable information on Fe homeostasis in plants. This could aid future biofortification approaches.

2. MATERIAL

2.1 Plant material

Arabidopsis thaliana plants of the Col-0 accession, or mutants in this genetic background, were used in all experiments. DK9 seeds were kindly provided by Dr. Michael J. Haydon (University of Cambridge, United Kingdom) and were obtained from a screen of an ethyl methanesulfonate (EMS)-mutagenized seedling population conducted at the University of Melbourne in the laboratory of Prof. C. Cobbett (Ph.D. thesis of Michael J. Haydon, chapter 3). In detail, a total of 14000 M2 plants were screened for leaf chlorosis, a phenotypic marker for a potential disturbance of metal homeostasis. A total of 226 putative mutants was recorded, and 36 of them were selected for re-screening in the M3 based on the strength of the phenotype. Eight confirmed mutants were backcrossed to Col-0. F2 seeds were harvested from two F1 individuals and scored for segregation of chlorosis on soil. For 3 of these mutants, the chlorotic phenotype segregated in a 3:1 ratio (3/4 of total seedlings were non chlorotic, 1/4 were chlorotic) suggesting the presence of a single recessive mutation causative of the phenotype. One of them, DK9, exhibited additional phenotypes, namely curly leaves and a low fertility, both of which co-segregated with leaf chlorosis (Ph.D. thesis of Michael J. Haydon, chapter 3). The mutant was backcrossed to the wild-type twice again before performing the experiments.

The T-DNA insertion mutants *rail-2* (SALK_103157.40.20.X) and *bts2-1* (SALK_048470, Col-0 background) were obtained from the Nottingham Arabidopsis Stock Centre (<http://signal.salk.edu>), and T3 homozygous seeds were used for the experiments. The RNAi lines *BTS2*-RNAi (N228712) and *RAII*-RNAi (N225134), both in Col-0 background, are part of the Arabidopsis Genomic RNAi Knock-out Line Analysis AGRIKOLA collection (<http://www.agrikola.org/index.php?o=/agrikola/main>). Seeds of a transgenic line carrying a *DR5-GUS* reporter construct were provided by Prof. Dr. Ida Ruberti (La Sapienza University, Rome, Italy) (Ulmasov et al., 1997).

2.2 Bacteria and localisation vectors

The *Escherichia coli* strain DH5 α (F⁻ ϕ 80*lacZ* Δ M15 Δ (*lacZYA-argF*)U169 *recA1 endA1 hsdR17*(r_k⁻, m_k⁺) *phoA supE44 thi-1 gyrA96 relA1* λ) was used to propagate plasmids. The pSP-eGFP vector (Supplemental Figure 1) (Pollmann et al., 2006) was provided by Prof. Dr. Danja Schünemann (Ruhr University Bochum, Bochum, Germany), and it was used to generate an *AtRAII::GFP* fusion construct for expression under the control of the CaMV 35S promoter. pRTds-*DCP2-Cherry* (Weber et al., 2008) was obtained by Prof. Dr. Markus Fauth (Goethe University, Frankfurt, Germany). Both constructs were suited for transient transformation of *Arabidopsis thaliana* protoplasts.

2.3 Chemicals and reagents

Chemicals were obtained as *per analysis* grade from the following companies: Applichem (Gatersleben, Germany), Applied Biosystems (Darmstadt, Germany), J. T. Baker (Center Valley, PA, USA), Becton Dickinson (Franklin Lakes, NJ, USA), Difco (Lawrence, KA, USA), Merck (Darmstadt, Germany), Roth (Karlsruhe, Germany), Riedel-de Haën (Seelze, Germany), Roche (Basel, Switzerland), Sigma-Aldrich (St. Louis, MO, USA), Syngenta (Basel, Switzerland), Strem Chemicals (Kehl, Germany).

For standard molecular biology procedures (restriction, ligation, PCR, cDNA synthesis), the following enzymes were used:

Restriction enzymes	New England Biolab (Ipswich, MA, USA) Roche (Basel, Switzerland)
T4 DNA ligase	New England Biolabs (Ipswich, MA, USA)
RedTaq (DNA polymerase)	Bioline (Luckenwalde, Germany)
PHUSION DNA polymerase	Finnzymes (Vantaa, Finland)
RevertAID retro-transcriptase	Fermentas (St. Leon-Rot, Germany)

Reagents for quantitative real-time PCR (SybrGreen) and High Resolution Melting (MeltDoctor) analysis of gDNA were purchased as 2x master mixes from Applied Biosystems (Darmstadt, Germany). Deoxyribonucleotide-triphosphates were from New

England Biolabs (Ipswich, MA, USA). Oligonucleotide primers were from Eurogentec (Köln, Germany). All reagents were used according to the instructions given by the respective manufacturers.

2.4 Equipment

The equipment employed to carry out the experiments is reported in Table 1.

Instrument	Model (Company, City, State)
Inductively Coupled Plasma - Atomic Emission Spectrometer	iCAP 6500 DUO (Thermo Scientific, Waltham, MA, USA)
Bead mill	MM200 (Retsch, Haan, Germany)
Centrifuges	Sorvall RC5B (Thermo Scientific, Waltham, MA, USA)
	Heraeus Multifuge XR3 (Thermo Scientific, Waltham, MA, USA)
	Perfect spin P (Erlangen, Germany)
	Microfuge 22R (Beckman Coulter, Indianapolis, IN, USA)
Confocal microscope	TCS SP5 (Leica Microsystems, Wetzlar, Germany)
Drying cabinet	TK/L E117 (EHRET, Emmendingen, Germany)
Electroporation instrument	Gene Pulser II (Bio-Rad, Hercules, CA, USA)
Gel documentation	GelDoc XR+ (BioRad, Hercules, CA, USA)
Gel electrophoresis	i-My Run (Cosmo Bio, Tokyo, Japan)
Growth cabinets	CU-41L4 (CLF, Wertingen, Germany)
	Adaptis CMP 6010 (Conviron, Berlin, Germany)
Heating block	HBT130 HLC (VLM, Bielefeld, Germany)
	HBT130 EC2 (VLM, Bielefeld, Germany)
Light microscope	Axioskop (Carl Zeiss, Göttingen, Germany)
Magnetic stirrers	MR3002 (Heidolph, Schwabach, Germany)
	IKAMAG RCT (IKA Werke, Staufen, Germany)
Spectrophotometer	Biomate 3 (Thermo Scientific, Waltham, MA, USA)
Real-time PCR machine	LightCycler 480 (Roche, Indianapolis, IN, USA)
Balance	Model 470 and Model 770 (Kern, Germany)
Shaker	GFL (Burgwedel, Germany)
Stereo microscope	M212 (Leica Microsystems, Wetzlar, Germany)
Sterile workbench	Fortuna Cabinet (LaboGene, Lyngø, Denmark)

Instrument	Model (Company, City, State)
Thermocycler	DNA Engine Thermal Cycler (BioRad, CA, USA)
Ultrapure water filtration	18,2 MΩ system (Merck, Billerica, MA, USA)
Vortex mixer	Genie 2 (Scientific Industries, Bohemia, NY, USA)

Table 1. List of equipment.

2.5 Media and soils for plant growth

To germinate and select plants carrying T-DNA insertions, solid 0.5x Murashige-Skoog (MS) medium (Murashige and Skoog, 1962) was used. 2.2 g l⁻¹ MS salts with vitamins (Duchefa, Haarlem, Netherlands), 10 g l⁻¹ sucrose and 3 ml l⁻¹ 1 M MES were diluted in water and adjusted to pH 5.7 with KOH. 1% (w/v) Agar M (Sigma-Aldrich, St. Louis, MO, USA) was added prior to autoclaving. Kanamycin was added to a final concentration of 50 µg ml⁻¹ to *ca.* 60°C warm medium from sterile-filtered 1000x stock solutions.

In all other experiments, *Arabidopsis thaliana* seeds were plated and grown on 0.25x modified Hoagland medium (Hoagland, 1948) supplemented with 1% (w/v) sucrose and 1% (w/v) washed agar type M (see paragraph 3.1.3). Hoagland medium was prepared by adding the nutrients to water representing *ca.* 50% of the final volume (Table 2) with stirring, and filling up to the desired final volume.

Stock solution	Final concentration	Volume of the stock solution required for 1l of medium
1 M Ca(NO ₃) ₂	1.5 mM	1.5 ml
1 M KH ₂ PO ₄	0.28 mM	0.28 ml
1 M MgSO ₄	0.75 mM	0.75 ml
1 M KNO ₃	1.25 mM	1.25 ml
1000 x micronutrient		1 ml
0.5 mM CuSO ₄	0.5 μM	
1 mM ZnSO ₄	1 μM	
5 mM MnSO ₄	5 μM	
25 mM H ₃ BO ₃	25 μM	
0.1 mM Na ₂ MoO ₄	0.1 μM	
50 mM KCl	50 μM	
1 M MES, pH 5.7 with KOH	3 mM	3 ml
10 mM FeHBED (10 mM Fe(NO ₃) ₃ + 10.5 mM HBED)	5 μM	0.5 ml

Table 2. Composition of 0.25x modified Hoagland medium.

Prior to autoclaving, volume was adjusted to ~95% of the final volume with ultrapure water, pH was adjusted to 5.7 with KOH with stirring, and ultrapure water was then added to reach the final volume.

For propagation and phenotypic analysis of the aerial part of 2- to 5-week-old plants, seedlings were transferred onto GS90 or minitray soil (Balster, Stommeln, Germany).

2.6 Medium for bacterial growth

For growth of *E. coli*, Luria-Bertani (LB) medium (Bertani, 1951) was used. To prepare liquid medium, 5 g l⁻¹ yeast extract, 10 g l⁻¹ tryptone and 10 g l⁻¹ NaCl were added to sterile water. For solid medium, 1% (w/v) Bacto Agar was also added before autoclaving. Antibiotics were added to *ca.* 60°C warm medium as sterile filtered 1000x stock solutions

as appropriate. The final concentrations were: ampicillin $100 \mu\text{g ml}^{-1}$, kanamycin $50 \mu\text{g ml}^{-1}$.

3. METHODS

3.1 PLANT GROWTH METHODS

3.1.1 Sterilisation and plating of *Arabidopsis thaliana* seeds

The desired quantity of seeds was placed in a 1.5 ml eppendorf tube and sterilized for 5 min in 1 ml 70% (v/v) Ethanol (EtOH) solution. After washing twice with 1 ml ultrapure sterile water, seeds were incubated in 1 ml bleach solution containing 0.05% (w/v) Tween 20 and 2.5% (v/v) NaOCl for 10 min. Seeds were washed 4 times with 1 ml ultrapure sterile water, and single seeds were plated onto solid Hoagland medium by using sterile toothpicks. After plating, the square, 12 cm x 12 cm plastic petri plates containing 40 ml of the growth medium were wrapped with Leucopore tape (Duchefa, Harleem, Netherlands) and placed in the dark at 4°C for 2 days to synchronize seed germination.

3.1.2 Plant growth conditions

Plates were placed vertically in a growth cabinet (CU-41L4, CLF, Wertenigen), with a photoperiod of 11 h light, 22°C/13 h dark, 18°C. Light intensity during the day was set to 120 $\mu\text{mol photons m}^{-2} \text{s}^{-1}$ and relative humidity was constantly kept at *ca.* 65%. Depending on the experiment, seedlings were grown for either 12 or 14 days before harvesting shoots and/or roots. For seed propagation, crosses, phenotypic and transcript level analyses in mature tissues, 14-d-old seedlings were moved onto autoclaved minitray soil by using tweezers and grown in 11 h light, 22°C/13 h dark, 18°C cycles in Grobanks (GroBank BB-XXL³, CLF Plant Climatics, Wertenigen, Germany). Light intensity during the day was set to 120 $\mu\text{mol photons m}^{-2} \text{s}^{-1}$, and relative humidity was constantly kept at *ca.* 65%. Eight pots were placed in trays and kept under a transparent lid for 3 days. Unless specified otherwise, plants were watered every three days with tap water until opening of the first siliques. Other used treatments are reported in Supplemental Table 1.

3.1.3 Preparation of chelator-washed agar

To obtain Fe-deprivation conditions leading to Fe deficiency symptoms in *A. thaliana* seedlings (chlorosis and reduced size), agar was treated to remove bound metal cations. In an Erlenmeyer flask, 20 g agar M were washed three times with 1 l of 50 mM EDTA, pH 8, with continuous stirring. The first two washes were carried out for 5 h while the last one was performed overnight (O/N). Agar was then washed six times with ultrapure water. Except the third wash carried out O/N, all others were conducted for 2 h. After the final wash, agar was filtered using Whatman paper for *ca.* 1 h. The agar was immediately used to prepare 2 l of Hoagland medium (paragraph 2.5). To prepare Fe deficient medium, FeHBED was omitted from the recipe.

3.2 MOLECULAR BIOLOGY METHODS IN *Arabidopsis thaliana*

3.2.1 Polymerase Chain Reaction (PCR) and agarose gel preparation

PCR was routinely used to amplify specific DNA sequences from genomic DNA or cDNA. Phusion DNA polymerase was used to obtain amplicons suitable for cloning, whereas RedTaq was used for all other applications. The manufacturer's protocols were followed. Oligonucleotide primers used for PCR applications are listed in Supplemental Table 2. The steps of a typical PCR reaction were:

1. Pre-heating: 95°C for 180 s
2. Denaturation: 95°C for 45 s
3. Amplification: $x^{\circ}\text{C}$ for 60 s
4. Elongation: 72°C for y min
5. Cooling: 10°C

Unless specified otherwise, steps 2-4 were repeated 30 times (30 cycles).

x was dependent on the annealing temperature of the primers (unless specified otherwise, 52°C were used).

y was dependent on the length of the amplicon (values between 1 and 3 min used).

To visualise the amplified DNA fragments, 5 µl PCR products and 2 µl 1 kb DNA ladder (PeqGold 1 kb, PEQLAB, Erlangen, Germany) were loaded in parallel on 1% (w/v) solid agarose gel (LE agarose, Biozym, Oldendorf, Germany) stained with Sybr-Safe (Life Technologies, Darmstadt, Germany) (1 : 20,000 dilution), and run for 25 min at 100 V in 0.5x TAE buffer. Gels were exposed to UV and pictures were taken using a gel documentation system. 1x TAE buffer was used to prepare the gels.

3.2.2 Purification of genomic DNA from tissues

This method was routinely used to extract genomic DNA from seedlings and other tissues (leaves, inflorescences). 50-100 mg material were placed in 1.5 ml tubes and ground manually in 50 µl ice-cold buffer (200 mM Tris-HCl, pH 7.5, 250 mM NaCl, 25 mM EDTA, 0.5 % (w/v) SDS) with a small pestle. A volume of 450 µl buffer was then added, and the mixture was briefly vortexed and left to stand at room temperature for 2 min. The sample was vortexed again, centrifuged at 12,000 rpm for 5 min and the supernatant was carefully transferred to a new tube. One volume of isopropanol, as well as 0.1 volume of 3 M Sodium Acetate, were added, and DNA was allowed to precipitate at room temperature for 10 min. DNA was then pelleted by centrifugation at 4°C for 15 min. The supernatant was discarded, and the pellet was washed with 1 ml 70% (v/v) EtOH, before centrifuging again at 4°C for 2 min. The supernatant was discarded, and the pellet was air-dried. The pellet was then resuspended in 100 µl T0.1E buffer (10 mM Tris-HCl, 0.1 mM EDTA, pH 8.0). Absorbances at 260 nm and 280 nm were measured with a spectrophotometer and DNA concentration was calculated as follows:

$$[\text{DNA}] (\mu\text{g ml}^{-1}) = A_{260} / [\epsilon (\mu\text{g ml}^{-1} \text{ cm}^{-1}) \times D (\text{cm})]$$

ϵ is the extinction coefficient for DNA (0.02 ml⁻¹ µg cm⁻¹) and D is the length of the cuvette's path (1 cm).

A260/A280 ratios were also measured to assess potential protein contamination and the purification degree of the obtained DNA. This ratio of highly pure DNA ranges between 1.8 and 2.1 (Sambrook et al., 2001).

3.2.3 Purification of total RNA from tissues

Total RNA was extracted using RNeasy Plant Mini Kit (QIAGEN, Hilden, Germany). *Ca.* 50 mg of tissues were harvested and immediately frozen in liquid nitrogen. Samples were then ground with stainless steel beads using a homogenizer MM200 (Retsch, Haan, Germany) (25 s^{-1} for 30 s), and the manufacturer's protocol was followed. Briefly, after incubation in a lysis buffer, samples were loaded and centrifuged on columns to remove cell debris. The nucleic acid-containing flow-through was mixed with EtOH, and loaded and centrifuged on a second column. The buffer-rich flow-through was discarded and DNase was used to degrade genomic DNA in the preparation. Additional washes with the provided buffers were performed and, subsequently, RNA was eluted in 30 μl RNase-free water. RNA concentrations were determined according to the formula reported in the previous paragraph, using an extinction coefficient (ϵ) of $0.025\text{ }\mu\text{g cm}^{-1}\text{ ml}^{-1}$. A260/A230 ratios were also calculated to assess potential phenol or carbohydrates contamination and the purification degree of the obtained RNA

3.2.4 cDNA synthesis

To generate cDNA for use in Retro Transcript-PCR (RT-PCR) and quantitative real-time RT-PCR, First Strand synthesis kit from Fermentas (St. Leon-Rot, Germany) was used. One μg total RNA was mixed with 100 pmol Oligo(dt)18 and DEPC-treated water was added to a final volume of 12.5 μl . The mix was briefly centrifuged, incubated at 65°C for 5 min and transferred onto ice. Four μl 5x reaction buffer, 0.5 μl Ribolock RNase inhibitor (20 u), 2 μl dNTP mix (10 mM each) and 1 μl reverse transcriptase (200 u) were added. After a gentle mix and a brief centrifugation, the reaction was incubated at 42°C for 1 h, followed by 70°C for 10 min to inactivate the enzyme. The final solution containing the cDNA was stored at -20°C .

A slightly different protocol was used to obtain cDNA from specific miRNAs (Varkonyi-Gasic et al., 2007). Instead of Oligo(dt)18, 1 μ l miRNA-RT (1 μ M) primers were used (see Supplemental Table 3), and a pulsed RT was performed after addition of reverse transcriptase (30 min at 16°C , followed by 60 cycles at 30°C for 30 s, 42°C for 30 s and 50°C for 1 s). Incubation at 85°C for 5 min was used to inactivate the reverse transcriptase.

5x Reaction buffer

250 mM Tris-HCl (pH 8.3)

250 mM KCl

20 mM MgCl₂

50 mM DTT

3.2.5 Quantitative real-time PCR

To perform quantitative real-time PCR, the fluorescent dye Sybr-Green (Applied Biosystems, Darmstadt, Germany) was used according to the manufacturer's instructions. For each primer combination, a mix consisting of 2.5 μ M forward and 2.5 μ M reverse primers was prepared. cDNA obtained from 1 μ g RNA was diluted in sterile water (for each reaction 0.08 μ l cDNA were diluted in 4 μ l water). PCR master mixes were prepared by scaling the volumes listed below to the desired number of amplification reactions:

4 μ l cDNA dilution

5 μ l 2x Sybr-Green PCR master mix

1 μ l primer mix

Sample preparation and pipetting in 384-plates were carried out on ice and in sterile conditions. Prior loading into the LightCycler 480 instrument, plates were briefly mixed with a vortex mixer and centrifuged at 1500 g for 2 min.

The following conditions were used for a typical 2-step run:

1) Pre-incubation	50°C	2 min
	95°C	10 min
2) Denaturation	95°C	15 s
3) Annealing + elongation	60°C	1 min
4) Melting curve analysis	95°C	10 s
	65°C	5 s
	95°C	1 min (ramp rate 2.8°C s ⁻¹)
5) Cooling	40°C	30 s

Steps 2-3 were repeated 40 times (40 cycles).

Fluorescence data was exported to Microsoft Excel using the Roche LightCycler 480 software, and transcript levels were determined as follows:

$$\text{Relative Transcript Level (in \% of HK)} = \text{APE}_{\text{YFG}}^{-\text{CT}} / \text{APE}_{\text{HK}}^{-\text{CT}} \times 1000$$

APE is Averaged Primer Efficiency, i.e. the average of all the reaction efficiencies for the respective primer pair, calculated by using the LinRegPCR program. CT is the cycle number at which the fluorescence generated by Sybr-Green bound PCR product corresponds to a threshold of fluorescence intensity of 0.6. At least 2 constitutively expressed housekeeping genes (HK) were used for each run and two technical replicates were run for each reaction. Primers were designed using PRIMER EXPRESS software (version 2.0; Applied Biosystems). Primers with a low penalty score (< 30), T_M between 58°C and 62°C and amplicon lengths between 60 and 200 bp were used. All primers used for the experiments are listed in Supplemental Table 4.

3.2.6 Preparation of nuclei-enriched genomic DNA

To obtain nuclear DNA for sequencing *via* a whole genome shotgun (WGS) strategy, nuclei were isolated and DNA was extracted according to a combination of protocols previously described (Schneeberger et al., 2009; Uchida et al., 2011). A total of 80 seedlings grown on Hoagland medium for 7 days in light and 3 days in dark (*ca.* 300 mg) were dried on tissue paper, ground in liquid N₂ with sterile mortar and pestle, and placed

in 50 ml Falcon tubes. Three ml of ice-cold homogenization buffer were added and samples were incubated on ice for 5 min with occasional shaking. The homogenate was filtered through cheesecloth into a 15 ml tube placed on ice, and the flow-through was centrifuged for 10 min at 1260 g, 4°C. The supernatant was removed and the precipitate was carefully resuspended with a small paint-brush in 500 µl homogenisation buffer. A volume of 15 µl Triton X-100 (final volume 0.3%) was added to the sample very slowly and under agitation. After 5 min incubation on ice, the lysate was loaded on the top of a 800 µl sucrose cushion and the sample was centrifuged for 10 min at 12,000 x g at 4°C. The green supernatant containing chloroplasts was removed, and 1 ml washing buffer was added to resuspend the pellet. The sample was centrifuged again (5 min, 12,000 x g, 4°C) and the supernatant was removed. DNA extraction was performed with each obtained sample following the DNeasy Plant Mini Kit protocol from QIAGEN. Briefly, the protocol included the use of a lysis buffer and RNase A to ensure complete degradation of plant material and RNA, respectively. Precipitates and debris were removed using a column and a DNA-binding solution was added to the cleared lysate to promote binding of the DNA to a second column. Contaminants were removed with wash steps and, eventually, DNA was eluted in 50 µl ultrapure water. To concentrate DNA, the flow-through containing the DNA was eluted a second time with the same column. The whole protocol consisting of nuclei enrichment and DNA extraction was repeated 4 times, and the volumes resulting from all single preparations were combined. DNA was further concentrated by evaporation in an incubator at 60°C to obtain 1.2 µg DNA/50 µl total volume.

Homogenization buffer

10 mM Tris, pH 9.4

80 mM KCl

10 mM EDTA

1 mM spermin

1 mM spermidin

0.5 M sucrose

0.15% (v/v) β-mercaptoethanol

Sucrose cushion (in homogenization buffer)

1.5 M sucrose

Washing buffer (in homogenization buffer)

0.5 M sucrose

0.3 % (v/v) Triton X-100

3.2.7 Preparation and transformation of protoplasts

Localization of chimeric GFP fusion proteins was carried out in mesophyll protoplasts. 10 leaves from 5-week-old plants grown on minitray soil in a growth cabinet (GroBank BB-XXL³) set at 11 h light, 22°C/13 h dark, 18°C cycles, were rinsed in water, blotted dry with Whatman paper and, after removal of the petiole, cut perpendicularly to the leaf axis in 1 mm-wide strips with a sterile razor-blade. Strips were immediately moved into 30 ml enzymatic solution in a tissue culture container (53 mm diameter, 100 mm height) (PlantCon, Thermo Fisher Scientific, Waltham, MA, USA). The material was vacuum infiltrated at 100 mbar for 1 min and vacuum was then released over *ca.* 1 min. The vessel containing leaf strips and enzymatic solution was placed in the dark for 3 h. During this time, protoplasts were released by manually swirling the solution. After addition of CaNO₃ to a final concentration of 50 mM, cell debris and undigested material were removed by filtering the protoplast suspension through a 41 µm nylon net filter (Merck Millipore, Billerica, MA, USA). The protoplast-containing filtrate was then stored on ice and handled with care. The suspension was centrifuged at 300 x g for 5 min at room temperature. The supernatant was carefully removed and the pelleted protoplasts were resuspended in 20 ml WI solution. After centrifugation at 300 x g for 5 min, the supernatant was removed, and the pellet was resuspended in 2 ml WI solution. The protoplast suspension was pipetted on top of 5 ml of a 21% (w/v) sucrose cushion in a 15 ml tube. Another centrifugation at 300 x g for 10 min allowed the collection of intact protoplasts in a visible interphase. *Ca.* 1.5 ml protoplasts were carefully aspirated with a pipette and incubated on ice for 30 min.

For each transformation, 200 µl protoplast suspension were transferred into a 1.5 ml eppendorf tube. Each sample was centrifuged at 1000 x g for 3 min and resuspended in

100 μl mannitol solution. 110 μl PEG solution and 25 μg of each plasmid DNA at a minimum concentration of 400 $\text{ng } \mu\text{l}^{-1}$ were added to each vial, and samples were mixed by tapping the tube. After an incubation of 15 min at room temperature, 440 μl W5 solution was added and mixed by tapping. Samples were then centrifuged again at 1000 $\times g$ for 3 min and pellets were resuspended in 100 μl WI. Each transformation reaction was moved into 500 μl WI solution in a 24-well plate. Protoplasts were incubated at room temperature in constant light in a standard fume hood for 14 h before observation with a confocal microscope.

2-(N-Morpholino) ethanesulfonic Acid (MES) solution was used as an autoclaved 1 M stock solution. All other solutions were prepared by dissolving chemicals in ultrapure water. Enzymatic and PEG solutions were used at room temperature, whereas WI, W5 and mannitol solutions were used at 4°C. pH was adjusted with KOH.

Enzymatic solution (in ultrapure water)

0.4 M mannitol

20 mM KCl

10 mM CaCl_2

0.1% (w/v) BSA fraction IV

20 mM MES, pH 5.7

1% (w/v) cellulase Onozuka R-10 (Serva, Heidelberg, Germany)

0.25% (w/v) macerozyme R-10 (Serva, Heidelberg, Germany)

WI solution

0.5 M mannitol

4 mM MES, pH 5.7

Mannitol solution

0.5 M mannitol

15 mM MgCl_2

PEG solution (for a final volume of 10 ml)

4 g Polyethyleneglycol 4000 (Merck, Darmstadt, Germany)

3 ml H₂O

0.2 M mannitol

0.1 M CaNO₃

0.5 ml H₂O

W5 solution

0.5 M mannitol

154 mM NaCl

125 mM CaCl₂

5 mM KCl

5 mM glucose, pH 5.8 with KOH

3.3 MOLECULAR BIOLOGY METHODS IN *Escherichia coli*

3.3.1 Transformation of *E. coli* cells by heat-shock

Chemically competent *E. coli* cells were used to amplify the DNA of desired constructs. A 50 µl aliquot of bacteria was thawed on ice and *ca.* 100 ng of plasmid DNA diluted in 5 µl of a ligation reaction were added and mixed by tapping the tube. The sample was heat-shocked at 42°C for 30 s and immediately placed on ice. 250 µl of liquid LB medium were added and cells were incubated at 37°C for 1 h, before being plated on solid LB medium containing the appropriate antibiotic for selection of transformants. Volumes ranging between 50 and 200 µl were used. Colonies could be observed after incubation at 37°C for at least 6 h.

3.3.2 Plasmid DNA isolation from large *E. coli* culture volumes

To isolate larger amounts of plasmid DNA from *E. coli*, Plasmid Maxi Kit from QIAGEN was used following the manufacturer's instructions. A single colony was inoculated in 5 ml of liquid LB medium containing the appropriate antibiotic and grown at 37°C with shaking at 200 rpm for 8 h. Half the volume of the initial culture was then used to inoculate 100 ml of liquid LB medium supplemented with antibiotic. After growth at 37°C for 16 h with shaking at 200 rpm, pelleted cells were obtained by centrifugation at 6,000 g at 4°C for 15 min. The supernatant was removed and cells were resuspended. Then bacteria were subjected to alkaline lysis and the lysate was centrifuged at 20,000 g at 4°C for 30 min. After transfer to a new tube, the solution was centrifuged again for 15 min. The supernatant was loaded on the top of a QIAGEN-tip 500 anion-exchange column and allowed to pass through it by gravity flow while DNA bound to the resin. After 2 washes aimed at removing contaminants from the column, plasmid DNA was eluted in a provided high-salt buffer. Plasmid DNA was precipitated with isopropyl alcohol, centrifuged and washed with 70% (v/v) EtOH. After drying for 1 h on a bench at RT, DNA was resuspended in 300 µl T0.1E buffer (10 mM Tris-HCl, 0.1 mM EDTA, pH 8).

3.3.3 Plasmid DNA isolation from small *E. coli* culture volumes

To isolate plasmids from *E. coli*, plasmid Mini Kit from QIAGEN was used following the manufacturer's instructions. A single colony was inoculated in 3 ml LB medium containing the selective antibiotic. Cultures were incubated at 37°C for 16 h (200 rpm). Cells were then harvested by centrifugation at 11,000 rpm at room temperature for 3 min. The bacterial pellet was resuspended in a provided lysis buffers (P1 and P2) for 5 min, prior to be neutralized for other 5 min (buffer N3) Centrifugation at 11,000 rpm for 10 min permitted a pellet to sediment. The supernatant was loaded on a QIAprep spin column and centrifuged for 1 min to allow DNA to bind to the silica matrix. Additional washes with the provided buffer PE were performed to remove salts. The QIAprep column was then placed on a sterile 1.5 ml microcentrifuge tube for elution. 50 µl Buffer T0.1E were

added to the center of the column, and a centrifugation at 11,000 rpm for 1 min was performed to harvest the final volume of pure plasmid DNA.

3.3.4 Cloning strategy

Traditional cloning involving restriction and ligation reactions (Sambrook et al., 2001) was used to generate a construct expressing *AtRAI-GFP* under the control of a CaMV 35S promoter in mesophyll protoplasts of *A. thaliana*. Total cDNA from wild-type seedlings grown for 14 days in sterile conditions (see paragraph 3.1.2) was used as a template for PCR to amplify the full-length *AtRAI* coding sequence (T_a 52°C, T_e 72 s for 2 min, 30 cycles). The combination of a forward and a reverse primer containing *ACC65i* and *BamHI* restriction sites, respectively, was used (Supplemental Table 2). Digestion of the obtained amplicon and pSP-eGFP (Pollmann et al., 2006) with *ACC65i* and *BamHI* was conducted using 1 unit of restriction enzyme in a 1X buffer solution (buffer 2, New England Biolab Ipswich, MA, USA) containing 2 µl of the DNA substrate (total volume 10 µl). Digestion was followed by ligation of the two components. Vector (1 µl, ca.100 ng), insert (5 µl, 5x molar) and 1 µl T4 DNA ligase were incubated in a solution containing 1X DNA T4 ligase buffer at RT for 2 hours. The construct was used for the transformation of *E. coli* according to paragraph 3.3.1. The vector was isolated from 3 different colonies (paragraph 3.3.3) and the cloned sequence was amplified with primers listed in Supplemental Table 2. The sequence of the fusion construct was verified by commercial DNA sequencing.

3.4 GENETIC METHODS

3.4.1 Map-based cloning

A genomic region with the putative localisation of the EMS-mutation was identified by genetic mapping (Jander et al., 2002). Sequencing of the whole genome permitted to identify putative mutations in the obtained window. The map-based cloning approach is based on the fact that, as physical distance between the mutation and a molecular marker

decreases, so does the genetic recombination frequency. The genetic mapping process consisted of 3 steps:

1) Generation of a population of F2 seeds for mapping: 8 homozygous DK9 plants were crossed to 8 Ler plants. Ler was used as male parent because DK9 was male sterile under the growth conditions used. F1 seeds were harvested and planted. 25 CAPS (Cleaved Amplified Polymorphism Sequences) markers polymorphic between Col-0 and Ler and spread across the Arabidopsis genome were chosen from the TAIR website (http://www.arabidopsis.org/servlets/Search?action=new_search&type=marker) and used to test the F1 generation and parents, in order to verify the success of the cross. The markers were tested on genomic DNA extracted from 6 F1 plants obtained from 3 independent crosses (2 plants per cross). All CAPS markers used for the mapping are listed in Supplemental Table 5 and their position in the chromosomes is given in Supplemental Figure 2. F1 plants were selfed and F2 seeds were harvested from single plants. No decrease in fertility was observed in F1 plants.

2) First-pass mapping: *ca.* 400 F2 seeds harvested from a single F1 plant were plated on Hoagland medium, grown for 10 days and plants homozygous for the causal mutation were scored on the basis of their recessive chlorotic phenotype. DNA was extracted from 104 chlorotic seedlings and for genotyping of these individuals employing molecular CAPS markers to determine meiotic recombination frequency: a bulk segregant analysis permitted to rapidly identify the markers located near the mutation (21 pools of five plants were tested with the markers). The markers close to the mutation (FCA3b, SC5, G4539) were tested again on the DNA from single individuals and an approximate distance from the putative mutation was calculated (Supplemental Table 6). An example of CAPS analysis is reported in Supplemental Figure 3. The marker G4539, localized on chromosome 4 (position between 9631247 and 9631811 bp, according to the AGI map) was determined to be closely linked to the DK9 locus.

3) Fine-scale mapping: HRM (High Resolution Melting) analyses with SNP (Short Nucleotide Polymorphism) markers were employed to narrow down the area containing the mutation to a window of about 100 kb (0.6 cM, according to the RI map) containing 40 genes, using a total of 656 F2 chlorotic seedlings (Supplemental Figure 4). The used

SNPs are reported in Supplemental Table 7. Detailed information about HRM methodology is given in the next paragraph.

4) Mutation identification: to identify the mutation, genomic DNA was extracted from homozygous (chlorotic) DK9 mutant individuals (see paragraph 3.2.6) and sent to the Fasteris company (Geneva, Switzerland) for sequencing with a Whole Genome Shot Gun approach (Solexa technology). Briefly, the prepared DNA was randomly fragmented and end-repaired. Adapters were ligated onto the fragments, providing a fully-representative genomic library of DNA templates. DNA molecules, attached on a slide, were amplified with polymerase so that local clonal colonies (clusters) were generated. To assess the sequence, four types of reversible terminator bases were added and non-incorporated nucleotides were washed away. SNPs and Indels relatively to the reference sequence (*Arabidopsis thaliana* genome, version TAIR10) were detected in a region between 9 and 11 Mb in the chromosome 4. Heterozygous SNPs were not considered. The company provided 100 random sequenced fragments to assess the level of chloroplast DNA contamination. 5/100 sequences resulted from chloroplast DNA, suggesting a successful nuclear DNA isolation. A table providing information about the two SNPs found in the region between 9 and 11 Mb, chromosome 4 (position, type of substitution, reference number of the affected gene) was also given (paragraph 4.1.2). The presence of the putative mutations on DK9's genome was verified by commercial sequencing (see Results section for details).

3.4.2 High Resolution Melting

High Resolution Melting is a method to differentiate heterozygous plants from either one of the homozygous parents employing SNPs. It is based on the detection of differences in PCR melting (dissociation) curves between amplicons obtained by amplification of the genomic region around a specific SNP in a heterozygous and homozygous background. DNA was extracted from F2 chlorotic seedlings according to the protocol described in paragraph 3.2.2, and for each reaction the following mix was prepared (final volume 10 μ l):

5 μ l 2 x MeltDoctor master mix (Applied Biosystems, Darmstadt, Germany)

0.6 µl forward primer (5 µM)
 0.6 µl reverse primer (5 µM)
 0.5 µl DNA (20 ng µl⁻¹)
 3.3 µl ultrapure water

To design primers suitable for HRM analysis, polymorphisms between Col-0 and Ler in specific chromosomal regions were searched in the SNP collection reported at the TAIR website. Combinations of primers amplifying a region comprising the desired SNP were designed using PRIMER EXPRESS software (version 2.0; Applied Biosystems). Primers with a low penalty score (< 30) and amplicon length around 60 bp were used.

Sample preparation and pipetting in 384-plates were carried out on ice and in sterile conditions. Prior to loading into the LightCycler 480 instrument, plates were briefly mixed with a vortex and centrifuged at 1500 x g for 2 min.

The following conditions were used for HRM runs:

1) Pre-incubation	50°C	10 min
2) Denaturation	95°C	10 s
3) Annealing	52°C	15 s
4) Elongation	72°C	10 s
5) High Resolution Melting	95°C	5 s
	64°C	30 s
	95°C	1 min (ramp rate 4.8°C s ⁻¹)
6) Cooling	40°C	30 s

Steps 2-4 were repeated 55 times (55 cycles). The LightCycler 480 software (Gene Scanning mode) permitted to distinguish heterozygous from homozygous samples. The sensitivity parameter, a function that influences the stringency with which melting curves are clustered into different groups, was adjusted to a value of 0.30. To confirm the results, a second melting curve was carried out with the amplicons obtained from the first run.

3.5 BIOCHEMICAL AND ANALYTICAL METHODS

3.5.1 Protein extraction

Shoots were harvested from 10-d-old seedlings grown on square petri plates and frozen in liquid N₂. Samples were homogenized with stainless steel beads (25 s⁻¹ for 30 s) using a homogenizer (MM 200, Retsch, Haan, Germany). Soluble proteins were extracted with ice-cold 50 mM Tris-Cl, pH 6.8 by vortexing for 20 s. Samples were centrifuged at 4°C and 14000 g for 15 min, before protein concentrations in the supernatant were determined with the Bradford protein assay. The method is based on the use of Coomassie Brilliant Blue G-250, a compound that, after binding proteins (prevalently aromatic and basic , residues) acquires a blue stain and absorbs at 595 nm (Bradford, 1976).

3.5.2 Catalase activity

Catalase activity was determined according to Aebi, 1983. A volume of 6 µl of protein extract was added to 600 µl of a 50 mM potassium phosphate buffer, pH 7.0, containing 5 mM H₂O₂. The decrease in absorbance at 240 nm was followed with a spectrophotometer for 40 s and catalase activity was calculated using an absorbance coefficient for H₂O₂ of 0.039 mM⁻¹ cm⁻¹. The reaction solution without added protein extract was used as blank.

3.5.3 Superoxide dismutase activity

An in-gel staining method based on the reduction of the colourless NBT (Nitroblue Tetrazolium) to the blue formazan compound was used to determine superoxide dismutase (SOD) activity (Beauchamp and Fridovich, 1971). The protein extract (15 µg) was loaded on a 15% (v/v) polyacrylamide gel (see below). After running at 200 V, 4°C, for 2 h, the gel was incubated in 100 ml 50 mM potassium phosphate buffer, pH 7.8, at room temperature in the dark for 1 h. After the incubation, the substrate NBT was added to the solution to a final concentration of 0.48 mM. The gel was left in the solution for 30 min with gentle swirling. After addition of riboflavin (final concentration 30 µM) and 0.02% (v/v) TEMED, the gel was incubated for 30 min with gentle swirling. The gel was

finally washed with 100 ml 50 mM potassium phosphate buffer, pH 7.8, for 5 min, and developed under fluorescent light for 5 min.

Concentrator gel (for a final volume of 5 ml)

1.25 ml 0.5 M TRIS-HCl, pH 6.8
0.65 ml acrylamide/bisacrylamide 30% (v/v)
6.1 ml ultrapure sterile H₂O
25 µl APS 10% (w/v)
4.5 µl TEMED

Running gel (for a final volume of 5 ml, corresponding to 1 gel)

1.25 ml 1.5 M TRIS-HCl, pH 8.8
2.5 ml acrylamide/bisacrylamide 30% (v/v)
1.25 ml ultrapure sterile H₂O
25 µl APS 10% (w/v)
4.5 µl TEMED

Running buffer

25 mM TRIS-HCl, pH 8.3
192 mM glycine

Loading buffer

0.25 mM TRIS-HCl, pH 6.8
50% (v/v) glycerol
0.02% (w/v) bromophenol blue

Potassium phosphate buffer (50 mM), pH 7.8

0.05 M K₂HPO₄
0.05 M KH₂PO₄

3.5.4 Root-surface ferric-chelate reductase activity

Sterile water (1 ml) was placed in single wells of a 24-well plate (BD Falcon, Franklin Lakes, NJ, USA) and 8 roots harvested from 14-d-old seedlings grown on Hoagland medium were placed in each well. The plate was gently shaken to remove agar from roots. The water was removed and roots were washed again with the same volume of water. Roots were incubated with 1 ml reaction buffer for 20 min, at RT in the dark. An aliquot of the solution of each well (0.5 ml) was transferred to a cuvette and absorbance at 562 was measured with a spectrophotometer. The reaction buffer was used as blank. Roots were then dried on Whatman paper and their weight was measured. The enzymatic activity was calculated using an extinction coefficient of $28.6 \text{ mM}^{-1} \text{ cm}^{-1}$

Buffer (for a total volume of 50 ml)

7.2 g Ferrozine (Sigma-Aldrich, St. Louis, MO, USA)

0.5 mM Na[Fe(EDTA)]

3.5.5 Chlorophyll quantification

Shoot fresh biomass of 10-d-old seedlings (*ca.* 20 mg) was determined, samples were placed in 2 ml eppendorf tubes and frozen in liquid nitrogen. Samples were homogenized with stainless steel beads at 28 s^{-1} for 30 s with a homogenizer MM200 (Retsch, Haan, Germany). To extract chlorophyll, tissues were incubated at 70°C in 2 ml methanol with shaking (300 rpm). Samples were then transferred onto ice and absorbance was measured at 650 and 665 nm with a spectrophotometer (Porra et al., 1989). Chlorophyll concentration was determined as follows:

$$\text{Chl TOT } (\mu\text{g ml}^{-1}) = 22.5 \times A_{650} + 4 \times A_{665}$$

The values were normalised to tissue fresh biomass and multiplied by the total extraction volume.

3.5.6 Multi-element analysis

Roots and shoots from 14-d-old seedlings grown on square petri plates were harvested separately. For desorbing apoplastically bound cations including those of Fe, tissues were washed for 10 min with an ice-cold solution containing 2 mM CaSO₄ and 10 mM EDTA, before incubating for 5 min with an ice-cold solution of 0.3 mM bathophenanthroline disulphonate and 5.7 mM sodium dithionite (Cailliatte, 2010). Pools of 5 shoots/roots harvested from one plate were washed in beakers containing 100 ml of the above-mentioned solutions. Samples were then rinsed twice in deionized water for 1 min and blotted dried on Whatman paper. After desorption, tissues were placed in paper bags, dried at 65°C for 3 days and left at room temperature for 2 days to equilibrate. After weighing the dry biomass (5 to 50 mg) into glass tubes (Duran, Wertheim, Germany), samples were digested overnight with 2 ml 65% (v/v) HNO₃. The material was then kept at 80°C for 1 h and at 120°C for 90 min, with occasional mixing. After cooling down, 1 ml 30% (v/v) H₂O₂ was added to each tube and samples were heated again (30 min at 60°C, followed by 30 min at 100°C), before filling up to 10 ml with ultrapure water. Tubes were capped and stored at 4°C. In parallel to the plant samples, a blank containing no plant material and a certified standard reference material sample containing 10 mg tobacco INCT-PVTL-6 (LGC Standards, Bury Lancashire, United Kingdom) were processed. Measurement of metal concentrations was carried out using the inductively coupled plasma atomic emission spectrometer (Table 2.4). The instrument was calibrated with multi-element standards made from analytical grade chemicals. Quality control was performed by measuring a reference material made from Virginia tobacco leaves (CTA-VTL2) (Dybczyński et al., 1998). Samples were measured by Petra Dütching.

3.6 HISTOCHEMICAL METHODS

3.6.1 Perls' stain

Perls' stain is a method used to detect the presence of Fe(III) in tissues. Ferric Fe reacts with K₄FeII(CN)₆ to form the insoluble Prussian blue dye *in situ*. 10-d-old seedlings grown on square plastic petri plates were placed in a solution containing 1 ml 4% (v/v) HCl and 1 ml 4% (v/v) K₄Fe(CN)₆, and immediately placed under vacuum for 15 min

(100 mbar). The vacuum was released over 30 s. The samples were then placed at room temperature for 20 min, and seedlings were rinsed with water for 20 s, before being stored in 70 % (v/v) EtOH. Observation of the roots was performed using a stereo microscope.

3.6.2 Histochemical β -glucuronidase (GUS) stain

GUS staining is a method to determine the tissues where a specific promoter is active in transgenic reporter lines carrying a gene encoding β -glucuronidase under control of a promoter under analysis (Jefferson et al., 1987; Marathe and McEwen, 1995). The assay relies on the ability of β -glucuronidase to convert the substrate 5-bromo-4-chloro-3-indolylglucuronide (X-Gluc) into an intermediate that further dimerizes to give a blue compound. Inflorescences at stage 12 were placed in 1 ml staining buffer and vacuum infiltrated for 5 min (100 mbar). Samples were then incubated O/N at 37°C and stored in 70% (v/v) EtOH. Observation of the samples was performed using a stereo microscope.

Staining buffer

2 mM Potassium Ferrocyanide

2 mM Potassium Ferricyanide

0.2% (v/v) Triton X-100

50 mM sodium phosphate pH 7.2 (34.2 ml 1 M Na₂HPO₄ + 15.8 ml 1 M NaH₂PO₄)

2 mM X-Gluc

All solutions were prepared in sterile ultrapure water.

3.6.3 Alexander's stain

Alexander's stain is a technique to assess pollen viability, and it is based on the ability of the stain to penetrate cell wall and cytoplasm of non-aborted pollen. In particular, two components of the stain, malachite green and acid fuchsin, stain pollen walls and cytoplasm, respectively (Alexander, 1969). After treatment, viable pollen acquires a strong red colour, whereas aborted pollen is not stained. Anthers of open flowers (stage 12) were collected and placed on a microscope slide. Three drops of the stain solution

were applied and the sample was incubated for 15 minutes at room temperature to ensure that the solution was completely absorbed by the pollen. A cover slip was gently applied on the stained anthers, and stained anthers were observed using a light microscope.

Staining solution (for a final volume of 100 ml). Storage at RT for a maximum of 6 months.

10 ml 95% (v/v) EtOH

1 ml 1% (w/v) malachite green (4-[(4-dimethylaminophenyl)phenyl-methyl]-N,N-dimethylaniline) in 95% (v/v) EtOH

25 ml glycerol

5 ml 1% (w/v) acid fuchsin (4-[4-Aminophenyl)-(4-imino-1-cyclohexa-2,5-dienylidene)methyl]aniline hydrochloride) in water

0.5 ml 1% (w/v) orange G (Na₂(8Z)-7-oxo-8-(phenylhydrazinylidene)naphtalene-1,3-disulfonate) in water

4 ml glacial acetic acid

Distilled water added to a final volume of 100 ml.

4. RESULTS

4.1 CHARACTERIZATION OF *rai1-1*

4.1.1 The phenotype of the DK9 (*rai1-1*) mutant is partly rescued by the administration of exogenous Fe

DK9 seeds were obtained from a screen of an ethyl methanesulfonate (EMS)-mutagenized seedling population and gently provided by Dr. Michael J. Haydon (Ph.D. thesis of Michael J. Haydon, chapter 3). Homozygous seedlings of the mutant grown on standard medium (containing 5 μM FeHBED) showed a $\sim 25\%$ reduction in biomass production and $\sim 55\%$ reduction in chlorophyll content compared to wild-type seedlings grown under the same conditions (Figure 1). As chlorosis and reduced plant growth are the most prominent visible Fe deficiency symptoms in *Arabidopsis thaliana*, it was assessed whether the administration of exogenous Fe could rescue the phenotype. Shoot biomass of DK9 seedlings grown in the presence of 5 and 50 μM FeHBED was twice greater than the biomass of seedlings grown in absence of Fe. Under Fe luxury conditions, chlorosis was fully rescued in the DK9 mutant. The mutant *irt1*, known to be drastically impaired in root Fe uptake (Varotto et al., 2002), showed a partial recovery of chlorophyll concentrations (to $\sim 50\%$ of wild type levels) under high Fe concentrations. Also in this case, the shoot biomass was slightly increased when Fe was supplemented in the medium. A similar experiment carried out on soil showed that chlorophyll content of DK9 plants was also restored when watering with 0.5 mM sequestrene (FeEDDHA) (Supplemental Figure 5).

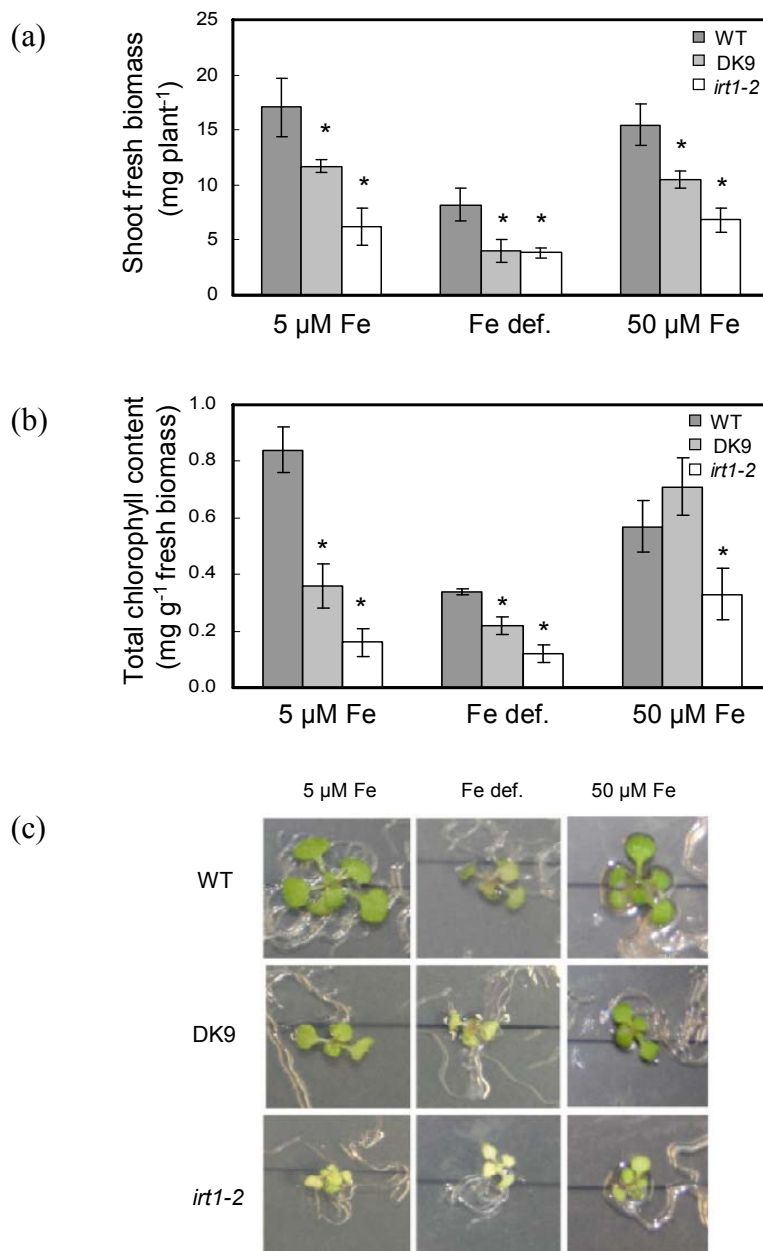


Figure 1. Partial phenotypic complementation of DK9 by high FeHBED supply.

(a) Shoot fresh biomass, (b) shoot chlorophyll concentrations and (c) photographs of WT, DK9 and *irt1-2* cultivated in media containing different Fe concentrations. WT, homozygous DK9 and *irt1-1* mutant seedlings were grown on control Hoagland medium (5 $\mu\text{M FeHBED}$), Fe deficient medium (no added Fe) and in Fe luxury conditions (50 $\mu\text{M FeHBED}$) for 12 days in short days, before documentation and harvest for analysis. Bars represent means \pm SD of 4 replicate plates, from which material was pooled from 10 seedlings per genotype. A two-way-ANOVA test was carried out comparing the whole set of values for the mutants and WT ($P < 0.05$ for interaction between treatment and genotype for (a), and $P < 0.05$ for (b)).

Asterisks denote significant differences between mutant and WT seedlings ($P < 0.05$, Student's T -test with Bonferroni corrections).

In addition to chlorosis and small size, the DK9 mutant grown on soil shows curly leaves and reduced fertility characterized by the formation of small siliques carrying a small number of seeds (Figure 2). Complete sterility was observed in the mutant grown at high temperatures (paragraph 4.1.12) Treatments with 0.5 mM FeEDDHA did not restore fertility or leaf development to those observed in the wild type. The fact that chlorosis is rescued in the mutant grown under high Fe conditions suggests a disturbance of Fe homeostasis in DK9. Fe can not rescue the other aberrant phenotypes, indicating that, in addition to Fe homeostasis, other processes are disturbed in the mutant. Alternatively, the fact that the fresh biomass of the control mutant *irt1* is not completely rescued by addition of Fe may indicate that the rescue conditions are not suitable to fully recover biomass of mutants impaired in Fe homeostasis. It is likely that Fe did not reach the target tissues/cells or is not active in the FeEDDHA and FeHBED forms.

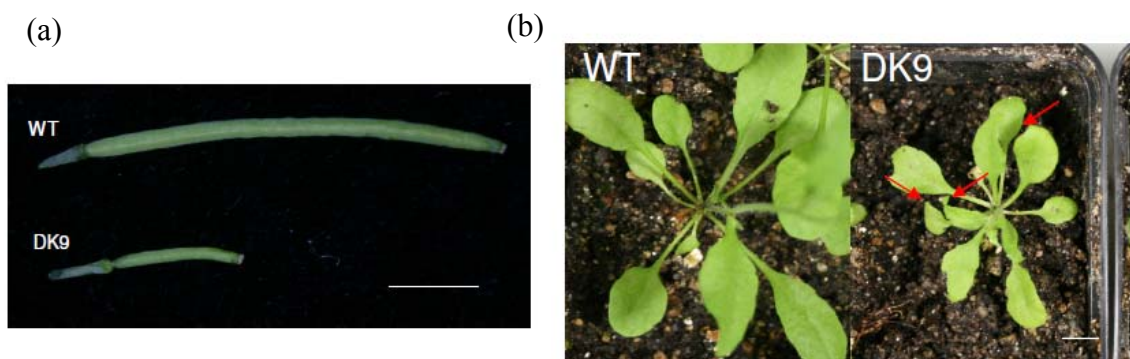


Figure 2. Fertility defect and abnormal leaf shape in the DK9 mutant grown on soil

(a) Photographs of siliques harvested from 45-d-old WT and DK9 mutant plants. The size bar corresponds to 0.25 cm. (b) Photographs of WT and DK9 plants grown on soil for 18 days after seedling establishment on Hoagland medium for 14 days. Arrows indicate upward curled leaf edges in the DK9 mutant. Size bar corresponds to 1 cm.

4.1.2 Mapping of the mutation in DK9

In order to map the DK9 mutation on Arabidopsis genome, fine mapping of the mutation followed by Whole Genome Shotgun sequencing was employed (see paragraph 3.4.1). The sequencing results identified only two single point mutations in the final window of 40 genes obtained by genetic mapping. The first putative mutation (a C->T substitution) was identified at the position 9720648 of the fourth chromosome, in the fifth intron of the gene At4g17410. According to the TAIR annotation, the gene encodes a protein containing a DWNN domain, a ~75 residues sequence which is typical of Ubiquitin-like modifiers (Pugh et al., 2006). To confirm this mutation, the DNA region containing the putative substitution was sequenced twice again in 10-d-old newly grown homozygous DK9 and wild-type seedlings. Interestingly, both DK9 and wild type had a T in the above-mentioned position. It is worth noting that the Whole Genome Shotgun sequencing was performed using DNA of the DK9 mutant only, and that the resulting sequence data were then compared with the available *Arabidopsis thaliana* genomic sequence provided by the TAIR10 database. Indeed, different from the wild type used in this work, TAIR10 reports a C in the position 9720648. The substitution at the position 9720648 of the fourth chromosome in DK9 is unlikely to cause its phenotype because it is shared with the corresponding wild type. This wild type used in all the experiments of the thesis. The second mutation identified by whole-genome shotgun sequencing in the region of interest was a G->A substitution at the position 9823388, in the gene At4g17620. To confirm the alteration, genomic DNA was extracted from DK9 and wild type, and the region around the predicted mutation was sequenced again. Our result confirmed the presence of an A in the position 9823388 of chromosome 4 in the DK9 mutant (Figure 3a), as well as the G in the wild type. According to the TAIR10 annotation, At4g17620 consists of 13 exons, and the mutation affects the last nucleotide of the fifth intron (Figure 3b), suggesting that it might interfere with correct splicing of the transcript of At4g17620 in DK9.

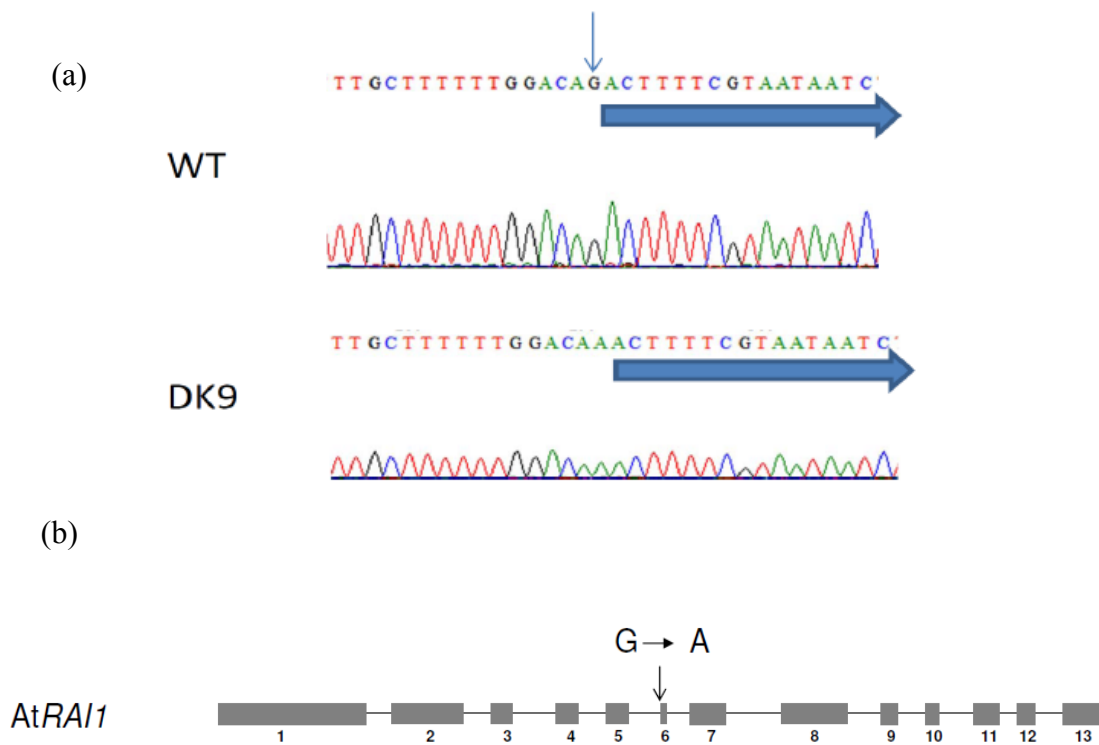


Figure 3. Confirmation of the mutation in DK9 by Sanger sequencing.

(a) Comparison between the sequences of At4g17620 in the WT and DK9 background. The panels show the sequencing results from nucleotide 1369 to 1400 of the open-reading frame At4g17620 in both WT and DK9. The thin vertical arrow indicates the position of the substitution whilst the thick horizontal arrow marks the sixth exon of the gene. (b) Schematic representation of the structure of the gene At4g17620. The gene consists of 13 exons (grey boxes) and 12 introns (lines), comprising a total of 2885 nucleotides from the translational start codon ATG to the TAA stop codon at the DNA sequence level. The arrow indicates the location of the mutation.

4.1.3 At4g17620 transcript in *rail-1* lacks an exon

Mutations affecting intron/exon boundaries have been reported to disrupt assembly of the splicing components at these sites, leading to a loss of interaction/stabilization across the exon and possibly to exon skipping by removal of two consecutive introns including the exon in between them from the pre-mRNA (Yanofsky et al., 1990; McNellis et al., 1994; Brown, 1996).

To examine the effect of the identified splice site mutation on the transcript of At4g17620, cDNA was synthesized from total RNA of DK9 and wild type seedlings and

amplified with primers spanning the affected nucleotide (Supplemental Table 2). The sequencing of the amplicons revealed that the transcript of At4g17620 in the mutant lacks the 24 nucleotides corresponding to exon 6, corroborating the hypothesis of exon skipping (Figure 4a). No differences in the abundance of At4g17620 transcript were detected between DK9 and wild type seedlings (Figure 4b).

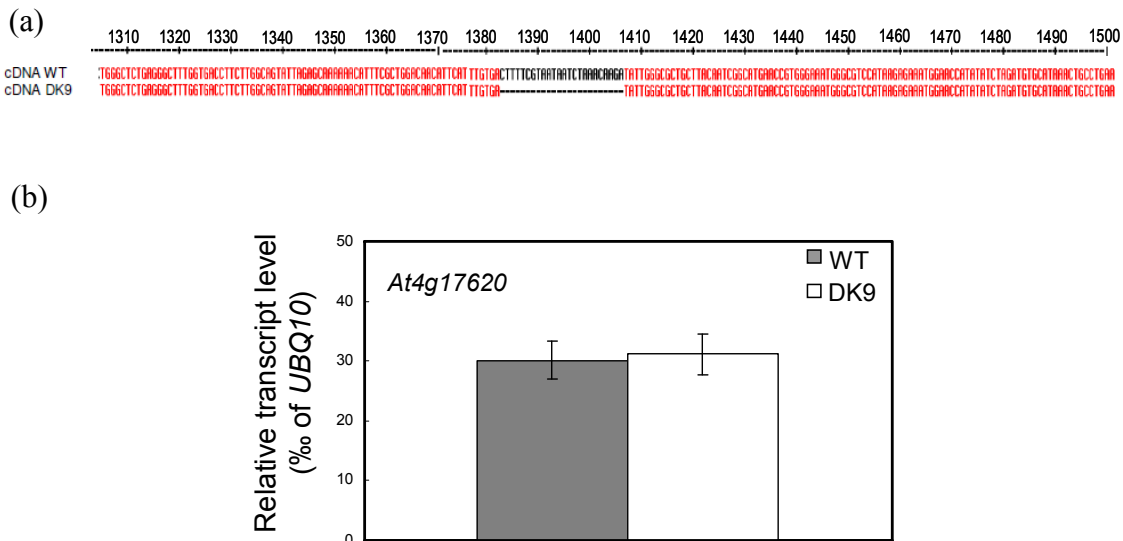


Figure 4. Analysis of the transcript of At4g17620.

(a) Alignment of part of the amplicons obtained from DK9 and WT spanning the region containing the mutation based on sequencing. The program Multalin was used. (b) At4g17620 transcript levels in 10-d-old seedlings of DK9 mutant and WT were quantified using real-time RT-PCR. Bars correspond to arithmetic means of the ratio between the expression of the reaction for At4g17620 and the constitutively expressed control gene *UBQ10*, then multiplied by 1000. Bars represent arithmetic means \pm SD of $n = 3$ replicate plates. Two technical replicates were run for each reaction.

4.1.4 The At4g17620 gene encodes a putative activator of 5'-to-3' exoribonucleases

At4g17620 is the unique *A. thaliana* homolog of *RAI1* of the yeast *Saccharomyces cerevisiae*, a gene encoding an activator of 5'-to-3' exoribonucleases (XRNs), enzymes with important functions in RNA metabolism (Xue et al., 2000). According to a recent study, *ScRai1p* enhances XRN activity by two distinct mechanisms: a 5' pyrophosphohydrolase activity decaps the target RNA, making it prone for degradation by XRNs, whereas the second mechanism probably involves a physical interaction between the activator RAI1 and XRN, with no catalytic role of the activator in RNA

processing (Xiang et al., 2009). Different from the *ScRai1p*, the human homolog DOM3Z is likely to have only decapping activity (Xiang et al., 2009). To our knowledge, no function has been reported for the *A. thaliana* protein (here called *AtRAI1*).

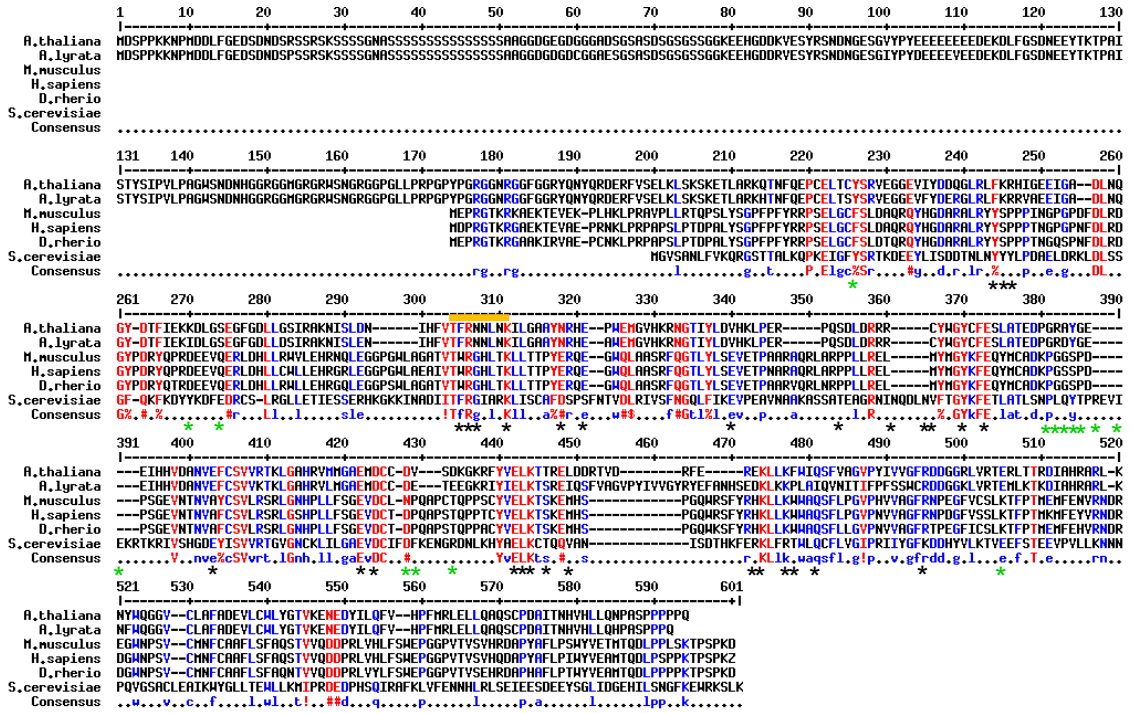


Figure 5. Multi-alignment of amino acid sequences of *AtRAI1* and homologous proteins from other organisms.

AtRAI1 sequence was used as input for a BLASTp search against the NCBI non-redundant protein database. The retrieved sequences from representative organisms were aligned using the program Multalin (Blosom 62-12-2 symbol comparison table). Residues conserved in all included sequences are highlighted in red, and residues conserved in only a subset of sequences are marked blue. The yellow bar indicates the string of 8 residues encoded by the exon lacking in DK9. Black asterisks denote residues in the active site pocket of *ScRai1*. Green asterisks denote residues located at the interface with the exoribonuclease *ScRat1p*. Numbers shown are the residues from the N-terminus.

An alignment of *AtRAI1* with homologs from different organisms showed that the protein sequence, in common with that of *A. lyrata*, possesses an additional N-terminal domain that the homologous proteins from the other (non-plant) organisms lack, albeit in the remainder of the amino acid sequence the similarity with the other homologs is quite high (> 70%) (Figure 5). Of particular interest is the fact that four codons in the 6th exon of *AtRAI1* encode amino acids that, according to the information available in yeast, are

localized in the active site of the enzyme (Phe305, Arg306, Gly307 and Lys311 in *AtRAI1*): studies on *S. pombe* and *H. sapiens* showed that the residue corresponding to Arg306 of *AtRAI1* plays a fundamental role in binding the β -phosphate of m^7 GDP. The decapping enzyme exhibits a specific hydrolase activity (pyrophosphohydrolase activity) resulting in cleavage between the α - and β -phosphates of the m^7 Gp $^{\gamma}$ p $^{\beta}$ p $^{\alpha}$ N cap structure. This generates both m^7 GDP and 5'-monophosphorylated RNA products (Xiang et al., 2009).

4.1.5 *RAI1* is expressed in all organs of *A. thaliana*

According to the microarray and Affimetrix data available through the BAR website (<http://bar.utoronto.ca/efp/cgi-bin/efpWeb.cgi>), *RAI1* is expressed in all tissues of *A. thaliana*. To confirm these data, transcript levels were determined in several organs by real-time RT-PCR. The results suggested that both roots and shoots of 14-d-old WT seedlings contain the *RAI1* transcript, as well as leaves, inflorescences and siliques of plants grown for 14 days on growth medium followed by 24 days on soil (Figure 6). Except leaves, where *RAI1* transcript levels were lower, all other tissues contained comparable amount of *RAI1* transcript.

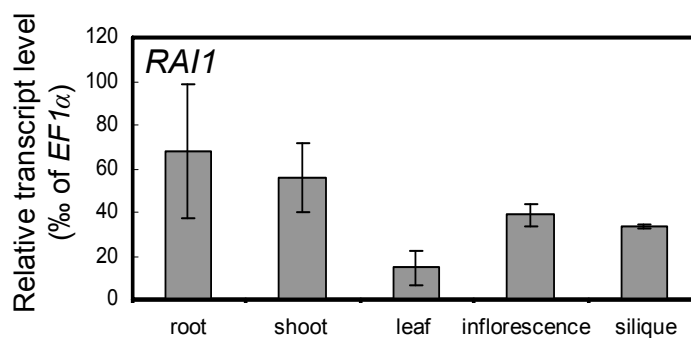


Figure 6. Steady-state *RAI1* transcript levels in different organs.

RAI1 transcript levels in several tissues were quantified using real-time RT-PCR. RNA was extracted from roots and shoots of wild-type seedlings grown on control Hoagland medium for 14 days, or from leaves, inflorescences and siliques of plants grown in short days (24 days for leaves and inflorescences, 38 for siliques). Bars correspond to arithmetic means of the ratios between the expression of the reaction for the tested gene and the constitutively expressed control gene, then multiplied by 1000. Bars represent

arithmetic means \pm SD of $n = 3$ replicate plates (10 seedlings per plate). Two technical replicates were run for each reaction.

4.1.6 Root-shoot partitioning of metals is altered in *rail-1*

In *rail-1*, those constitutive Fe deficiency symptoms that can be rescued by Fe supplementation might result from a disruption of Fe uptake, as known, for example, in *irt1-2* (Varotto et al., 2002). To test for a potential impairment of Fe accumulation in the *rail-1* mutant, metal concentrations were analyzed in 14-d-old seedlings by ICP-AES. In accordance with the observed leaf chlorosis, shoots of *rail-1* seedlings accumulated on average about 75% of the Fe accumulated in the wild type (Figure 7a). This was associated with a trend in *rail-1* to accumulate more Fe in roots than the wild type (Figure 7b).

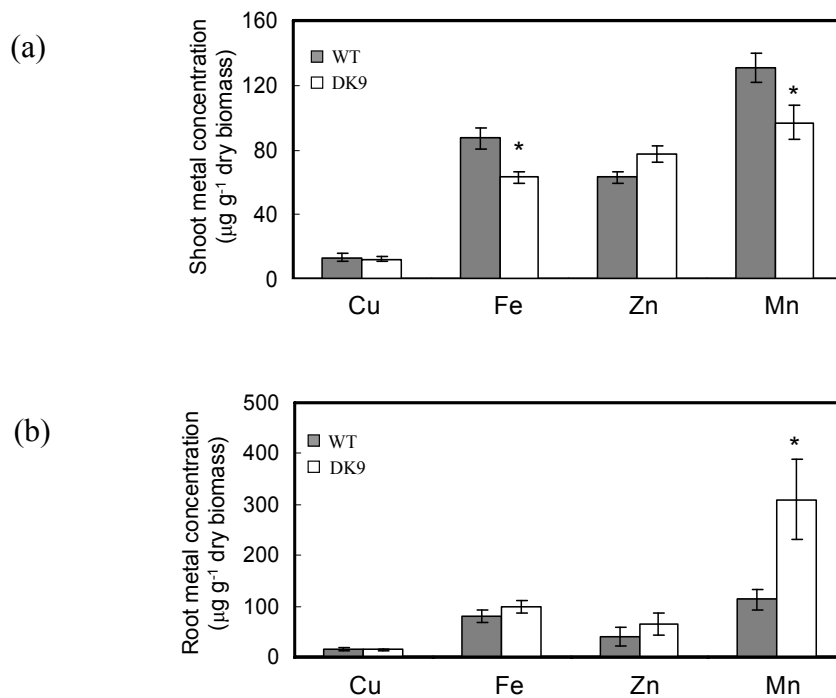


Figure 7. Concentrations of essential transition metals in shoots and roots of the *rail-1* mutant and wild-type seedlings.

Metal concentrations in (a) shoots and (b) roots of 14-d-old *rail-1* and WT seedlings grown on vertical plates containing Hoagland medium (including $5 \mu\text{M}$ FeHED) in short days. Values represent arithmetic means \pm SD of $n = 4$ replicate plates, for each of which material was pooled from 12 seedlings per genotype for analysis. Data are shown from one experiment representative of two independent experiments. An

asterisk above a pair of bars indicates that the corresponding value in *rail-1* is significantly different ($P < 0.05$) from the value determined for the WT for the respective organ according to a Student's *t*-test with no corrections.

Fe accumulation was then analyzed in seedlings grown under different Fe regimes. This confirmed lowered shoot Fe concentrations in *rail-1* in comparison to the wild type under control and also under Fe deficiency conditions. Under luxury Fe conditions, Fe concentrations in *rail-1* shoots were comparable to those of the wild type (Figure 8a), indicating a rescue of *rail-1* shoot Fe concentrations by Fe supplementation. This explains the rescue of chlorosis observed under these conditions (Figure. 1c). Interestingly, the extent of Fe accumulation in roots of *rail-1* compared to the wild type was more pronounced at high Fe supplementation (50% above those found in wild type) and not apparent in seedlings grown under Fe deficiency conditions (Figure 8b). The alterations in shoot Fe concentrations in *rail-1* are surprising given that shoot Fe concentrations are known to be under extremely tight homeostatic control and are rarely changed in mutants (Lahner et al., 2003). Instead, alterations in the accumulation of other transition metals, in particular manganese (Mn), were proposed to be diagnostic of Fe homeostasis defects.

Indeed, Mn partitioning was also found to be altered in *rail-1* seedlings. In comparison to the wild type, Mn concentrations were lower in shoots (but not below the threshold that usually causes Mn deficiency symptoms) and higher in roots of *rail-1* (Figure 7a and 7b). No differences in Zn and Cu accumulation were detected between *rail-1* and the wild type. The present results confirm that *rail-1* exhibits an altered root-shoot partitioning of metals. In particular, low concentrations of Fe in the shoot are associated with chlorosis observed in *rail-1* leaves.

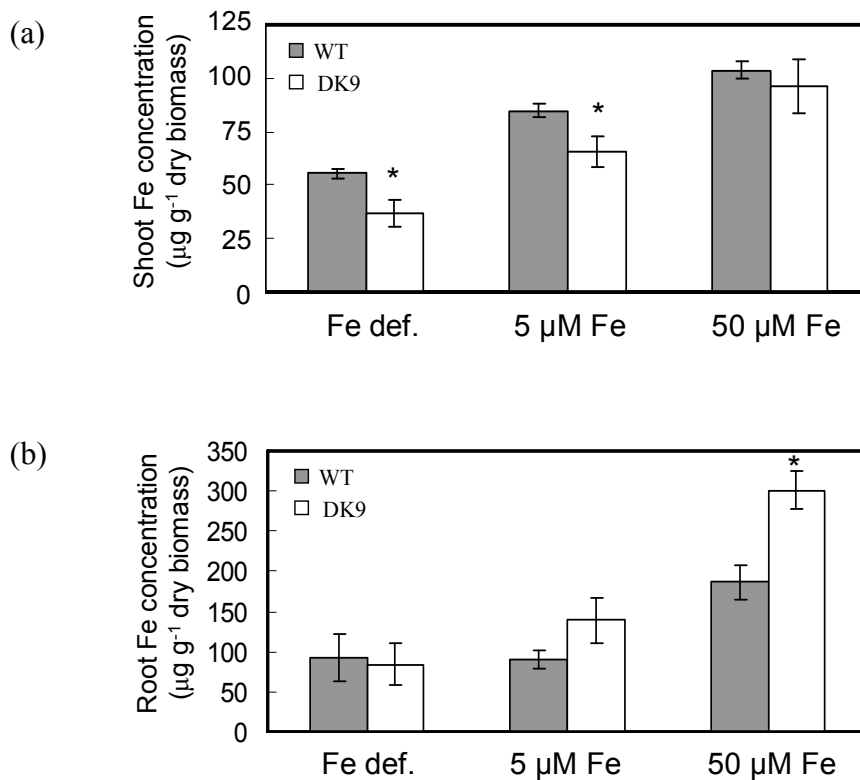


Figure 8. Fe accumulation in *rail-1* and wild type seedlings grown under different Fe conditions.

Shown are Fe concentrations detected in (a) shoots and (b) roots of WT and *rail-1* seedlings grown on vertical plates containing Hoagland medium (5 µM FeHBED), Fe deficiency and Fe excess conditions for 14 days. Roots and shoots were harvested separately, and Fe concentrations were quantified by ICP-AES. Bars represent arithmetic means \pm SD of $n = 4$ replicate plates, for each of which material was pooled from 12 seedlings per genotype for analysis. An asterisk above a bar indicates that the corresponding value for *rail-1* is significantly different ($P < 0.05$) from the value determined for the WT for the respective organ according to a Student's *t*-test with no corrections.

4.1.7 The reduction in shoot Fe concentration is associated with a physiological Fe deficiency in *rail-1*

In order to test whether reduced Fe concentrations and chlorosis in the leaves of *rail-1* were associated with a physiological Fe deficiency, several enzyme assays of Fe-dependent enzymes were conducted. Catalase is an enzyme which plays a key role in removing the potentially damaging compound H₂O₂, by converting it into H₂O and O₂. Due to its Fe requirement in the porphyrin heme groups measurement of catalase activity has been described as a marker to assess Fe status in *Arabidopsis* shoots (Aebi, 1983).

Consistent with the ICP-AES data, at 5 μM FeHBED catalase activity levels in *rail-1* were reduced to about 30% of wild type levels. Complementation with 50 μM FeHBED restored wild type levels of catalase activity (Figure 9a).

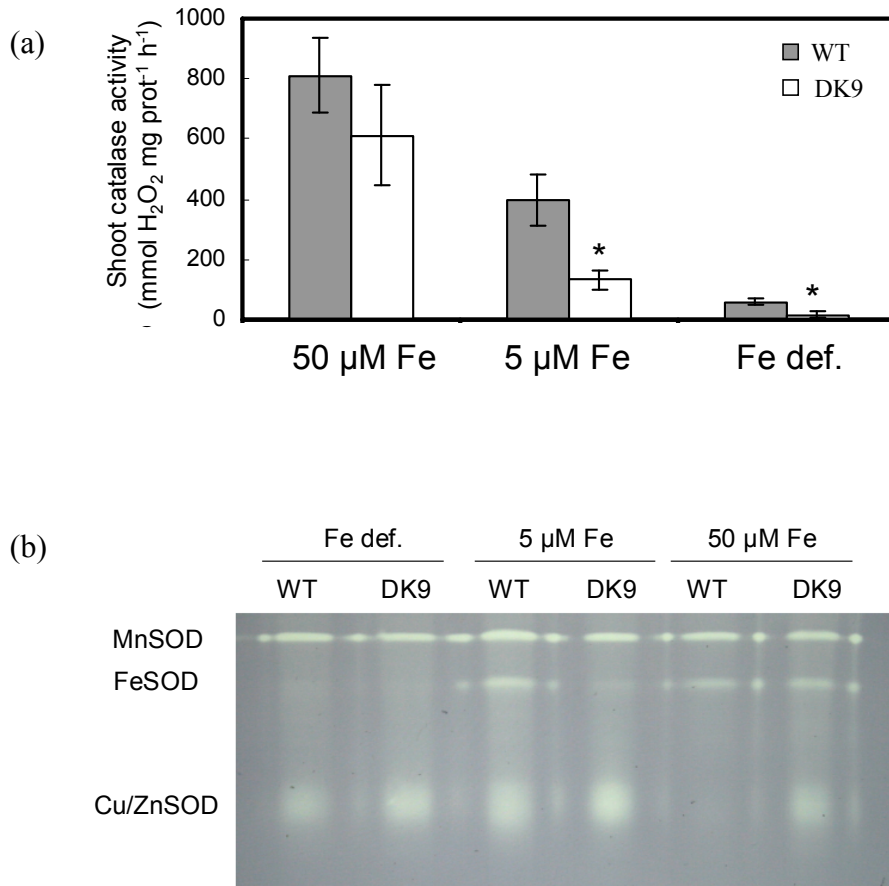


Figure 9. Catalase and SOD activities in wild type and *rail-1* mutant seedlings.

(a) Catalase activity measurements and (b) in-gel detection of superoxide dismutase isozyme activities. Assays were conducted in total protein extracts prepared from shoot tissues harvested from WT and *rail-1* seedlings grown for 14 days on control Hoagland medium (5 μM FeHBED), Fe deficiency (no FeHBED added) and luxury Fe (50 μM FeHBED). Bars represent arithmetic means \pm SD of $n = 4$ replicate plates, from each of which material was pooled from 10 seedlings per genotype for analysis. An asterisk above a bar indicates that the corresponding value is significantly different ($P < 0.05$) from the value determined for the wild type for the respective organ according to Student's *t*-test with Bonferroni corrections. A two-way ANOVA detected a significant interaction between genotype and treatment ($P < 0.05$) (a). Data are shown from one experiment representative of two independent experiments.

Under the same conditions, the activity of Fe superoxide dismutase (FeSOD), a Fe-dependent anti-oxidant enzyme able to dismutate O_2^- into O_2 and H_2O_2 , was also lower than in wild-type seedlings, whereas MnSOD activity remained approximately constant in all genotypes under all conditions. At high Fe concentrations, FeSOD activity in *rail-1* plants was restored to wild type levels (Figure 9b). The low level of activity observed for Fe-requiring enzymes in the shoot of *rail-1* seedlings confirms the Fe-deficient status in the shoot of the mutant. Although not directly relevant here, it was observed that under 50 μ M Fe, Cu/Zn SOD activity in wild type was not detectable, suggesting that high Fe levels favor the substitution of the Cu/Zn-dependent enzyme with the Fe-dependent enzyme. Indeed, superoxide dismutase isoform abundance is known to depend on metal availability in plants and Fe-Cu cross-talk was recently described (Cohu and Pilon, 2007; Waters et al., 2012).

4.1.8 Fe(III) accumulates in the outer cell layers of the root of the *rail-1* mutant

In order to localize Fe(III) accumulation detected by ICP-AES in *rail-1* roots, a Perls' stain was carried out of 10-d-old seedlings grown on a Fe-rich medium. An accumulation of Fe in the root epidermis and cortex of *rail-1* was observed, suggesting that the mutation affects the transfer of Fe from the outer cells of the root towards the central cylinder and thus the subsequent step of Fe translocation to the shoot *via* the xylem (Figure 10).

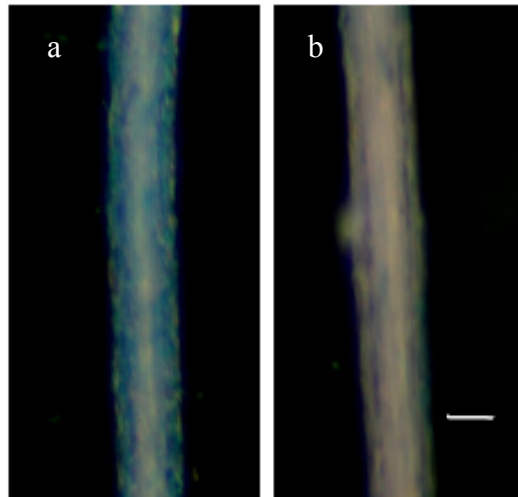


Figure 10. Localization of Fe(III) in roots of *rail-1* mutant and wild-type seedlings.

Shown are photographs of the primary roots of (a) *rail-1* and (b) wild-type seedlings were grown for 10 days on Hoagland medium containing 50 μM Fe, and Fe(III) in roots was visualized using Perls' stain. The shown images are representative of 8 seedlings grown on 3 independent plates per genotype. Size bar corresponds to 25 μm .

4.1.9 Root Fe deficiency responses are dampened in the *rail-1* mutant

Tight gene regulation in space and time is required for maintaining Fe homeostasis efficiently, thus providing correct amounts of this metal to the different tissues. In *Arabidopsis* roots, the core of the Fe uptake machinery consists of a ferric chelate reductase (*FRO2*) (Robinson et al., 1999), an enzyme that converts the Fe(III) in extracellular ferric chelates to Fe(II), and a transporter (*IRT1*) able to transport Fe^{2+} cations into the root cells (Varotto et al., 2002; Vert et al., 2002). An up-regulation of transcript levels of the genes encoding these proteins is known to occur under Fe deficiency conditions. To assess the regulation of these genes in the mutant background, transcripts were quantified by quantitative real-time RT-PCR. When compared to control conditions, root *IRT1* and *FRO2* transcript levels were up-regulated approximately two-fold under Fe deficiency conditions in wild-type seedlings. Even though under Fe deficiency a four-fold upregulation was observed in *rail-1* for both *IRT1* and *FRO2* transcripts, transcript levels were 4-fold lower than in the wild type under control conditions and 2-fold lower under Fe deficiency conditions (Figure 11). It should be noted that in the control medium employed by us, Fe deficiency responses are partly

activated, but plants exhibit no visible Fe deficiency symptoms, whereas control conditions employed by other researchers result in a full repression of Fe deficiency responses. In summary, transcript abundance suggests that expression of Fe deficiency-responsive Fe acquisition genes is dampened in *rail-1*, with a reduction in the transcript levels in comparison to the wild type that is particularly prominent under the employed control growth conditions (5 μ M FeHBED).

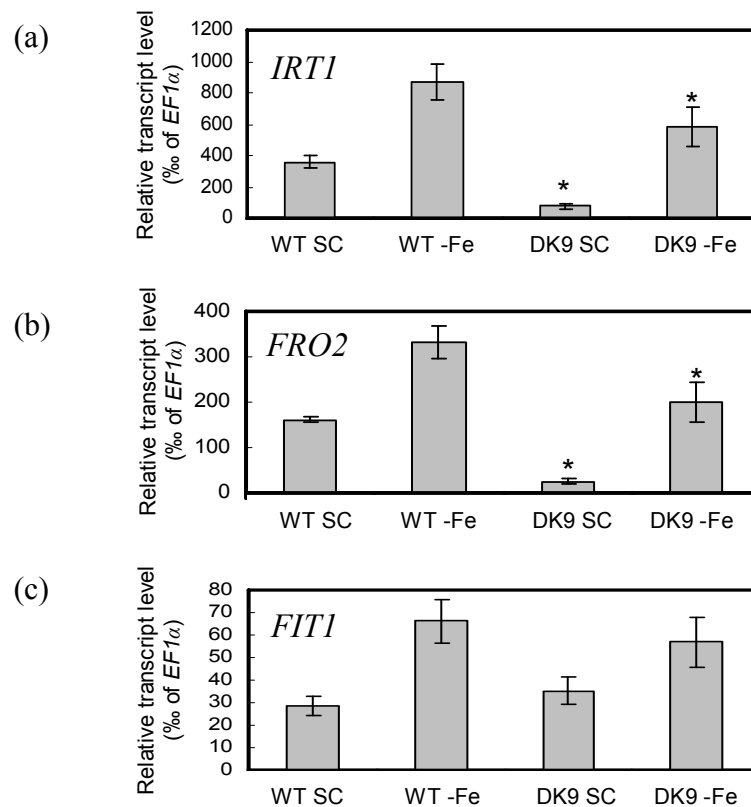


Figure 11. Fe deficiency marker transcript levels in roots of wild-type and *rail-1* seedlings.

(a) *IRT1*, (b) *FRO2* and (c) *FIT1* transcript levels were quantified using quantitative real-time RT-PCR. RNA was extracted from roots of *rail-1* and wild-type seedlings grown on control Hoagland medium supplemented with 5 μ M Fe (SC = Standard Conditions) or Fe deficient medium (-Fe) for 14 days. Bars correspond to arithmetic means \pm SD ($n = 3$ replicate plates of roots pooled from 12 seedlings) of the ratios between the expression of the reaction for the tested gene and the constitutively expressed control gene *EF1 α* , then multiplied by 1000. An asterisk above a bar indicates that the corresponding mean in *rail-1* is significantly different ($P < 0.05$) from the mean of the wild type under the same condition according to a Student's *t*-test with no corrections. Two technical replicates were run for each reaction.

The relationship between decreased transcript levels of genes of the Fe uptake machinery and the increased accumulation of Fe in roots can be explained in several ways. One hypothesis could be that the *rail-1* plant senses the accumulation of Fe in the root and shuts down the Fe acquisition in order to avoid further accumulation of the metal in roots. As an alternative, the *rail-1* defect could lead to a reduction in the synthesis or stability of *IRT1* and *FRO2* transcripts.

It is worth noting that Fe homeostasis is regulated both at the transcriptional and post-transcriptional level. It is also possible that, even though *FRO2* and *IRT1* transcript levels are reduced in *rail-1*, protein levels and/or activities may be comparable or even higher than in the wild type.

Interestingly, no differences were observed in the regulation of the expression of the *FIT1* gene under both conditions, an upstream component regulating transcript levels of *FRO2* and *IRT1* (Vert et al., 2002; Colangelo and Guerinot, 2004), suggesting that its regulation may take place at the protein level (Figure 11c).

4.1.10 FRO2 activity is reduced in the *rail-1* mutant

Fe deficiency responses are regulated at the protein level in addition to the transcript level. Therefore, root-surface ferric-chelate reductase activity, which corresponds to the activity of FRO2, was measured in seedlings grown on control medium and on Fe deficient medium. As expected, the FRO2 activity in roots of wild type was approximately four-fold higher in Fe deficient conditions than in control medium. *rail-1* plants showed lower levels of activity in both tested conditions, even though a Fe deficiency-dependent 4-fold increase in activity was still observed (Figure 12). These results corroborate the real-time RT-PCR data, suggesting that the Fe deficiency response in the *rail-1* mutant is attenuated in both standard and Fe-limited conditions.

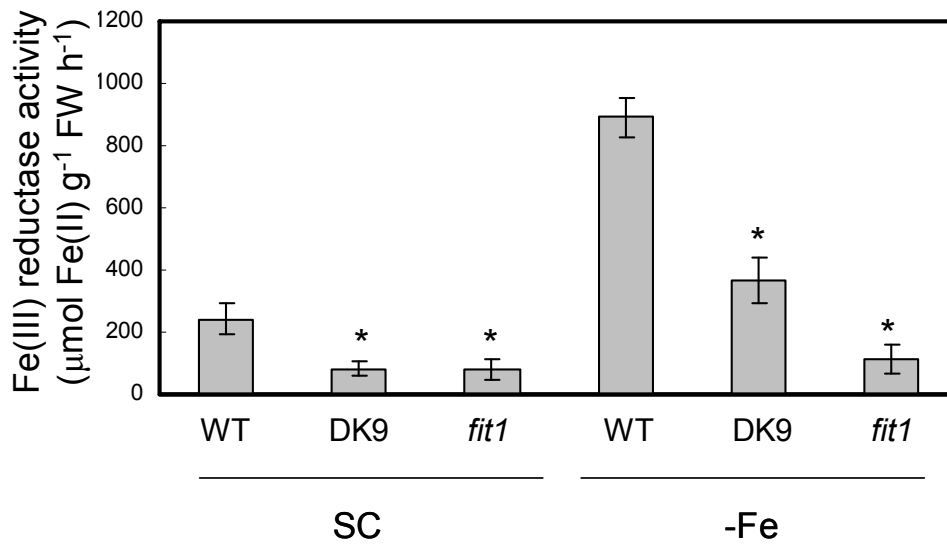


Figure 12. Dependence of Fe supply of root-surface ferric-chelate reductase activity in wild-type and *rail-1* seedlings.

Root surface ferric chelate reductase activity was measured in wild type, and *fit1-2* seedlings grown for 14 days on control (standard conditions SC) or Fe deficient medium. Bars represent arithmetic means \pm SD of $n = 4$ replicate samples, each consisting of roots pooled from 8 seedlings. Asterisks indicate a statistically significant difference ($P < 0.05$) between wild type and mutant grown in the same condition, based on a Student's *t*-test with Bonferroni corrections. Data are shown from one experiment representative of two independent experiments.

4.1.11 *rail-1* mutant has low fertility

As mentioned in paragraph 4.1.1, *rail-1* shows a low-fertility phenotype, characterized by the formation of small siliques carrying a low number of seeds. An analysis with Alexander stain suggested a defect in the release of mature pollen from the anthers (Figure 13).

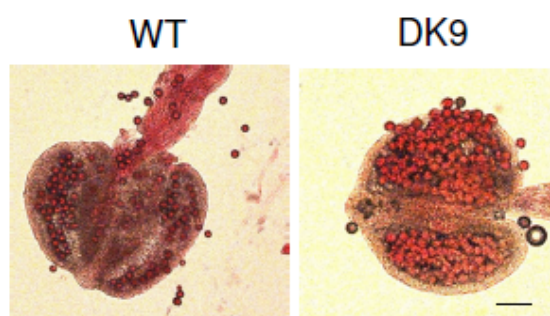


Figure 13. The *rail-1* mutant exhibits a fertility defect.

Alexander stain performed with anthers of WT and *rail-1* plants grown on soil for 38 days in short-day conditions. The shown images are representative of 9 anthers from 3 independent plants per genotype. The size bar corresponds to 100 μm .

A defect in male fertility was confirmed by crossing *rail-1* with wild type. Of the siliques produced using anthers from wild type on pistils of *rail-1*, 91% carried seeds, whereas only 17% of the siliques produced using anthers from *rail-1* and pistils of wild type contained seeds (Table 3). These data suggest that the dramatically reduced fertility of *rail-1* is largely a consequence of male sterility.

Table 3. Success of reciprocal crosses between wild-type and *rail-1* plants.

♂	♀	Success (no. of siliques with seeds/no. of pollinated pistils)
DK9	WT	2/12 (17%)
WT	DK9	11/12 (91%)
WT	WT	12/12 (100%)

4.1.12 Male sterility of *rail-1* is temperature-dependent and linked to an altered distribution of IAA in the mutant

Under our standard growth conditions, soil-grown *rail-1* mutant plants produced fewer seeds than the wild type, but they were completely sterile at higher temperatures (29°C) (Figure 14).

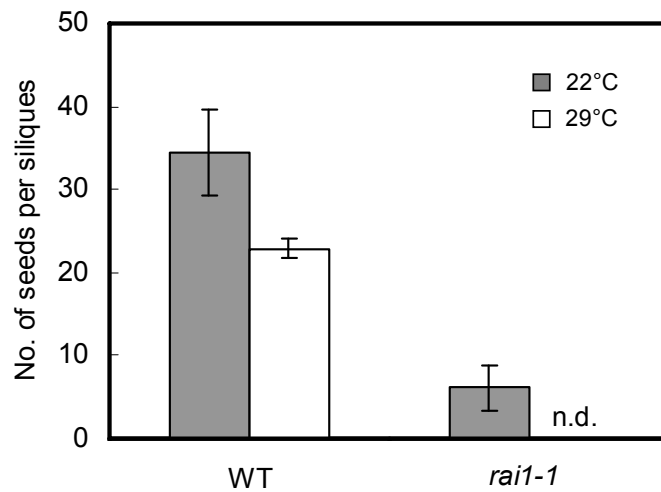


Figure 14. Determination of seed number in wild-type and *rai1-1* plants.

Number of seeds obtained from single siliques of 45-d-old *rai1-1* and WT plants grown in short days at 22°C or 29°C for both day and night. Bars represent arithmetic means \pm SD of a total of $n = 4$ plants per genotype (4 randomly selected siliques counted per plant). n.d.: no seeds detected.

In addition to Fe deficiency-related symptoms and a male fertility defect, *rai1-1* shows phenotypic features common to several IAA (indole-3-acetic acid)-related mutants. For example, upward curled leaves represent a typical phenotype of auxin-related mutants (Hu et al., 2003; Fleming, 2005).

To assess a potential involvement of IAA in the fertility defect, a GUS stain was performed with the inflorescences of *rai1-1* and wild-type plants carrying the auxin-responsive *DR5-GUS* construct. There was no visible staining at all in *rai1-1* anthers of plants grown at the higher temperature of 29°C, whereas the anthers of wild type still presented the stain (Figure 15). No major differences between wild type and *rai1-1* were detected at the standard temperature of 22°C. This data indicates that the absence of IAA or IAA responsiveness detectable through *DR5-GUS* staining is associated with male sterility of the mutant. However, application of exogenous IAA on inflorescences containing buds and open flowers did not rescue this phenotype, indicating that a possible lack of IAA in the inflorescence is not the only cause of the observed fertility defect in *rai1-1*. Alternatively, another form or amount of IAA may be required to restore male fertility.

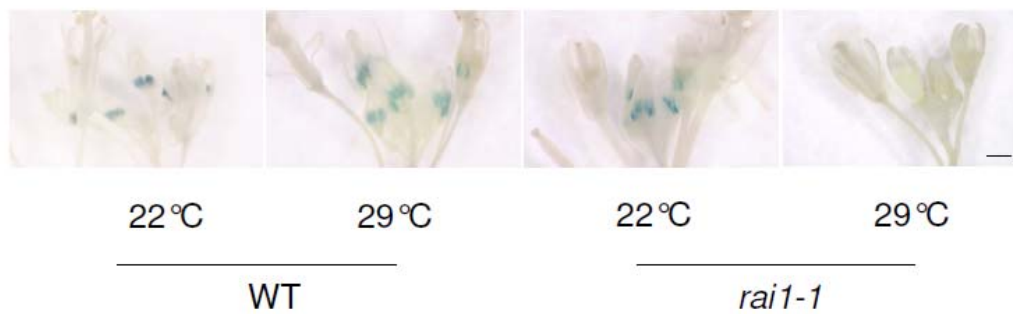


Figure 15. Histochemical detection of *DR5-GUS* activity in wild-type and *rail-1* plants.

Localization of GUS activity in inflorescences of WT and DK9 plants carrying a *DR5-GUS* construct grown for 38 days on soil at 22°C or 29°C. The shown images are representative of 4 inflorescences per genotype. The size bar corresponds to 1.5 mm.

4.1.13 The *rail-1* mutant displays an alteration in free IAA release

To obtain more information on auxin-related processes in the *rail-1* mutant, transcript levels of several genes involved in IAA conjugation were determined in seedlings by quantitative real-time RT-PCR. In comparison to wild type, the mutant showed decreases in average transcript levels of two *ILR* (*IAA-LEUCINE RESISTANT*) genes (Figure 16), *ILR1* and *ILR3*, by 50 and 60 %, respectively. *ILR1* is an amidohydrolase which generates free IAA from the IAA-Leu conjugate, an inactive form of auxin (Bartel and Fink, 1995). The second one, *ILR3*, encodes a bHLH leucine zipper transcription factor which was concluded based on the mutant phenotype to have a role in influencing IAA-conjugate hydrolysis by a poorly understood mechanism (Rampey et al., 2006). No significant changes in transcript level between wild type and *rail-1* were found for the other tested auxin-responsive genes.

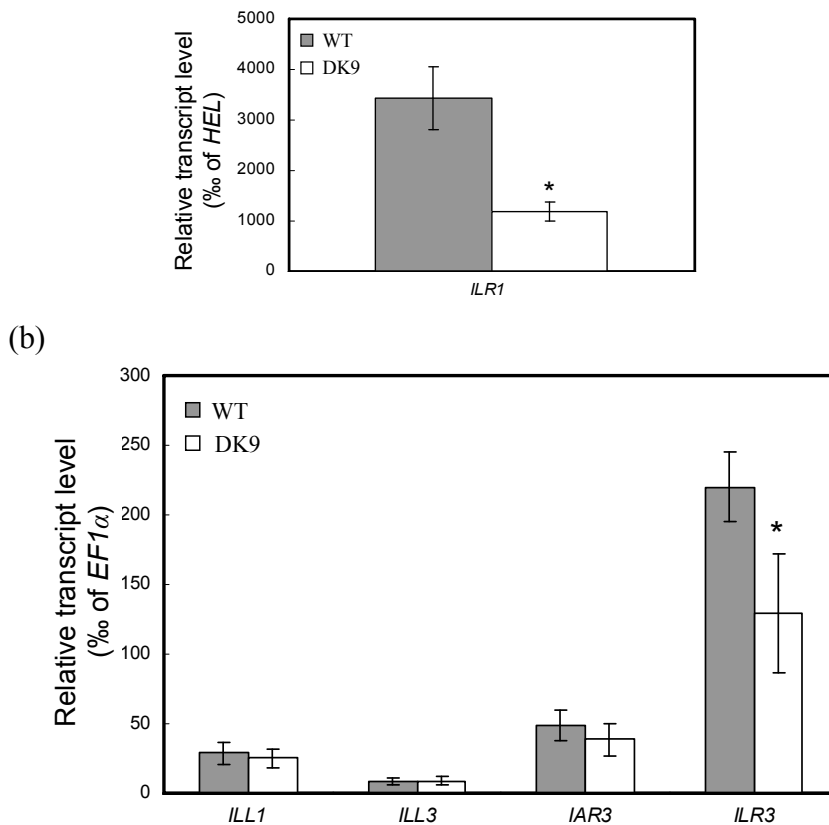


Figure 16. Transcript levels of genes related to IAA-amide conjugation and hydrolysis.

RNA was extracted from shoots of *rail-1* and WT seedlings grown on control Hoagland medium (5 μ M Fe) for 14 days. Bars correspond to arithmetic means of the ratio between the expression of the reaction for the tested gene and the constitutively expressed control gene *EF1 α* or *Hel*, then multiplied by 1000. Bars represent arithmetic means \pm SD of $n = 3$ replicate plates, for each of which material was pooled from 10 seedlings. An asterisk above a bar indicates that the corresponding mean in *rail-1* is significantly different ($P < 0.05$) from the mean for the wild type according to a Student's *t*-test with no corrections. Two technical replicates were run for each reaction.

To further investigate IAA conjugation in the mutant, wild-type and *rail-1* seedlings were grown on medium containing several concentrations of IAA-Leu and IAA-Ala. At 10 μ M IAA-Leu, root growth of the wild type was inhibited to a larger extent than in the mutant, suggesting that *rail-1* is slightly more tolerant than the wild type (Figure 17). No obvious differences were detected between root growth of wild type and mutant growing on medium supplemented with IAA-Ala. Taken together, these results suggest decreased rates in the *rail-1* mutant of release of free IAA from IAA-Leu. However, it is worth

noting that the interpretation of the results of this experiment is not easy, as wild type and mutant perform differently already in medium without added IAA-amide conjugates.

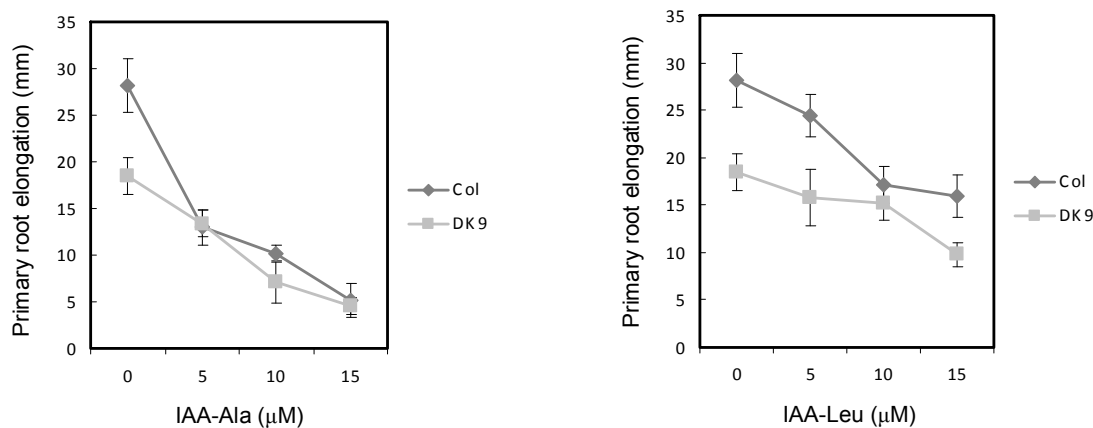


Figure 17. Sensitivity of root elongation in wild-type and *rail-1* seedlings to IAA-amide conjugates.

WT (Col) and *rail-1* seedlings were grown for 10 days on Hoagland medium and then transferred for 4 days onto medium supplemented with several concentrations of IAA-Ala or IAA-Leu. The length of the portion of the root grown after transfer was then measured. The data points represent arithmetic means \pm SD of $n = 4$ replicate samples, each consisting of roots from 6 seedlings grown on a common plate. Data are shown from one experiment representative of two independent experiments.

4.1.14 *LCR* transcript levels in *rail-1* are lower than in wild type

When grown on soil, the *rail-1* mutant shows abnormal leaves, with the leaf edges curling upwards (Figure 2b). The establishment of a proper leaf morphology is regulated by a complex network of genes (Byrne, 2005) involving *LEAF CURLING RESPONSIVENESS (LCR)* in *A. thaliana* (Song et al., 2012). The gene encodes a protein containing a 50-amino acid F-box domain, which is conserved among all plant orthologs. Low transcript levels of *LCR* in a loss-of-function mutant (*lcr*) resulted in semi-dwarfism and upward leaf curling. Little is known about the direct targets of *LCR*, but misregulation (both up-regulation and down-regulation) of auxin-responsive genes in *lcr* suggested a role in the degradation of components in the auxin signaling pathway (Song et al., 2012).

To determine the transcript levels of *LCR* in the shoot of the *rail-1* mutant by quantitative real-time RT-PCR, total RNA was isolated from leaves of plants grown for 14 days on

Hoagland medium, followed by another 14 days on soil. Transcript levels of *LCR* were reduced by *ca.* 50% compared to those in the wild type (Figure 18). This result indicates the possibility that the curly leaf phenotype of the mutant is caused by low expression of *LCR*.

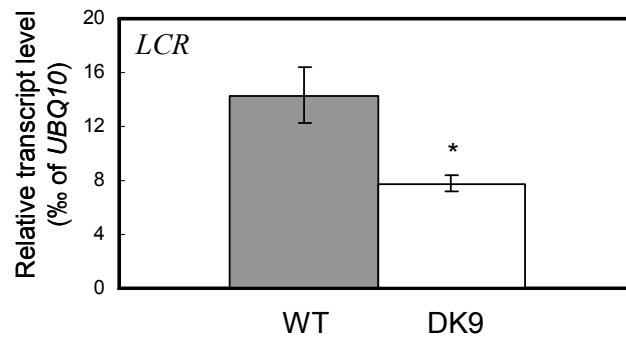


Figure 18. *LCR* transcript levels in wild-type and *rail-1* rosette leaves.

LCR transcript levels determined in shoots of *rail-1* and WT seedlings grown for 14 days on Hoagland medium, followed by another 14 days on soil. Bars correspond to arithmetic means of the ratio between the expression of the reaction for the tested gene and the constitutively expressed control genes, then multiplied by 1000. Bars represent arithmetic means \pm SD of $n = 3$ replicate individuals. The corresponding mean in *rail-1* is significantly different ($P < 0.05$) from the mean for the wild type according to a Student's *t*-test. Two technical replicates were run for each reaction.

4.1.15 miRNA accumulation is aberrant in the *rail-1* mutant

MicroRNAs (miRNAs) are short non-coding RNAs (19-24 nucleotides in plants) which bind to complementary sequences on target messenger RNA transcripts, thus initiating target mRNA degradation or translational repression (Chen, 2005). As post-transcriptional regulators, plant miRNAs have a role in several biological processes including development, stress responses, and defense against viruses (Perez-Quintero et al., 2010). miRNAs have also been implicated in long-distance nutrient signaling pathways. For an example, mi399 is a phloem-mobile miRNA which regulates phosphate homeostasis (Pant et al., 2008). As it was hypothesized that *rail-1* may have a problem in long-distance Fe signaling, a potential misregulation of miRNAs found to be regulated under Fe deficient conditions (miR159, miR172 and miR162) (Kong and Yang, 2010)

was assessed by real-time RT-PCR. Even though a potential role for the three tested miRNAs in Fe homeostasis has not been studied so far, the analysed miRNAs have already been implicated in several processes. miRNA159 plays a role in seed germination (Palatnik et al., 2007), miR172 in flower development (Zhao et al., 2007), and miR162 in the resistance to bacterial and viral pathogens (Azevedo et al., 2010).

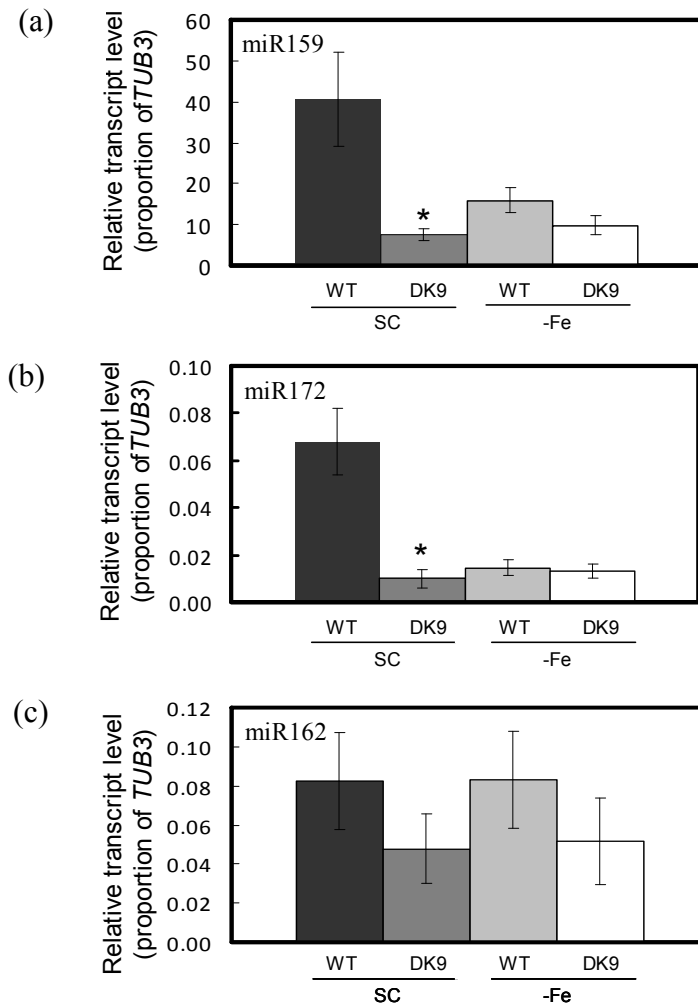


Figure 19. Levels of Fe responsive miRNAs in wild type and *rail-1*.

Relative levels of miRNAs (a) miR159, (b) miR172 and (c) miR162 determined in shoots of *rail-1* and WT seedlings grown on Hoagland medium supplemented with 5 μM FeHBED (SC = Standard Conditions) or without Fe (-Fe) for 14 days. Bars correspond to arithmetic means of the ratio between the expression of the reaction for the tested mature miRNA and the constitutively expressed control gene *TUB3*. Bars represent arithmetic mean \pm SD of $n = 3$ replicate petri plates, with 12 seedlings pooled per plate. Asterisks denote significant differences ($P < 0.05$) between WT and *rail-1* grown under the same conditions according to a Student's *t*-test. Two technical replicates were run for each reaction. Data are shown from one experiment representative of two independent experiments.

Under Fe deficiency, wild type accumulated about 15-20 % of the miR159 and miR172 levels accumulated under standard-Fe growth regime, confirming the regulation of these two miRNAs dependent on Fe availability as reported in the literature (Song et al., 2012). In all tested conditions, miR159 and miR172 levels in the *rail-1* mutant were comparable to the levels detected in the wild type under Fe deficient conditions (Figure 19). Taken together, the data show that in the presence of Fe abundance of the Fe-responsive miR159 and miR172 is lowered in DK9. The fact that the levels of these two miRNAs are similar in *rail-1* and wild type under Fe deficiency conditions suggests that the miRNA levels reflect a differing physiological Fe status of the seedlings of these two genotypes when cultivated in standard media. Alternatively, *rail-1* may be defective in miRNA biogenesis. In contrast to the literature, we could not observe any dependence of miR162 levels on Fe status in either the wild type or *rail-1*. Abundance of miR162 was *ca.* 20% lower in *rail-1* than in the wild type, suggesting Fe-independent misregulation of this miRNA.

4.1.16 A chimeric 35S:AtRAI1-GFP fusion protein localizes in the cytosol of *A. thaliana* mesophyll protoplasts

To assess the localization of AtRAI1, *A. thaliana* mesophyll protoplasts were transformed with a 35S:AtRAI1-GFP construct (see paragraph 3.3.4 for details about the generation of the construct). The GFP signal was detected in the cytosol (Figure 20). To confirm this result, protoplasts were co-transformed with 35S:AtRAI1-GFP and 35S:Dcp2-cherry, a marker construct for cytosol. DCP2 is the main enzyme with a decapping activity in *A. thaliana* as well as in other eukaryotes. Studies on yeast Dcp1/Dcp2 have shown that the two proteins bind non-translating mRNAs in the cytosol and, after recruiting additional activators of the decapping process, they remove the cap at the 5'-end. In turn, this leads to the degradation of the target mRNA by 5'-to-3' exoribonucleases or by the exosome (Balagopal and Parker, 2009). It is known that eukaryotic RNA processing occurs in specific cytoplasmic foci, known as processing bodies (PBs) (Anderson and Kedersha, 2006). The signals of the two fluorescent proteins completely co-localized (Figure 20). The finding that AtRAI1 co-localizes in the cytosol with AtDCP2 is consistent with a possible role of the protein in mRNA degradation. Recently, a role for the human

homolog DOM3Z in the cytoplasmatic degradation of mRNAs was proposed (Zheng et al., 2011a).

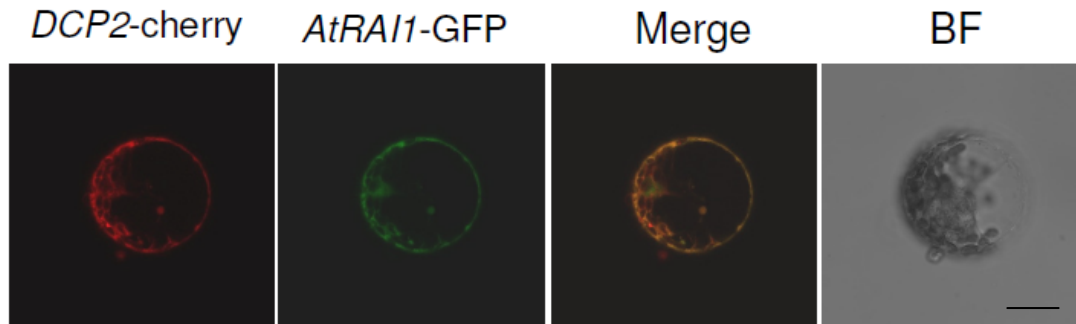


Figure 20. Localization of *AtRAI1* in *Arabidopsis thaliana* mesophyll protoplasts.

Shown are images of protoplasts transiently co-transformed with 35S:*DCP2*-cherry and 35S:*AtRAI1*-GFP constructs. Each image consists of 10 superimposed z-slices covering a distance of *ca.* 30 μ m in total, obtained with a confocal laser-scanning microscope. Two independent transformations were performed with the combination of constructs. The images are representative of six recorded images per transformation. Merge is an overlay of the GFP and the RFP channel. BF, Bright Field. Scale bar: 25 μ m.

4.1.17 *rai1-1* seedlings are ethylene-insensitive (data from Dr. M.J. Haydon)

XRN4 is the only 5'-to-3' exoribonuclease localized in the cytosol of *A. thaliana* cells. Two independent publications have demonstrated that *XRN4* is allelic to *EIN5*, a gene involved in the ethylene signaling pathway, the genomic position of which remained unknown for a long time (Van Der Straeten et al., 1993; Roman et al., 1995; Olmedo et al., 2006; Potuschak et al., 2006). *XRN4* is supposed to direct the degradation of the transcript encoding the F-box proteins EBF1/2, which in turn controls EIN3 stability in the nucleus (paragraph 1.1.5) When grown in the dark in the presence of the ethylene precursor 1-aminocyclopropane-1-carboxylic acid (ACC), the allelic loss-of-function mutants *xrn4-3* and *ein5-1* do not display the typical ethylene response consisting of a thick and short hypocotyl, excessively pronounced apical hook and short root (Potuschak et al., 2006). Because *AtRAI1* is localized in the same compartment as *XRN4* and an interaction between 5'-to-3' exoribonucleases and Rai1p was proposed in yeast, we tested whether disruption of *AtRAI1* function could lead to failure of the triple response. As expected, and different from the wild type, the *rai1-1* mutant showed a reduced ethylene

response (Figure 21). This result shows that *rail-1* is defective in ethylene responses, as already known for *xrn4*. This finding is consistent with the hypothesis of a link between these two proteins, the activator RAI1 and the exoribonuclease XRN4.

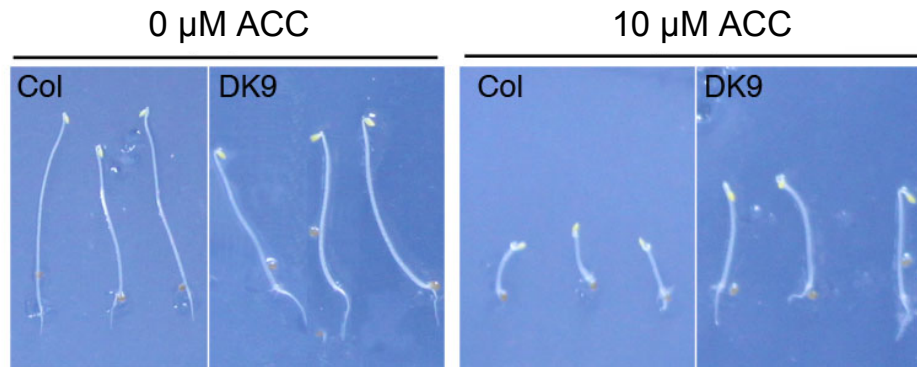


Figure 21. Wild type and *rail-1* response to administration of ACC.

Photographs of representative 3-d-old WT and *rail-1* seedlings grown in dark on standard Hoagland medium in the absence or the presence of 10 μ M ACC.

4.1.18 The *xrn4/ein5-1* mutant does not show iron-dependent defects

A large proportion of the information regarding the function of XRN4 was obtained in studies on loss-of-function mutants (Souret et al., 2004; Olmedo et al., 2006; Potuschak et al., 2006). As stated in the literature, none of mutant alleles show any obvious visible phenotype when grown on sterile medium or soil under normal conditions. The genome of *ein5-1* exhibits an X-ray-induced deletion in the fifteenth exon of *XRN4*, leading to a frame-shift mutation and the production of a truncated protein (Roman et al., 2005). *XRN4* transcript levels were also significantly lower than in wild type (Potuschak et al., 2006). To assess whether modulating Fe concentrations affect the growth or leaf colour of the *ein5-1* mutant showing a loss-of-function of *XRN4*, the mutant was grown medium lacking Fe or supplemented with several Fe concentrations. No difference in root growth, shoot biomass or leaf colour was observed between wild type and mutant grown at the same conditions (Figure 22). As it was hypothesized that RAI1 and XRN4 are components of the same signaling cascade, it was expected that mutants for the corresponding genes would have resulted in similar phenotype. However, the unexpectedly subtle phenotype of loss-of-function and null alleles for *XRN4* has recently

been explained with the presence of other unidentified cytosolic XRNs that may take over (part of) XRN4 functions (Goeres et al., 2007).

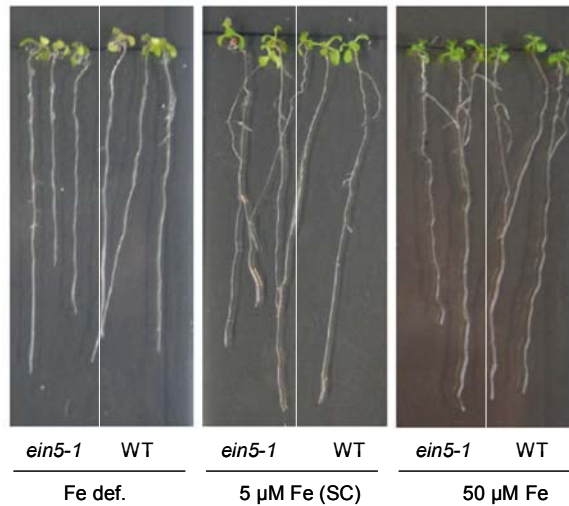


Figure 22. Photographs of *ein5-1* and wild-type seedlings grown in the presence of several different Fe concentrations.

Photographs showing WT and *ein5-1* seedlings grown on control Hoagland medium (5 µM FeHBED), Fe deficient medium (no FeHBED added) and Fe excess (50 µM FeHBED) for 12 days in short days.

4.1.19 Recapitulation of the *rail-1* phenotype in a *AtRAII*-RNAi line

To confirm that the phenotype of the *rail-1* mutant is caused by a mutation in the At4g17620 gene, *AtRAII*-RNAi lines were ordered from the AGRİKOLA collection and grown under standard conditions for 12 days. Transcript levels of *AtRAII* were determined in seedlings of the lines by RT-PCR (Figure 23a). Line 25 showed the strongest reduction among all RNAi lines, and it was used for further experiments. *AtRAII*-RNAi seedlings grown on petri plates for 16 days were smaller and more chlorotic than wild-type seedlings (Figure 23b, 23c). Supplementation with Fe was able to rescue chlorosis of line 25 (Figure 23d). After 14 days of growth on medium and 14 days on soil, plants were smaller than the wild type and exhibited upward curly leaves (Figure 23e). These results show that the phenotype of an *AtRAII*-RNAi line resembles that of *rail-1*, suggesting that hypomorphism at the At4g17620 locus is associated with small size, chlorosis and curly leaves.

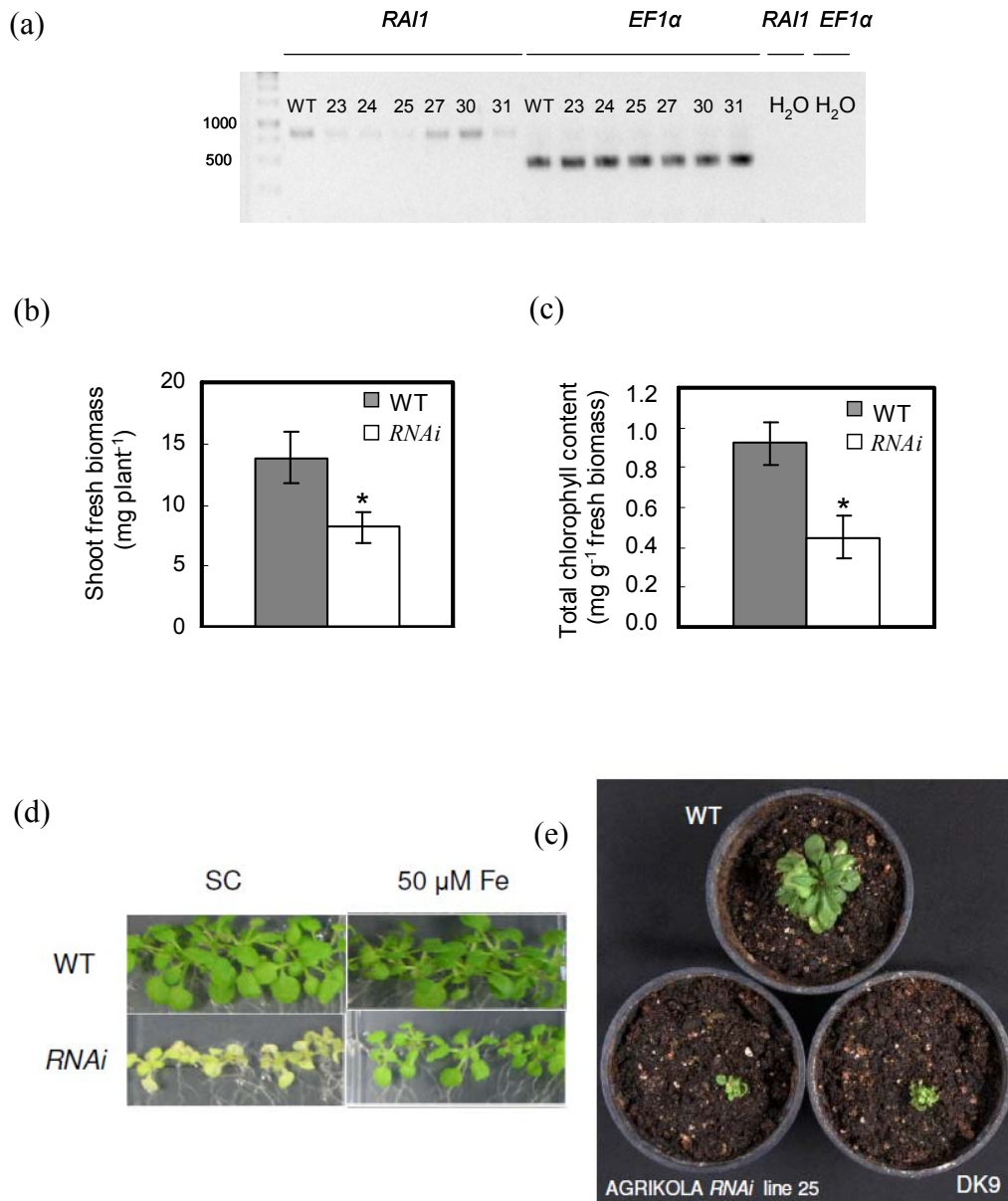


Figure 23. Molecular and phenotypic characterization of *AtRAII*-RNAi seedlings.

(a) Gel of RT-PCR products obtained by amplification of cDNA from 12-d-old seedlings of several *AtRAII*-RNAi lines. Specific primers for *RAII* were used (Supplemental Table 2). *EF1α* was used as constitutively expressed control gene. 25 and 30 cycles were used for amplification of *RAII* and *EF1α*, respectively. Negative controls with water instead of DNA template are also shown (H₂O). The expected size of the amplicon obtained with the combination of transcript-specific primers (*RAII*) is 832 bp. The expected size of the amplicon obtained with the combination of *EF1α*-specific primers is 475 bp. (b) Shoot fresh biomass and (c) chlorophyll concentrations of WT and *AtRAII*-RNAi (line 25) seedlings were grown on standard Hoagland medium (5 μM FeHBED) for 12 days in short days, before phenotypes were recorded. Asterisks

indicate significant differences between mutant and WT seedlings ($P < 0.05$, Student's T -test). Bars represent means \pm SD of 4 replicate plates, each containing 10 pooled shoots per genotype. (d) Photographs showing wild type and *AtRAII*-RNAi grown under standard and Fe luxury conditions for 16 days. (e) Photographs of wild-type, *rai1-1* and *AtRAII*-RNAi plants grown for 14 days on sterile Hoagland medium, followed by 14 days on soil.

4.1.20 The homozygous knockout mutant *rai1-2* is not viable

T-DNA insertion mutants are a valuable tool to determine the roles of genes, because insertions in promoters or coding sequences of specific genes eliminate or compromise their functions. Heterozygous seeds of a T-DNA mutant putatively carrying an insertion in the *AtRAII* gene (SALK_103157.40.20.X) were ordered *via* the TAIR website <http://www.arabidopsis.org/>. The seeds were germinated and grown on routine Hoagland before DNA was extracted from seedlings for genomic characterization (see paragraph 3.2.2). PCRs carried out with combinations of one primer annealing to the left border sequence (LB) of the T-DNA and one primer annealing in the adjacent genomic region upstream the insertion resulted in the amplification of a product for 4/12 of the tested seedlings. An amplicon was obtained for all the tested seedlings, when the genomic DNA was amplified with primers upstream and downstream the T-DNA insertion. This data indicated that all the tested seedlings were either wild-type or heterozygous, suggesting the possibility that homozygous seeds were either absent from the seed population or not viable. The T-DNA insertion was localized just after the nucleotide 1204 from the translational start codon of the *RAII* gene, inside intron 4 (Figure 24).

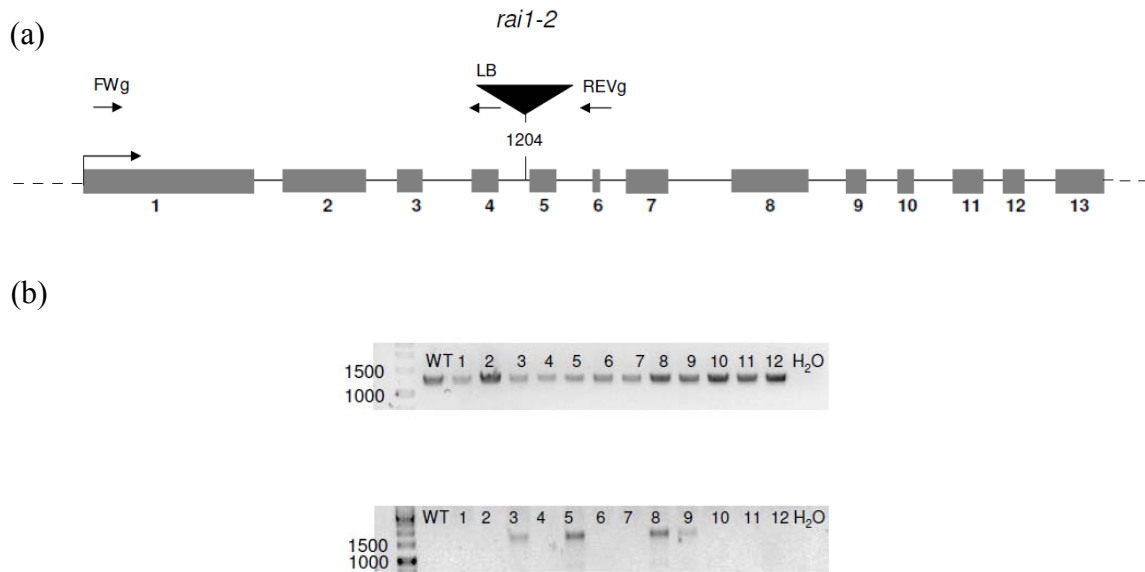


Figure 24. Genomic characterization of *rai1-2*.

(a) Schematic representation of the *RAIL* locus. Arrows indicate the positions of the primers used to characterize *rai1-2* at the genomic level. FWg, forward primer annealing to the genomic sequence upstream the T-DNA insertion. REVg, reverse primer annealing to the genomic sequence downstream the insertion. LB, Left Border primer specific for the insertion. Grey boxes correspond to exons and the black triangle indicates the T-DNA insertion. (b) Image of agarose gels showing the amplicons obtained by PCR with a combination of FWg and REVg (upper panel) and FWg and LB (lower panel). Expected amplicon sizes are 1339 bp and 1577 bp for the PCR reported in the upper and lower panel, respectively. H₂O indicates the lane of the negative control reaction performed without DNA template. No PCR products were obtained when a primer annealing to the right border was used in combination with FWg or REVg (data not shown).

To confirm that homozygous *rai1-2* seeds are not viable, heterozygous plants were grown, and an analysis of siliques was performed. The observed siliques looked normal, but some seeds inside did not develop (Figure 25a). A smaller subset of these siliques also contained some small aberrant seeds (Figure 25b). The number of fully developed seeds per silique was quantified, and siliques from the heterozygous mutant were lacking on average *ca.* 1/4 of the seeds (Chi-square test, $P < 0.01$) (Figure 25c). This finding is in agreement with the ratio we would expect, if homozygous *rai1-2* seeds were developmentally arrested. Together, these results show that *AtRAIL* is essential for seed development. Furthermore, the fact that homozygous *rai1-1* seeds are viable and *rai1-1*

seedlings are similar to the *AtRAII*-RNAi ones, suggests that *rail-1* may be a weak allele in which RAI1 function is strongly reduced, but not completely lost.

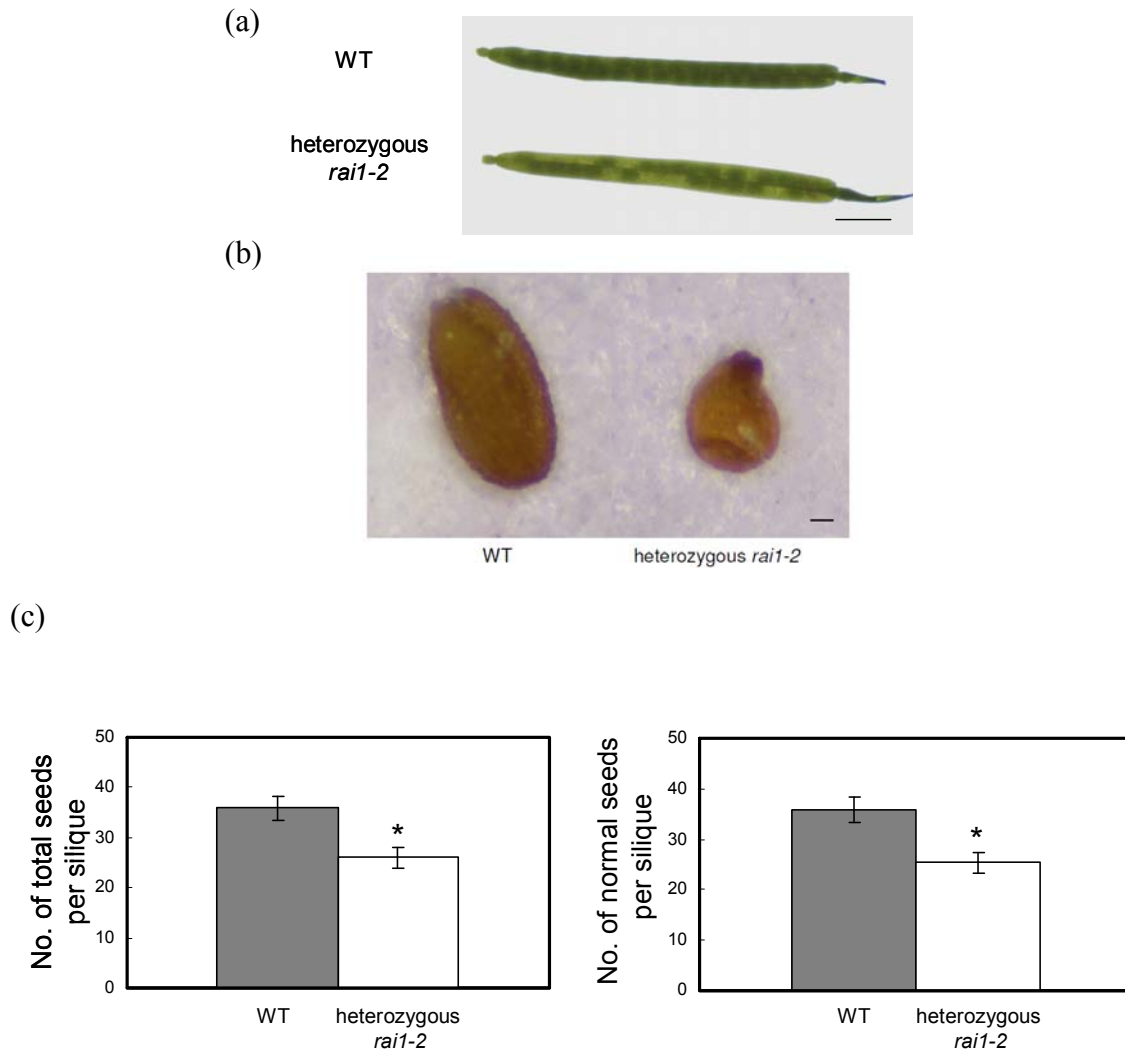


Figure 25. Phenotypic characterization of heterozygous *rail-2* plants.

(a) Photographs of representative siliques from 42-d-old *rail-2* heterozygous and wild-type plants grown on soil in short days. Bar corresponds to 0.25 cm. (b) Comparison between normal and aberrant seeds harvested from siliques of heterozygous *rail-2* plants. Bar corresponds to 50 μ m. (c) Number of seeds obtained from single siliques comprising (panel on the left) or not comprising (panel on the right) aberrant seeds. Bars represent arithmetic means \pm SD of seeds counted from single siliques. A total of 16 siliques was pooled from each of $n = 4$ plants per genotype.

4.2 CHARACTERIZATION OF *bts2-1*

4.2.1 The amino acid sequence of the BTS2 protein exhibits two hemerythrin motifs and two zinc finger domains

The *BTS* family in *Arabidopsis thaliana* consists of three homologous genes encoding putative E3 ubiquitin ligases: At3g18290 (*BTS*), At1g18920 (*BTS2*) and At1g74760 (*BTS3*) (Long et al., 2010). To gain more insight into the domain structure of *BTS2*, an *in silico* analysis was performed by using ScanProsite, Smart and Pfam packages. The analysis indicated the presence of two hemerythrin domains (one localised near the N-terminus and one in the central part of the protein sequence) and two zinc finger domains (CHY- and C3HC4-type) close to the C-terminus (Figure 26a). According to the InterPro database (<http://www.ebi.ac.uk/interpro/>), all of these motifs are predicted to bind metals. In the canonical hemerythrin domain, two iron atoms bind to the imidazole rings of four histidine residues and the carboxyl group of an aspartic acid and a glutamic acid. Variations in the amino acid composition of the domain are quite common (Supplemental Figure 7a) (Stenkamp, 1994). Interestingly, some bacteria and some phyla of marine invertebrates possess a protein consisting of only a single hemerythrin domain. A role for these proteins in transfer and storage of O₂ has been proposed (Demuyneck et al., 1993). Different from hemerythrin motifs, zinc finger motifs coordinate Zn atoms *via* cross-braces containing histidines and cysteines (Supplemental Figure 7b). These finger-like folds are often stabilised by salt bridges (Laity et al., 2001). At least in mammals, CHY and C3HC4 domains have been found in many E3 ubiquitin ligases (Lorick et al., 1999). One of them, PIRH2, contains the CHY domain and targets the cancer-related factor p53 for degradation (Corcoran et al., 2004).

Furthermore, pBLAST analyses indicated that *BTS2* is more similar to *BTS3* (69% identity, 80% similarity) than to *BTS* (41% identity, 59% similarity) (Figure 26b). In comparison to *BTS2* and *BTS3*, *BTS* contains an additional hemerythrin motif in the central region of the protein (residues 327-440). Intriguingly, the domain structure of the members of the *BTS* family (C-terminal zinc finger domains and N-terminal hemerythrin motifs) is reminiscent of *FBXL5*, a E3 ubiquitin ligase that regulates Fe homeostasis in *Homo sapiens* (Salahudeen et al., 2009; Vashisht et al., 2009).

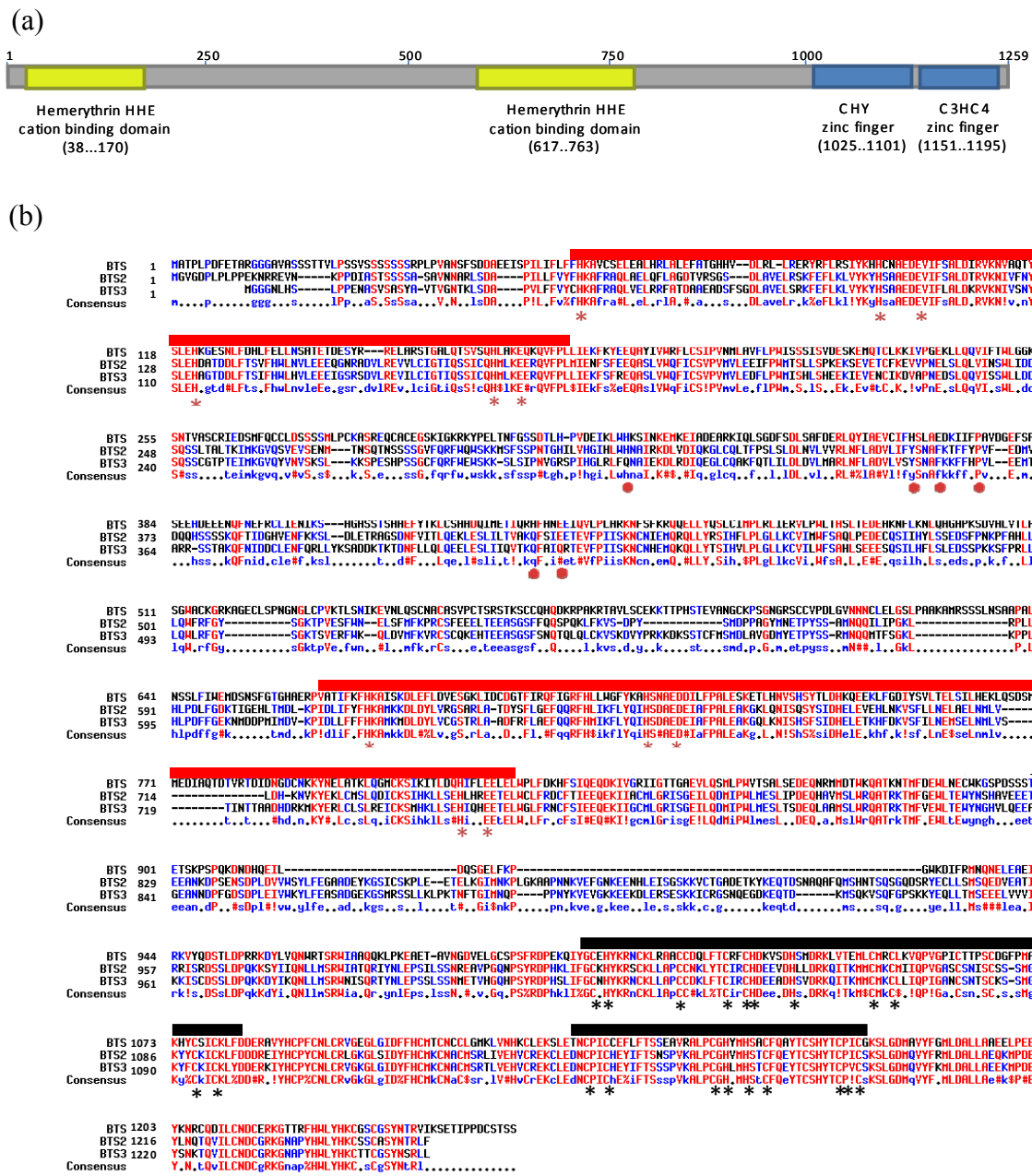


Figure 26. BTS2 contains hemerythrin motifs and zinc finger domains.

(a) Schematic representation of the protein structure of BTS2 with its motif and domain structure. The amino acid sequence of BTS2 was used as query input in the Scanprosite, SMART and Pfam packages to identify motifs and domains. All of these programs found two hemerythrin motifs and two zinc fingers domains (CHY- and C3HC4-type). (b) Multi-alignment of the amino acid sequences of BTS (At3g18290), BTS2 (At1g18910) and BTS3 (At1g74770). The BTS sequence was BLASTed against the *Arabidopsis thaliana* non-redundant protein database and the retrieved sequences were aligned using the program MultiAlin (Corpet et al., 1998). Residues conserved in all the three paralogs are shown in red whilst residues conserved only in two of them are shown in blue. Red asterisks mark essential residues of the hemerythrin domain conserved in

the three sequences. Black asterisks mark essential residues of the CHY and C3HC4 zinc finger domains conserved in the three sequences. Hemerythrin domains are indicated with a red bar, while the zinc finger domains are indicated with a black bar. Red circle mark residues of a hemerythrin domain present in BTS, but not in BTS2 and BTS3.

4.2.2 *BTS2* is highly expressed in seedlings and siliques, and transcript levels increase under Fe deficiency conditions

To assess the spatio-temporal regulation of *BTS2*, transcript levels were quantified by real-time RT-PCR in roots and shoots of 14-d-old seedlings. Additionally, transcript levels were determined in leaves, inflorescence and siliques of 38-d-old mature plants grown on soil. Expression of *BTS2* was detectable in all analysed tissues. However, the transcript abundance was 4.0-fold higher in seedlings (similar levels in roots and shoots) and siliques, when compared to leaves and inflorescences (Figure 27a). Furthermore, in order to determine whether the regulation of *BTS2* is metal-dependent, transcript levels were analysed in 10-d-old whole seedlings cultivated under Fe deficiency and excess Zn conditions. Compared to standard control media, the *BTS2* transcript levels in seedlings were up-regulated approximately 2-fold under Fe deficiency and were also slightly increased on media containing toxic Zn concentrations (Figure 27b). These results are consistent with expression profiling data showing a 2.8-fold up-regulation of *BTS2* in the roots of wild-type seedlings grown on Fe-depleted growth medium (Colangelo and Guerinot, 2004). Together, these results indicate that transcript levels of *BTS2* are highest in young seedlings and siliques and increase moderately in response to Fe deficiency.

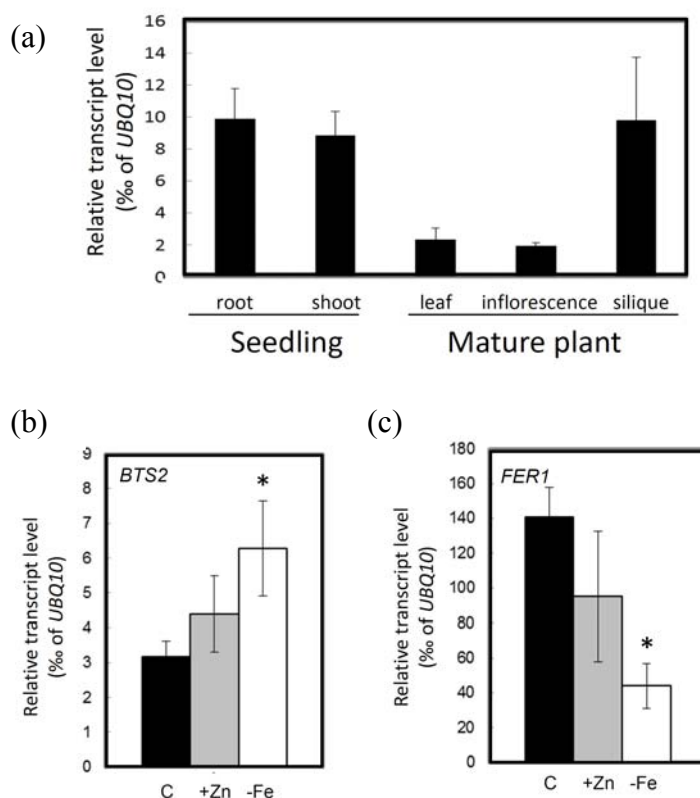


Figure 27. Developmental and metal-dependent regulation of steady-state *BTS2* transcript levels.

(a) RNA was extracted from roots and shoots of wild-type seedlings grown on Hoagland medium (1 μM Zn, 5 μM Fe) for 14 days, and from leaves, inflorescence and siliques of plants after transfer and cultivation on soil for 24 days. (b) RNA was extracted from whole wild-type seedlings grown for 10 days on control Hoagland medium (C) or on medium supplemented with 100 μM Zn (+Zn) or depleted of Fe (-Fe). *BTS2* and *FER1* transcript levels were quantified using real-time RT-PCR. Bars correspond to arithmetic means \pm SE of $n = 3$ replicate plates (seedlings) or $n = 3$ plants (leaf, inflorescences, siliques) of the ratio between the expression of the reaction for *BTS2* and for the constitutively expressed control gene *UBQ10*. Asterisks denote significant differences between control and treated seedlings according to Student's *t*-test ($P < 0.05$) with no corrections.

4.2.3 The *bts2-1* knockout mutant is more tolerant to high Zn concentrations than the wild type

To obtain information about *BTS2* function, a SALK T-DNA mutant line (here called *bts2-1*) was ordered, and the T-DNA insertion was localised in the genome by PCR using combinations of gene and insert-specific primers. The combination of primers spanning the predicted location of the insertion (a forward primer annealing to the 6th exon and a

reverse primer annealing to the 12th exon of *BTS2*) resulted in a product of the expected size in wild type but not in *bts2-1* (Figure 28b). The combination of a primer annealing to the left border (LB) of the T-DNA insert and the reverse primer annealing to the 12th exon of *BTS2* resulted in the amplification of a sequence in the mutant but not in wild type (Figure 28b). Sequencing of this PCR product revealed that the T-DNA insert is located in the sixth exon between nucleotides 2986 and 2987 of the predicted coding sequence (Figure 28a). Homozygous T3 seeds were obtained and used for experiments. Quantification of *BTS2* transcript levels by RT-PCR of regions that are upstream, spanning and downstream of the insertion showed that the *bts2-1* mutant completely lacks *BTS2* transcript, suggesting that *bts2-1* is likely to be a null allele (Figure 28c).

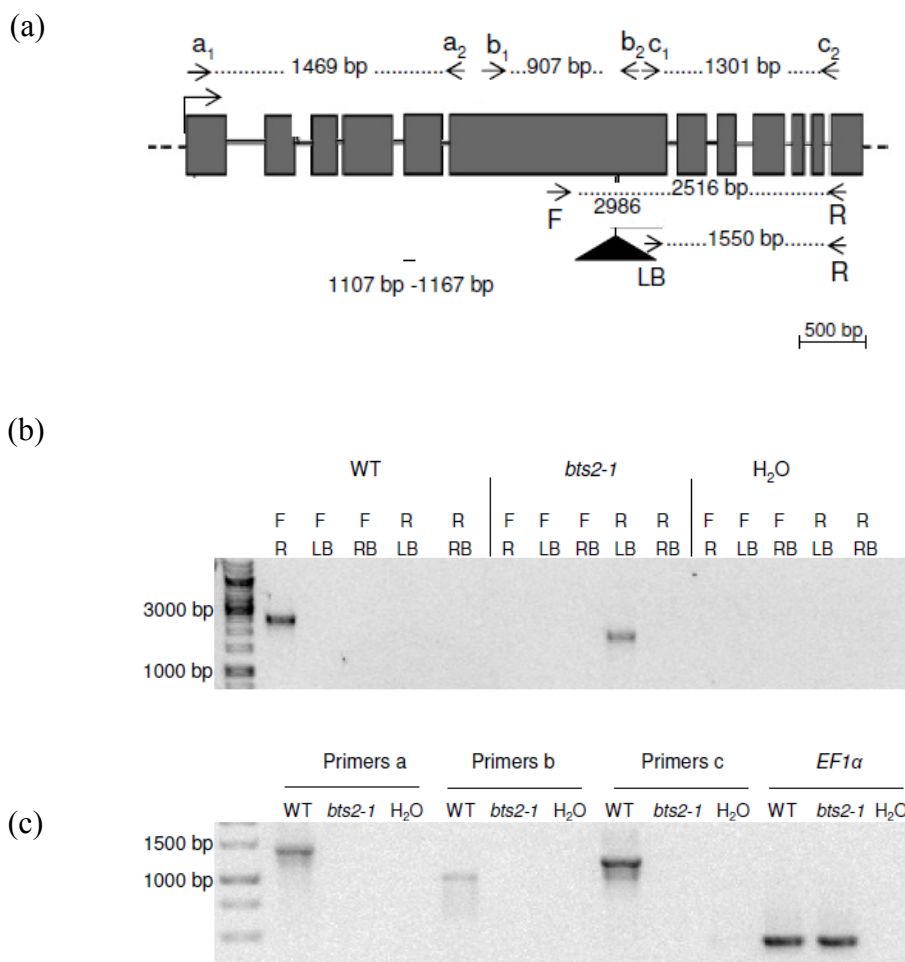


Figure 28. Genetic characterization of the *bts2-1* knockout mutant.

(a) Scheme of the *BTS2* locus. The position of the integration of the T-DNA insertion in *bts2-1* is indicated relative to the predicted translational start of *BTS2* according to the TAIR website (www.arabidopsis.org/). Grey boxes correspond to exons, lines to introns, dashed lines to untranslated regions. The segment below

the scheme indicates the transcript region targeted by the interfering RNA in *BTS2*-RNAi (see Figure 33). Arrows indicate the positions of the primers used for the genomic and transcript analysis. (b) Agarose gel showing the genomic characterisation of a homozygous *bts2-1* line. Specific regions of the genomic DNA from *bts2-1* were amplified using the combination of a primer upstream (F) and downstream (R) of the predicted insertion, or T-DNA-specific primers (LB and RB) in combination with F and R. (c) Analysis of *BTS2* transcript levels in *bts2-1* seedlings. cDNA from wild-type and *bts2-1* was amplified with combinations of primers upstream (Primers a: a1 and a2), spanning (Primers b: b1 and b2) and downstream (Primers c: c1 and c2) of the T-DNA insertion. *EF1 α* was used as constitutively expressed control gene. Wild type (positive control) and H₂O (negative control) were included in each analysis. Labels on the left of the gels indicate the sizes of the ladder fragments.

To investigate the effect of different concentrations of Zn and Fe on the phenotype of the *bts2-1* mutant, shoot biomass and chlorophyll concentration were measured in 12-d-old seedlings. No differences were detected in shoot biomass and chlorophyll content between wild type and *bts2-1* under routine conditions (1 μ M ZnSO₄, 5 μ M FeHBED). Shoots of *bts2-1* seedlings grown on medium supplemented with high levels of Zn (50 μ M and 100 μ M) were bigger and contained more chlorophyll than the wild type (Figure 29). A similar experiment varying the Fe concentrations in the medium between deficient, standard and luxury (0, 5, 50 μ M FeHBED) showed no difference between the mutant and the wild type (Figure 30). Taken together, these results suggest that *bts2-1* is more tolerant to excess Zn, but grows like the wild type under Fe deficiency.

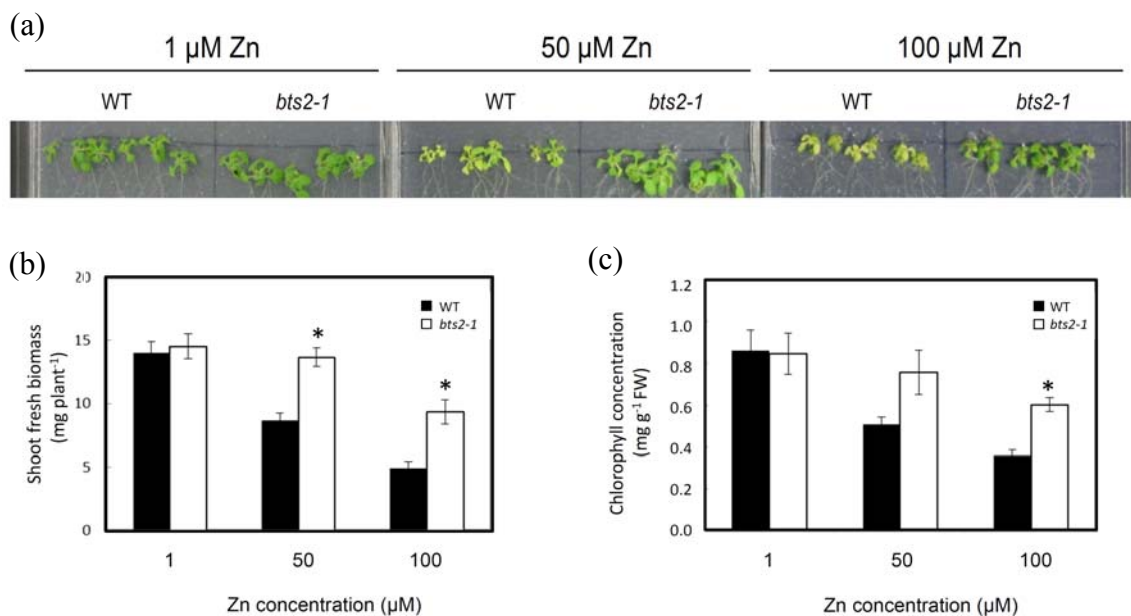


Figure 29. Zn sensitivity of wild-type and *bts2-1* seedlings.

Shown are (a) photographs, (b) measurements of the shoot fresh biomass and (c) the rosette chlorophyll concentrations of 12-d-old seedlings grown on Hoagland medium supplemented with 1, 50 or 100 μM Zn. Values in (b) and (c) are arithmetic means \pm SD of $n = 3$ replicate plates from each of which 5 shoots were pooled per genotype and treatment for each of the two independent biological experiments. Asterisks indicate statistically differences ($P < 0.05$) between means according to Student's t -test with Bonferroni corrections. FW, fresh biomass.

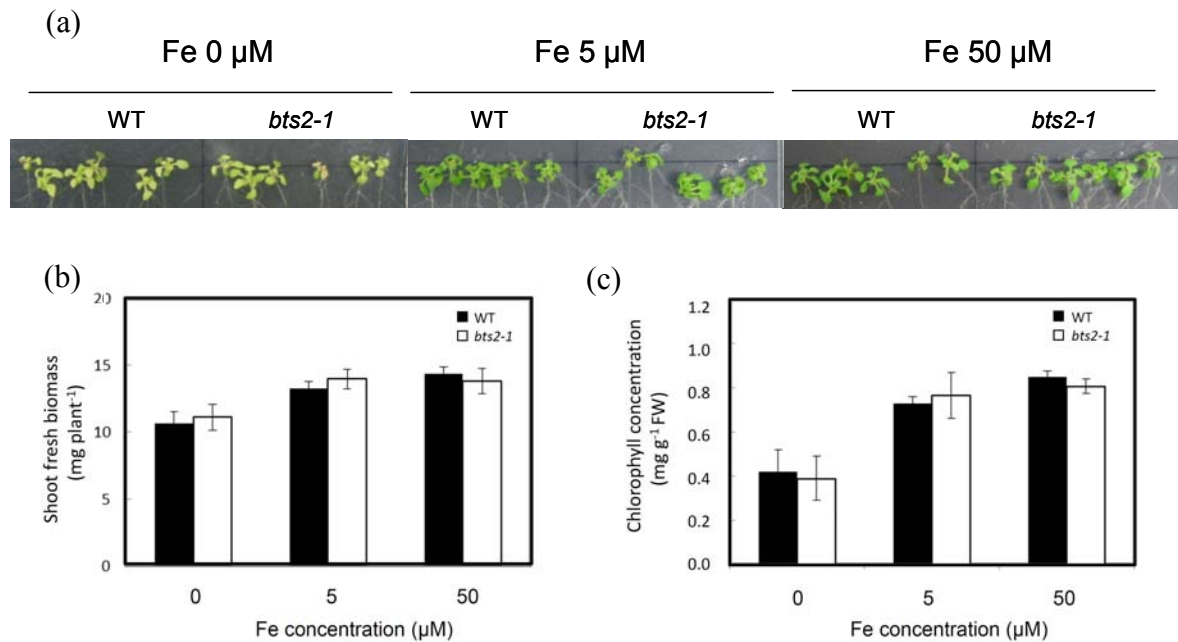


Figure 30. Sensitivity to Fe deficiency of wild-type and *bts2-1* seedlings.

Shown are (a) photographs, (b) measurements of the shoot fresh biomass and (c) the rosette chlorophyll concentrations of 12-d-old seedlings grown on Hoagland medium (1% (w/v) Agar M, 1% (w/v) sucrose), supplemented with 0 μM , 5 μM or 50 μM FeHBED. Values in (b) and (c) are arithmetic means \pm SD of $n = 3$ replicate plates, from each of which 5 shoots were pooled per genotype and treatment, from one experiment of two independent biological experiments. No statistically significant differences were detected between wild type and mutant under any condition according to Student's t -test with Bonferroni corrections. FW, fresh biomass.

4.2.4 *bts2-1* exhibits an altered distribution of metals under excess Zn conditions

To test for a potential alteration in Zn and Fe accumulation in *bts2-1* mutants, metal concentrations were analysed in 14-d-old seedlings by ICP-AES. Under excess Zn conditions, shoots of the mutant accumulated 40 % less Zn than the wild-type shoots (Figure 31b). In accordance with previous data (Arrivault *et al.*, 2006; van de Mortel *et*

al., 2006), wild-type seedlings exposed to excess Zn accumulated about 2.0-fold higher Fe concentrations in the roots than seedlings grown in control media (Figure 31d). However, this trend was not observed in *bts2-1*. The data reported here suggest that the enhanced Zn tolerance of *bts2-1* seedlings might result from a decreased accumulation of Zn in shoots.

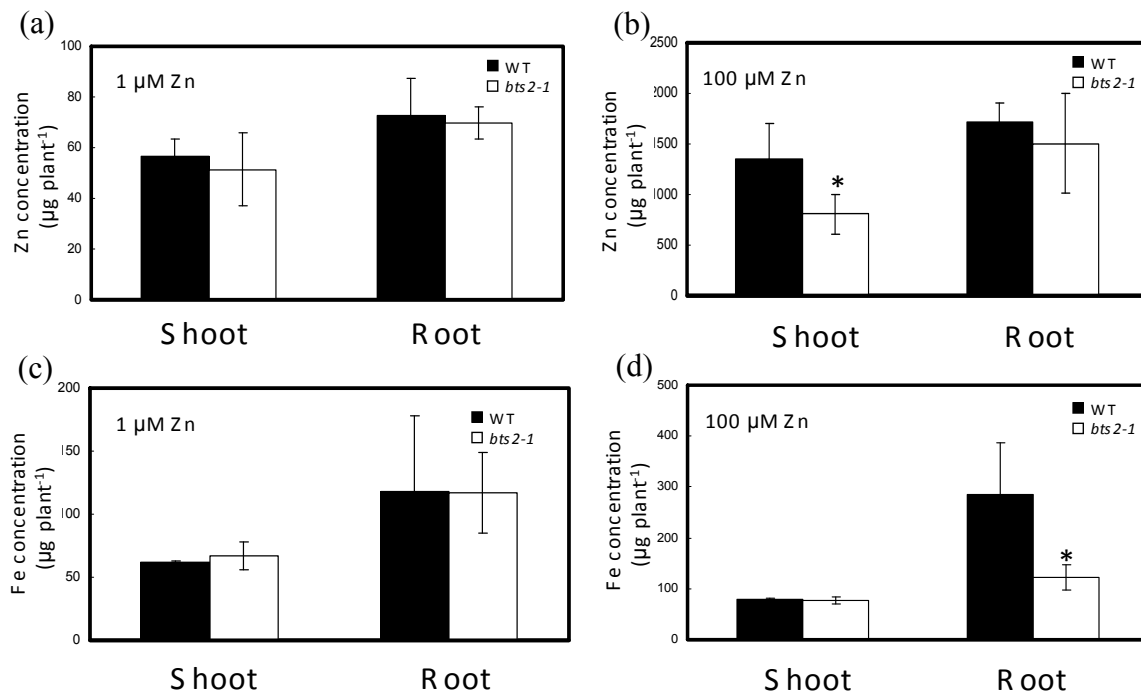


Figure 31. Zn and Fe accumulation in wild-type and *bts2-1* seedlings.

Wild-type and *bts2-1* seedlings were grown for 14 days on vertical plates containing standard Hoagland medium (1 $\mu\text{M ZnSO}_4$) or Hoagland medium supplemented with 100 $\mu\text{M ZnSO}_4$. Zn concentrations were measured in shoots and roots of wild-type and *bts2-1* seedlings grown on (a) control medium and (b) excess Zn conditions. Fe concentrations were measured in shoots and roots of wild-type and *bts2-1* seedlings grown on (c) control medium and (d) excess Zn conditions. Values are arithmetic means \pm SD of $n = 4$ replicate plates with material pooled from 12 seedlings per condition and genotype. An asterisk above a bar indicates a significant difference ($P < 0.05$) between mutant and wild-type mean according to Student's *t*-test with Bonferroni corrections.

4.2.5 Zn excess- and Fe deficiency-responsive genes in the shoot of *bts2-1* are repressed under stress Zn conditions

To analyze the Zn and Fe status in the shoot, transcripts of marker genes for excess Zn and Fe deficiency were quantified in 14-d-old *bts2-1* by real-time RT-PCR. *ZIF1* and

FRO3 transcript levels in shoots of wild-type seedlings were higher under excess Zn conditions compared to control conditions, corroborating published data (Mukherjee et al., 2006; Haydon and Cobbett, 2007). However, toxic levels of Zn in the growth medium did not lead to the up-regulation of these marker genes in the *bts2-1* mutant (Figure 32). This further substantiates the hypothesis that the mutant does not experience a physiological Zn excess in the shoot.

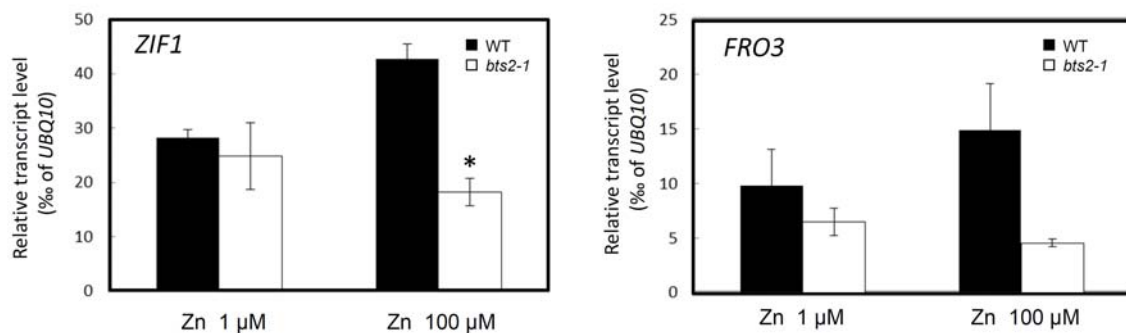


Figure 32. Zn-dependent regulation of Zn and Fe excess marker genes in wild-type and *bts2-1* seedlings.

RNA was extracted from shoots of wild-type and *bts2-1* seedlings grown for 14 days on routine Hoagland medium (1 μ M Zn) or supplemented with 100 μ M Zn. Transcript levels of (a) *ZIF1* and (b) *FRO3* were measured by real-time RT-PCR. Bars correspond to arithmetic means (\pm SE of $n = 3$ replicate plates) of the ratio between the expression of the reaction for *BTS2* and the constitutively expressed control gene *UBQ10*. Asterisks denote significant differences between wild type and *bts2-1* according to Student's *t*-test ($P < 0.05$) with Bonferroni corrections.

4.2.6 *BTS2*-RNAi lines exhibit tolerance to high Zn concentrations

To confirm that Zn tolerance of the *bts2-1* mutant is caused by loss-of-function of *BTS2*, RNAi lines were ordered from the AGRİKOLA collection (Hilson et al., 2004). The obtained lines are transgenic for a short hairpin RNA construct targeting the region between nucleotides 1107 and 1167 of the *BTS2* transcript (Figure 28a). RT-PCR analysis revealed that in the line N2287-10 *BTS2* transcript levels were reduced to 19% of control transcript level, while in the line N2287-12 *BTS2* transcript was undetectable (Figure 33a). The latter line was grown under standard, Fe deficiency and Zn toxicity conditions. No difference was observed between *BTS2*-RNAi and wild-type seedlings grown on standard and Fe-depleted medium (Figure 33b). However, the *BTS2*-RNAi line was more

tolerant to high Zn concentrations than the wild type (Figure 33b). The Zn-tolerant phenotype shared between *BTS2*-RNAi and *bts2-1* corroborates the hypothesis that the tolerance to high Zn concentrations is related to a reduction in (or a loss of) the function of *BTS2*.

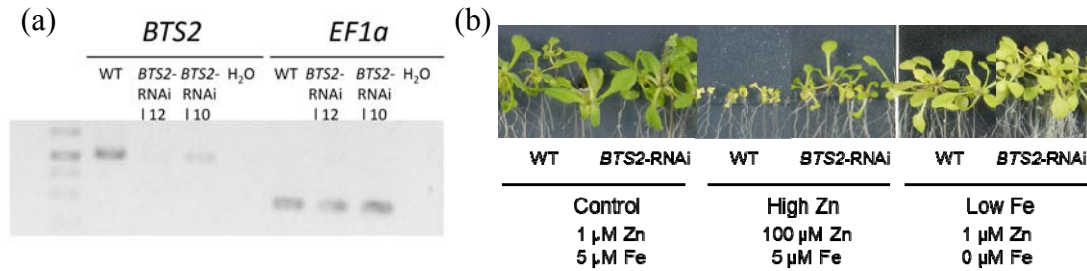


Figure 33. *BTS2* transcript levels and phenotypic characterisation of a *BTS2*-RNAi line.

(a) *BTS2* transcript levels in the *BTS2*-RNAi lines N2287-10 (l 10) and N2287-12 (l 12) (lines 10 and 12) and wild-type seedlings were assessed by RT-PCR. PCR products were amplified from cDNA of 14-d-old wild-type and *BTS2*-RNAi seedlings using the combination of primers b1 and b2 (see Figure 28). *EF1α* was used as constitutively expressed control gene. (b) Photographs of wild-type and *BTS2*-RNAi (line 12) seedlings grown for 17 days under routine (1 μM Zn, 5 μM Fe), Zn excess (100 μM Zn, 5 μM Fe) and Fe deficiency (1 μM Zn, 0 μM Fe) conditions.

5. DISCUSSION

5.1 CHARACTERIZATION OF *rail-1*

5.1.1 Disruption of a gene encoding a putative activator of 5'-to-3' exoribonucleases causes pleiotropic phenotypes

The work presented here includes the physiological and functional characterization of DK9, a recessive EMS-mutant isolated by Dr. Michael Haydon based on leaf chlorosis. When grown on Hoagland medium, the mutant showed chlorosis and reduced size, known as typical symptoms of Fe deficiency (Figure 1). In addition, mature DK9 (*rail-1*) plants grown on soil also exhibited abnormal leaf shape and reduced seed production, when compared to the wild type (Figure 2). Supplementation of the medium with Fe is known rescue mutants defective in Fe uptake (Varotto et al., 2002; Vert et al., 2002; Colangelo and Guerinot, 2004) and Fe translocation to the areal part (Roschztardt et al., 2011). Consistent with the hypothesis that DK9 (*rail-1*) may have a defect affecting Fe homeostasis, leaf chlorosis phenotype of the mutant was rescued by supplying high concentrations of FeHBED in the medium (Figure 1). However, the fact that the other defects could not be rescued by Fe supplementation indicates that the mutation is likely to impact additional pathways different from metal homeostasis.

Coarse and fine mapping combined with whole-genome sequencing were used to identify the mutation in the genome. The mutant under analysis carries a G-to-A substitution at the position 9823388 of chromosome 4. This substitution corresponds to the most common mutation resulting from treatment with the alkylating agent EMS, as it represents 99 % of the induced lesions (Krieg, 1963; Kovalchuk et al., 2000). EMS is known to alkylate guanine at the O₆ position, producing O₆-ethylguanine, which pairs with thymine. Two rounds of DNA replication subsequently fix the mutation (O₆-ethylguanine - C base pair is replaced by a A-T pair).

The single-nucleotide substitution affected the last nucleotide of intron 5 of the gene At4g17620, at the level of the canonical splice acceptor site AG. This motif is universally

conserved and it is recognized and bound by trans-acting factors involved in the splicing process (Zhang, 1998). Mutations in these positions of intron-exon junctions are known to prevent the interaction of the splicing machinery with the DNA sequence, thus leading to aberrant splicing (Baralle and Baralle, 2005). Indeed, transcript analyses of the affected gene showed that the mature transcript formed in the mutant lacks exon 6, likely as a result of aberrant splicing (Figure 4). Since exon 6 contains a total of 24 nucleotides, the mutation does not affect the reading frame. Instead, a protein lacking 8 residues is likely to be produced in the mutant.

At4g17620 encodes a putative activator of 5'-to-3' exoribonucleases, enzymes involved in RNA metabolism. Even though no functional information is available about this gene in *A. thaliana*, the homolog from the yeast *Saccharomyces cerevisiae* (*ScRai1*), has been studied in some depth. No paralogous genes of At4g17620 were found in *A. thaliana*. Structural and biochemical studies have suggested that *ScRai1p* may have at least two functions inside the nucleus. Firstly, a pyrophosphohydrolase activity towards the 5'-cap of specific RNA substrates removes a pyrophosphate group from the 5'-end of mRNAs (decapping activity), thus enhancing their subsequent degradation by 5'-to-3' exoribonucleases. Secondly, *ScRai1p* activates *ScRat1p*, the nuclear 5'-to-3' exoribonuclease through a physical protein-protein interaction (Xue et al., 2000). Interestingly, the mammalian orthologs of *ScRai1p* and *ScRat1p*, DOM3Z and XRN2, respectively, do not physically interact with one another, and recent data showed that DOM3Z may act in the cytoplasm, where it co-localizes with the decapping enzymes DCP1 and DCP2 (Xiang et al., 2009; Zheng et al., 2011a). Different from the yeast *Rai1*, a biochemical role for DOM3Z has not been described so far.

Multi-alignment of the amino acid sequences of several *Rai1*-related proteins (Figure 5) showed that the similarity between *ScRai1p* and the *Arabidopsis thaliana* *AtRAI1* over their entire length is 52%, whereas the similarity between DOM3Z and *AtRAI1* is 74%. Despite the overall differences in the amino acid sequences between *ScRai1p* and the homologs in other organisms, the acidic residues involved in the pyrophosphohydrolase activity of *ScRai1p* (Figure 5) are highly conserved in all proteins, suggesting that they may all possess the enzymatic activity. Interestingly, the exon missing in the *rail-1* mutant contains the codon for Arg306, the side chain of which interacts with the diphosphate group of GDP, the product of the enzymatic activity. The lack of this residue, as well as the possible structural alterations at the site that may arise from the lack of

residues 304 to 311 of the protein, in *rail-1* are likely to abrogate the enzymatic activity of the protein completely or to a large extent.

Furthermore, the Rail sequences of *A. thaliana* and *A. lyrata* are the longest ones among all homologs, as the first translated codon of the mRNA is localised 510 base pairs (170 amino acids) upstream the translational start of the sequences from all other higher eukaryotes. It is unknown whether this additional domain at the N-terminus modifies the localization or function of the protein.

As previously published, the putative residues involved in the interaction of ScRailp with ScRat1p (residues 162-168 in ScRat1p) are conserved only among fungal proteins and they could not be found in DOM3Z (Xiang et al., 2009). Our alignment shows that, in analogy with other proteins from multicellular eukaryotes, AtRAI1 also lacks the 7 amino acids that correspond to those that mediate this protein-protein interaction in yeast. Even though no motifs similar to the ones required for ScRailp/ScRat1p interaction could be found in the AtRAI1 sequence, we cannot exclude that the enzyme can interact with exoribonucleases or other proteins *via* other undiscovered motifs. The high similarity shared with sequences of multicellular eukaryotes indicates that the protein in *A. thaliana* is likely to have a role more similar to these homologous than to the fungal ones. Although no information is available about the precise function of ScRailp orthologs in multicellular eukaryotes, the finding that DOM3Z does not bind the nuclear 5'-to-3' exoribonuclease XRN2 is indicative of a role different from the one of the homolog in yeast.

5.1.2 Impairment of Fe homeostasis in the *rail-1* mutant

In accordance with the observation that chlorosis could be rescued in *rail-1*, analysis of elemental content by ICP showed that shoot Fe concentrations of the mutant are lower than in the wild type (Figure 7). Furthermore, shoots of Fe-supplemented *rail-1* seedlings were not chlorotic and showed similar levels of Fe as the wild type, suggesting that in the presence of high levels of Fe, *rail-1* is able to maintain all biochemical processes requiring Fe. Indeed, determination of the enzymatic activity of Fe deficiency markers in shoots (catalase and FeSOD) confirmed that the mutant is not able to perform biochemically like wild type. At high levels of Fe supply the enzymatic activities were restored (Figure 9).

Under control and iron-deficiency growth conditions, lower levels of Fe mutant shoots were associated to a tendency to accumulate Fe in roots, when compared to the wild type (Figure 7, 8 and 10). Thus, *rail-1* has an aberrant partitioning of Fe between root and shoot. Interestingly, transcript levels of *IRT1* and *FRO2*, two major components of the root Fe uptake system of *A. thaliana*, were lower in *rail-1* than in the wild type both under routine and Fe-limited conditions (Figure 11). In accordance with these results, under these growth conditions root-surface ferric-chelate reductase activity, which is known to depend on *FRO2*, in the roots of *rail-1* was also lower than in wild type (Figure 12).

One possible hypothesis explaining these observations is a defect in the translocation of Fe through the root towards the xylem or in the subsequent translocation to the shoot the mutant, or in the regulation of this. Since our Perls' staining did not detect accumulation of Fe in the central cylinder or the xylem, the former is more likely than the latter. According to this hypothesis, reduced expression of genes of the Fe uptake machinery may be a result of the plant sensing the accumulation of Fe in the root and shutting down the Fe acquisition in order to avoid further accumulation of the metal in roots.

Alternatively, the *rail-1* mutant phenotype could be explained with a defect in Fe-dependent signalling. *rail-1* seedlings may not be able to sense or communicate information about the Fe status. In this case a signal generated in the shoot and transferred to the root under Fe deficiency would be compromised in *rail-1*. This would result in the premature repression of uptake and translocation of Fe that causes and is maintained under physiological Fe deficiency in the shoot. In this scenario, it would be difficult to explain why also under our routine conditions the mutant shows symptoms related to Fe deficiency. However, the finding that *IRT1* and *FRO2* transcript levels of the wild type at 5 μ M Fe are discretely high suggest that under our routine conditions seedlings may already experience some mild Fe-deficiency.

To explore a putative shoot-to-root signalling problem in the mutant, the accumulation was assessed of some known Fe-responsive miRNAs in both standard and Fe-deficiency conditions (Figure 19). According to our results, the levels of two miRNAs (miR159 and miR172) under routine conditions were higher in wild type than in *rail-1*, whereas they were low for both genotypes under Fe-limited conditions. It is possible that the aberrant expression pattern of these miRNAs in the mutant is rather a symptomatic effect than a causative one, as miRNAs levels in the mutant grown under standard conditions resemble

the ones detected under Fe deficiency. We also cannot rule out that our analysis missed the important targets, and movement of miRNAs was not addressed. To date, the nature of the systemic Fe deficiency signal that appears to move from vegetative leaves to the roots of Fe-deficient plants and governs Fe deficiency responses is unknown.

5.1.3 Impairment of IAA-conjugation in the *rail-1* mutant

Indole-3-acetic acid (IAA) is the main auxin in *A. thaliana*, and it is involved in numerous growth and developmental processes (Dharmasiri and Estelle, 2004). The levels of free IAA, the active form of IAA, are known to be tightly regulated. It has been estimated that only 1% of the total auxin is in the free form (Tam et al., 2000), whereas the remaining auxin is present in the inactive form of conjugates with sugars or amino acids. These conjugates are not active *per se* but can be converted to free IAA.

rail-1 has lower *ILR1* and *ILR3* transcript levels than the wild type (Figure 16). *ILR1* encodes a IAA-conjugate hydrolase with specificity for IAA-Leucine complexes (Bartel and Fink, 1995), whereas *ILR3* encodes a bHLH transcription factor modulating auxin-conjugate responsiveness (Rampey et al., 2006). *rail-1* roots were less sensitive than wild type to IAA-Leu but responded normally to IAA-Ala (Figure 17). This resistance profile is similar to the loss-of-function *ilr1-5* mutant (Bartel and Fink, 1995), suggesting that adequate transcript levels of *ILR1* are required for wild-type levels of responsiveness to IAA-Leu. It is possible that *ilr1-5* and *rail-1* are tolerant to exogenous IAA-Leu because high levels of the inactive conjugate cannot be hydrolyzed to form the active IAA, thus preventing a potentially harmful excess of free IAA.

A role for *ILR3* in the regulation of IAA-conjugation is still unclear. It has been hypothesized that *ILR3* may be involved in the modulation of IAA conjugation *via* regulation of *ILR1* activity, but experimental evidence supporting the model is still lacking (Rampey et al., 2006). Intriguingly, *ILR3* is the only protein that has been implicated in both Fe homeostasis and IAA conjugation, thus providing a possible link between the two pathways. In particular, *ILR3* is supposed to interact with the bHLH transcription factor *PYE* and the putative E3 ligase *BTS*, two proteins involved in the regulation of Fe-responsive genes (paragraph 1.1.4) (Long et al., 2010). Down-regulation of *ILR3* in *rail-1* may explain, at least in part, some defects in the regulation of Fe homeostasis and IAA-conjugation in the mutant.

5.1.4 Curly leaves and low fertility are associated with defects in auxin signalling and conjugation, respectively

Mutants defective in IAA-dependent regulation exhibit broad ranges of phenotypes, including abnormal development of leaf edges and low fertility, two features that are also carried by the *rail-1* mutant. Depending on their apical-basal axis formation, leaves can be clustered into hyponastic (downward curled at the leaf edges) and epinastic (upward curled at the leaf edges) ones. For example, the auxin signalling mutant *arf7* exhibits hyponastic leaves (Harper et al., 2000). A recent study reported that the F-box LCR has an essential role in establishing the curvature of leaves (Song et al., 2012). *LCR* transcript abundance could be correlated with the extent of the curvature in leaves, as the hypomorphic *lcr* mutant has epinastic leaves, whereas overexpression of the gene results in hyponastic leaves. *LCR* transcript levels were reduced in *rail-1* when compared to wild type (Figure 18). This finding is in accordance with previous results showing that even slight decreases of *LCR* transcripts result in leaf epinasty. Indeed, LCR is a master regulator of the auxin response and its overexpression drastically decrease the expression of auxin-responsive genes (Song et al., 2012). The proteins that LCR targets for ubiquitin-dependent degradation are still unknown.

Anther fertility defects related to the one found *rail-1* are also found in mutants defective in IAA homeostasis. For example, *IAMT1*-RNAi lines are dwarf and exhibit low fertility (Qin et al., 2005). *IAMT1* (IAA CARBOXYL METHYLTRANSFERASE) is an enzyme able to regulate free IAA levels by converting it into methyl-IAA ester (MeIAA). Analysis of the reproductive organs in *rail-1* revealed strongly suppressed opening of anthers and subsequent pollen release (Figure 14). To check free IAA distribution in anthers, the auxin responsive promoter *DR5* was used. According to the GUS analysis, under our routine growth condition (22°C), *rail-1* plants showed high GUS stain at the level of anthers, as the wild type (Figure 15). However, inflorescences of plants grown at 29°C, a condition leading to complete sterility of the mutant, did not exhibit any staining, indicating the absence or low levels of free active auxin or of auxin responsiveness of the *DR5* promoter in these organs.

It is already known that low levels of auxin are often associated with low fertility. *yuc1yuc4* and *yuc2yuc6*, two mutants impaired in the biosynthesis of auxin, do not produce pollen. *DR5-GUS* analyses indicate that auxin is absent in flowers of those

mutants (Cheng et al., 2006). *yuc1yuc4* and *yuc2yuc6* could not be rescued by exogenous application of IAA. Likewise, male sterility of *rai1-1* could not be rescued by treatment with the phytohormone. This implies that auxin is not the (only) cause of the male sterility in *rai1-1* or that the compound was not able to reach adequate concentrations in the cells in which its activity is required. The low levels of *DR5*-driven GUS activity found in *rai1-1* anthers may be a consequence of the finding that the mutant has low *ILRI* levels in the tissues and likely reduced ability to release free IAA from Leu-conjugates. However, analysis of *ILRI* transcript levels specifically in anthers of *rai1-1* is still lacking.

On the basis of our data, it is still unclear why male sterility of *rai1-1* is more severe at high temperature. However, it is worth noting that many mutants defective in components of the main decapping machinery in yeast and *A. thaliana* have a more severe phenotype at high temperatures. Yeast *dcp1* and *dcp2* mutants arrest growth at 36°C (Beelman et al., 1996). and loss-of-function alleles of *VARICOSA (VCS)*, which encodes a WD-domain containing protein interacting with *AtDCP2*, have reduced size and leaves carrying a unique thick vein only at 29°C (Goeres et al., 2007). All these data suggest that formation of the decapping machinery and/or the pyro phosphohydrolase activity of the enzymes may be sensitive to high temperature.

5.1.5 RAI1 is likely to impact the ethylene response, a pathway known to regulate transcripts of genes involved in Fe homeostasis

Like proposed recently for the human homolog DOM3Z, *AtRAI1* co-localizes with DCP2 in the cytosol (Figure 20), where critical steps of mRNA metabolism occur. For example, cytosolic mRNAs bound to ribosomes undergo repeated rounds of translation before they are degraded. The 5'-to-3' degradation pathway requires the binding of repressors of translation initiation (Dhh1/Rck in yeast) at the 5'-end of the target mRNAs. These proteins represent a docking site for enzymes which remove the cap (DCP1 and DCP2), leaving a 5' monophosphate which is the substrate of 5'-to-3' exoribonucleases (Balagopal and Parker, 2009). In yeast, the 5'-to-3' exonucleolytic digestion in the cytoplasm is carried out by Xrn1, a member of the 5PX family and paralog to the nuclear Rat1 (Zuo and Deutscher, 2001). Interestingly, *ScRat1p* is known to interact with

ScRai1p, but the respective homologs in *Homo sapiens* (XRN2 and DOM3Z) do not interact (Xiang et al., 2009).

The *A. thaliana* genome encodes three homologs of ScRat1 and ScXrn1: the nuclear *AtXRN2* and *AtXRN3*, and the cytosolic *AtXRN4*. XRN2 and XRN3 have overlapping functions, as both of them are endogenous RNA silencing suppressors (Gy et al., 2007). XRN2 is also required for primary cleavage of the pre-ribosomal RNA (Zakrzewska-Placzec et al., 2010). The role of XRNs in the process leading to the formation of miRNAs has been studied in-depth. XRN2 and XRN3 degrade excised miRNA loops, a by-product of the processing of pre-miRNAs carried out by DICER LIKE1 (DCL1) in the nucleus. As expected, mutations in *XRN2* and *XRN3* do not affect mature miRNA levels (Gy et al., 2007). Likewise, mutations in *XRN4* does not directly influence the formation of miRNAs, but the protein degrades the 3' fragments of the mRNAs targeted by miRNAs (Souret et al., 2004). Interestingly, in contrast to yeast ScXrn1, *AtXRN4* is not a general mRNA decay enzyme, but degrades only specific transcripts (Rymarquis et al., 2011). This is consistent with the finding that the predominant mRNA decay pathway in Arabidopsis operates *via* the exosome, a process involving 3'-to-5' exoribonucleases (paragraph 1.2.3) (Chekanova et al., 2007).

In addition to the above-mentioned functions, XRN4 is also an integral component of the ethylene response pathway, as it indirectly suppress the transcription of *EBF1/2*, two genes encoding F-box proteins involved in the degradation of EIN3 (Olmedo et al., 2006; Potuschak et al., 2006). Intriguingly, this pathway is required for correct stabilisation of FIT1, the transcription factor regulating Fe uptake response. FIT1 is known to be stabilised by direct interaction with EIN3 (Lingam et al., 2011). As ScRai1p interacts and activates a 5'-to-3' exoribonuclease in yeast, it is tempting to speculate that *AtRAI1* also acts to allow or facilitate the activity of the cytoplasmic XRN4. Consistent with this hypothesis, the *rail-1* mutant shows insensitivity to ethylene, a typical feature of *xrn4/ein5* mutants (Figure 21). However, according to our data, different from *rail-1*, Fe deficiency-driven chlorosis of *ein5-1* was no more severe than in the wild type. No visible difference between *ein5-1* and wild type was detected under all the tested Fe conditions (Figure 22). A scenario that might explain this result is that *AtRAI1* may affect the levels of transcripts influencing Fe homeostasis in an XRN4/ethylene-independent manner. An alternative hypothesis cannot be ruled out, as outlined next. In fact, it was already observed that, in striking disagreement with XRN4 central function in degrading cytosolic

RNAs, all available null and loss-of-function *xrn4* mutants have only subtle phenotypes when grown on medium or soil (Potuschak et al., 2006; Gy et al., 2007; Rymarquis et al., 2011). An explanation for this finding could be that low levels of XRN2 and/or XRN3 are also in the cytosol and in part compensate for the loss of function of XRN4. Indeed, Xrn1 and Rat1 in yeast are functionally interchangeable and low percentage (5-10%) of each enzyme is active in the respective compartment of the paralog (Johnson, 1997; Zuo and Deutscher, 2001). Furthermore, the mammalian XRN2, ortholog to *A. thaliana*'s XRN2 and XRN3, and originally localised to the nucleus, has been recently detected in small quantities also in the cytoplasm, where it degrades accumulated non-targeting siRNAs (Wei et al., 2012). In other publications, the unexpected mild phenotype of *xrn4* was also explained with the existence of another still unknown cytosolic 5'-to-3' exoribonuclease (Goeres et al., 2007). According to this scenario, it could be speculated that in wild type *AtRAI1* is necessary for all pathways requiring on XRN or XRN-related activities in the cytosol. Therefore, the more drastic phenotype in *rail-1* in comparison to *xrn4* mutants may be caused by the suppression of the activities of more or all cytosolic 5'-to-3' exoribonucleases. High levels of EBF1/2 and subsequent degradation of EIN3 would destabilize the FIT1 protein, thus attenuating Fe deficiency responses in the root, a phenomenon that we observed in *rail-1* (Figure 11 and 12).

Furthermore, it is important to note that aberrant ethylene signalling can affect auxin production. Ethylene-mediated activation of auxin biosynthesis was reported (Ruzicka et al., 2007; Swarup et al., 2007). For example, *WEI2/ASA1* and *WEI7/ASB1*, two genes encoding anthranilate synthase subunits that are required for the first step of Trp biosynthesis, are up-regulated in response to ethylene (Stepanova et al., 2005). There is evidence that some *GH3s*, genes encoding enzymes known to catalyse the synthesis of IAA amide conjugates, are up-regulated in response to ethylene exposure (Liu et al., 2005). The supposed involvement of *AtRAI1* in ethylene-dependent responses may indicate that, at least in part, the aberrant expression profile of IAA conjugation-related genes we observe in *rail-1* is a secondary effect of a defect in ethylene signalling.

5.1.6 Rationale for the phenotypes of *rail-1*, *rail-2* and *AtRAII*-RNAi

In addition to data related to the EMS-mutant *rail-1*, this thesis reports the physiological and molecular characterization of a *AtRAII*-RNAi transgenic line and a T-DNA insertional mutant affected in *AtRAII* locus.

Plants carrying a *AtRAII*-RNAi construct, which showed ~70% reduced transcript levels, exhibited a phenotype very similar to *rail-1* when grown in sterile conditions and on soil (reduced size, leaf chlorosis, curly leaves and low fertility) (Figure 23). Unlike *rail-1* and *AtRAII*-RNAi, homozygous seeds from the T-DNA accession (*rail-2*) were not viable (Figure 25). In fact, heterozygous plants carried normal siliques, but the number of produced seeds was *ca.* 1/4 lower than in wild type, indicating lethality in the homozygous status (Figure 25). It is likely that the insertion, localised just after nucleotide 1204 from the translational start at the level of intron 4 of *AtRAII*, disrupts the gene and a truncated non-functional transcript is produced. Differently from *rail-2*, *rail-1* may be a weak allele. This is consistent with the fact that the phenotype of *rail-1* resembles that of the *AtRAII*-RNAi line, where *AtRAII* is not completely silenced. The level of activity of *AtRAII* may be low, but not completely absent, in the EMS mutant and *AtRAII*-RNAi. In the first case, the lack of the exon carrying the codon for Arg306 could lead to a reduction in, but not a complete loss of, the catalytic activity of the enzyme. In the second case, the level of active *AtRAII* protein may be reduced as a result of lowered transcript levels.

Analysis of the phenotypes in *rail-2* indicates that *AtRAII* plays important roles in the development of *A. thaliana* and is essential for the formation of viable seeds. High levels of *DCPI* transcript in dry seeds and a decrease just after germination support that a timely expression of the decapping machinery may be necessary for proper seed development (Xu and Chua, 2009).

5.1.7 Towards a model explaining *AtRAII* function

Here it is shown that *AtRAII*, a putative activator of 5'-to-3' exoribonucleases, plays an important role in *Arabidopsis thaliana* development and, directly or indirectly, affects transcript levels of genes encoding components of auxin, ethylene and Fe homeostasis.

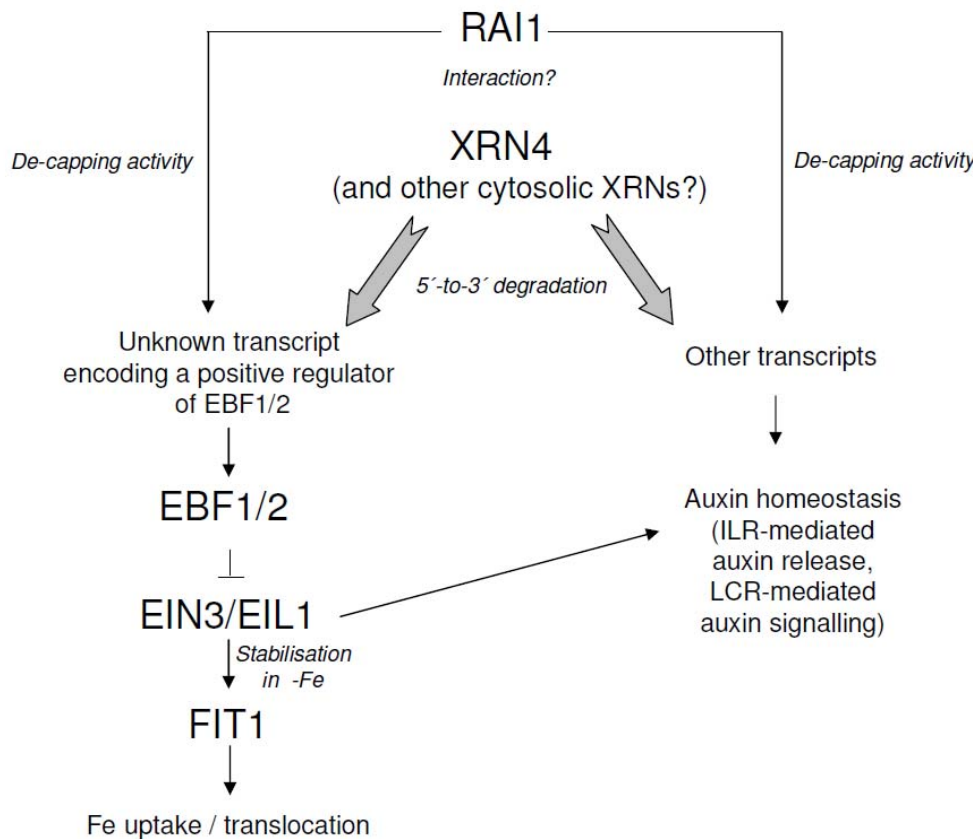


Figure 34. Hypothetical model describing RAI1 role in *Arabidopsis thaliana*.

AtRAI1 stimulates the 5'-to-3' exonucleolytic activity of cytosolic XRNs by decapping their target or, alternatively, but less likely, directly interacting with them. Among the RAI1-decapped transcripts which are degraded by the XRN enzymes are some mRNAs, encoding (still unknown) positive regulators of the F-box proteins EBF1/2. Lowered levels of EBF1/2 stabilize EIN3, a central component of the principal ethylene response pathway. Under Fe-limited conditions, EIN3 stabilizes FIT1, thus promoting the Fe deficiency response in roots and possibly also Fe translocation to the shoot. Correct auxin responses require RAI1- and XRN4-mediated degradation of transcripts. Proper auxin homeostasis can be ethylene response signalling pathway-dependent or - independent.

A model is proposed here in which *AtRAI1* acts in the cytosol at the level of processing bodies by preparing the substrate, i.e. decapped transcripts, for the RNA degradation activity of XRN4 (and likely other hypothetical cytosolic XRNs or other enzymes exhibiting comparable activities). It is still unknown whether *AtRAI1* only decaps transcripts, thus making them prone for XRN4 attack, or also activates the exoribonuclease by direct interaction. Based on considerations of domain conservation

among homologs of *ScRai1p* from different organisms, the latter seems less likely than the former, and the mutation in *rail-1* is likely to affect pyrophosphohydrolase activity.

According to previous work, only a few RNA transcripts are degraded by XRN4 (Rymarquis et al., 2011). Among them there are some transcripts encoding unknown positive regulators of EBF1/2, two F-box proteins that are able to target EIN3 for degradation (Olmedo et al., 2006; Potuschak et al., 2006). XRN4 activity is required to maintain low levels of these F-box proteins, thus controlling EIN3 stability. Strikingly, EIN3 is known to upregulate genes of the transcriptional cascade of the ethylene response and to stabilize FIT1 by physical interaction (Lingam et al., 2011). According to the model proposed here, *AtRAI1* is required for correct regulation of Fe uptake involving ethylene signalling including XRN4 and EIN3. Impairment of *AtRAI1* function leads to an impaired ethylene signalling, decreased FIT1 protein and, consequently, to a reduction in the Fe deficiency - induced transcriptional activation of Fe acquisition in roots. Indeed, the transcript levels of *IRT1* and *FRO2*, two components in the Fe uptake in roots, are lower in the *rail-1* mutant than in wild type (Figure 11) under both Fe-deficiency and standard growth conditions. This suggests that also under the standard conditions employed here, a basal ethylene-mediated Fe uptake activity is required. No differences in FIT1 transcript levels were observed between *rail-1* and wild type. Therefore, it is possible that FIT1 protein levels are decreased in the mutant. This is in agreement with previous findings indicating that the presence of EIN3 stabilizes the FIT1 protein and does not affect *FIT1* transcript levels.

Auxin production and conjugation is also known to be in part regulated dependent on ethylene (Ruzicka et al., 2007). It is possible that the auxin-conjugation defects in *rail-1* can be explained as secondary effects of an impaired ethylene signalling. However, according to the findings reported in this thesis, the phenotype of *rail-1* is reminiscent of auxin-related mutants, rather than ethylene-related ones. This may suggest that the misregulation of some transcripts implicated in auxin homeostasis in *rail-1* is not due to an impairment of the ethylene pathway.

Impaired auxin conjugation in *rail-1*, irrespective of whether this is a consequence of suppressed ethylene responses or arising independently of this, might explain the male infertility of the *rail-1* mutant. Complete sterility of the mutant was associated with absence of auxin in the anther, the reproductive organ that was found to be defective in

the mutant (Figure 13) It is worth noting that >45% of the transcripts with decreased accumulation in *xrn4* are expressed in stamens (Rymarquis et al., 2011). It is very likely that XRN4 has a major role in regulating transcripts involved in stamen development.

5.1.8 Outlook

This work is based on a mutant impaired in metal homeostasis newly identified in a forward genetic approach. In particular, the *AtRAI1* gene was found to have a critical role in to the maintenance of Fe and hormone homeostasis. Based on the experiments performed in this thesis, most of the phenotypic traits of the *AtRAI1* loss-of-function and null mutants can be explained. However, some questions still remain open. According to the model proposed here, RAI1 stimulates XRN4 activity, but it is unknown whether this occurs *via* a direct interaction between the two proteins. A yeast two-hybrid experiment may help to find potential binding partners of *AtRAI1*. Furthermore, both yeast and mammalian homologs of *AtRAI1* are likely to decap RNA substrates. The ability of *AtRAI1* to decap transcripts can be investigated by biochemical analyses. Assays verifying the ability of an enzyme to bind GDP, a critical step of the pyrophosphohydrolase reaction, have been successfully carried out with *ScRai1p* and they may be used with *AtRAI1*.

The reported experiments could attribute leaf chlorosis of *rail-1* to a physiological Fe deficiency in the shoot of the mutant. Administration of exogenous Fe was able to rescue this phenotype. Other phenotypes were apparently linked to an impairment in auxin homeostasis: epinastic leaves were associated with low expression of *LCR*, a main regulator of IAA signalling and abaxial/adaxial patterning in *A. thaliana* leaves, whereas low fertility could be linked to reduced levels of active auxin (or to a reduced response to active auxin) at the level of the anthers. However, treatments with IAA could not rescue the phenotypes. This may be explained by insufficient uptake of IAA due to the experimental procedure. Alternatively, transcripts unrelated to IAA homeostasis which are regulated by *AtRAI1*, have a role in the proper development of leaves and reproductive organs. A broader analysis of the expression profile employing microarrays could help to identify the transcripts that are misregulated in the mutant. If *AtRAI1* and XRN4 are components of the same pathway, as proposed here, a comparison between these data and the already available microarray data of *xrn4* mutants would reveal that the

same subset of transcripts are misregulated in the two mutants, with less pronounced phenotypes expected in *xrn4*.

In addition, crosses between *rail-1* and available mutants of components of ethylene signalling may provide more information about the exact position of *AtRAI1* in the pathway. Generation of transgenic plants carrying *AtRAI1*-GFP and *pAtRAI1-GUS* fusion constructs may give valuable information about the exact cells and tissues where the protein is localised and the *RAI1* promoter is active.

5.2 CHARACTERIZATION OF *bts2-1*

5.2.1 The predicted BTS2 domain structure is reminiscent of mammalian E3 ligases involved in Fe-dependent regulation

The involvement of E3 ubiquitin ligases in the maintenance of iron homeostasis has recently been reported in studies on mammals (Salahudeen et al., 2009; Vashisht et al., 2009). According to these findings, the E3 ubiquitin ligase FBLX5 (F-box and Leucine-rich Repeat Protein 5) binds the iron sensor IRP2 (Iron Regulatory Protein 2) under exposure to high Fe concentrations and targets it for degradation. IRP2 is known to bind the 28 nucleotide - sequence of the Iron Regulatory Element (IRE) at the 5' UTR of the ferritin transcript (paragraph 1.1.4) and represses its translation (Samaniego et al., 1994). FBLX5 consists of two functional domains: the N-terminal domain contains one hemerythrin motif responsible for sensing the cellular Fe status, and the C-terminal domain is necessary to bind a protein complex that in turn interacts with the E2 ubiquitin enzyme (for details about the ubiquitin-mediated protein degradation refer to paragraph 1.1.5). According to studies on sipunculid worms, the center binding two Fe atoms can also bind O₂ *via* a reaction leading to the oxidation of the di-ferrous centre and generation of a hydroperoxide (OOH⁻) complex (Holmes et al., 1991).

In this study, the function of BTS2, a putative E3 ubiquitin ligase in *A. thaliana* that possesses two hemerythrin motifs in its N-terminal domain, was investigated (Figure 26). BTS2 shares similarity at the level of the amino acid sequence to the E3 ubiquitin ligase

BTS, a protein that has a putative role in the regulation of Fe-deficiency responsive genes (Long et al., 2010). BTS3, another unknown protein of the BTS family, is more similar to BTS2 than BTS and also contains two predicted hemerythrin motifs. In contrast, BTS is predicted to contain three hemerythrin motifs. As in FBLX5, each motif exhibits four histidines and two acidic residues that can putatively coordinate two Fe^{2+} atoms. The C-terminal domain is conserved in the three Arabidopsis members of the BTS family and it comprises a series of zinc finger domains. These cysteine and histidine-containing structures may bind Zn atoms and serve as a docking site for E2 ubiquitin ligases (Freemont, 2000). For example, the C3HC4 domain of Sina (Seven in absentia), a protein required for specification of cell fate in *Drosophila melanogaster*'s eye, directly interacts with the E2 ubiquitin-conjugating enzyme (UbcD1) (Carthew and Rubin, 1990). Different from the BTS proteins, FBLX5 contains an F-box, a domain responsible to bind other components of the E3 multi-subunit complex. These, in turn, bind the E2 ubiquitin ligase. Despite some differences, the fact that both BTS2 and FBLX5 possess domains able to bind Fe (hemerythrins) and domains that may directly/indirectly interact with E2 ubiquitin ligases suggest a role also for BTS2 in coupling the cellular Fe status with the degradation of specific proteins.

5.2.2 BTS2 modulates Fe deficiency responses

According to the data presented here, *BTS2* transcript levels are up-regulated approximately 2.0-fold under Fe deficiency and also slightly increased under toxic Zn concentrations (Figure 27b). The greater response to Fe deficiency in comparison to the stressful Zn treatment might indicate that *BTS2* transcript levels are directly responsive to the physiological Fe-deficient status, a condition that is mostly driven by minimal levels of Fe in the growth medium and, to some extent, by oversupply of Zn (Arrivault et al., 2006). Growth of seedlings at several concentrations of Zn and Fe is necessary to draw a final conclusion on this issue. Interestingly, the data presented here on *BTS2* expression are similar to a previously reported analysis of *BTS* expression in roots, suggesting that both *BTS* and *BTS2* play a role in Fe response (Long et al., 2010). In addition, the results show that *BTS2* is predominantly expressed in seedlings and siliques, indicating a tissue- and developmental stage-specific regulation of this gene (Figure 27a).

In this study, no difference could be detected between wild-type and *bts2-1* seedlings grown on standard medium (5 μM Fe, 1 μM Zn) (Figure 29a) or on soil (data not shown). By contrast, a previous study reported that a complete loss-of-function allele for *BTS* is lethal at the embryonic stage under standard growth conditions (McElver, 2001). Even though it is still unclear whether the members of the *BTS* family have similar or redundant roles, it cannot be excluded that *BTS3* may partly take over the function of the lacking protein in the *bts2-1* mutant, thus preventing a more severe phenotype. It is worth noting that *BTS2* and *BTS3* genes are localised in two segmentally duplicated regions of chromosome 1, indicating paralogy between these genes (The genome Arabidopsis initiative, 2000).

The knockdown *BTS2*-RNAi line as well as the T-DNA mutant *bts2-1* were more Zn-tolerant than the wild type (Figure 29 and Figure 33). According to the hypothesis proposed here, the observed phenotypic differences between wild type and mutants are governed by an excess Zn-driven Fe deficient status, a phenomenon that has been described in previous publications (Shanmugam et al., 2012; Sinclair and Kraemer, 2012). However, it cannot be ruled out that a direct connection between *BTS2* function and cellular Zn status exists. The question remains why no differences between *bts2-1* and wild type could be observed on Fe-depleted medium. This might be due to difficulties in the detection of subtle differences in chlorophyll content at such low chlorophyll concentrations, as measured in this case.

Under Zn oversupply, Fe concentrations in roots of *bts2-1* were lower than in wild-type roots (Figure 31d). This could either be a consequence of lowered Zn toxicity in *bts2-1* (Arrivault et al., 2006) or a sign of reduced root Fe (and Zn) uptake rates, possibly via IRT1. Alternatively, it is possible that in the presence of excess Zn^{2+} , *BTS2* binds Zn^{2+} accidentally instead of its natural binding partner Fe^{2+} , and acts to repress root-to-shoot Fe translocation. According to this hypothesis, the biological function of *BTS2* is expected to be the control of shoot Fe accumulation. Under Fe-sufficient conditions, one would then expect enhanced Fe accumulation in shoots of *bts2-1*. At toxic levels of Fe in the medium, which are difficult to achieve experimentally, however, it is expected that *bts2-1* shows an enhanced Fe sensitivity.

It is tempting to speculate that when the cellular Fe concentration is low, *BTS2* is transcriptionally up-regulated (Figure 27), and the encoded protein may positively regulate Fe uptake. As *BTS2* is an E3 ubiquitin ligase, it is likely to target one or more

repressors of the Fe deficiency response for degradation. It is suggested that in the *bts2-1* mutant, Fe uptake is compromised, resulting in lower concentrations of this metal in roots. It is worth noting that under excess Zn conditions, Zn homeostasis also seems to be affected in the mutant, as shoot Zn content is considerably lower than in the wild type without a notable accumulation of Zn in roots (Figure 31b). Low levels of Zn concentration in the shoot were confirmed by the detection of low transcript levels of genes responsive to excess Zn (Figure 32) and may explain the tolerant phenotype observed in the *bts2-1* seedlings.

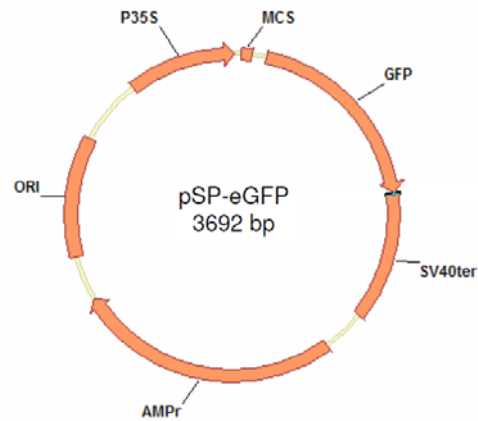
5.2.3 Outlook

The data presented here suggest a role of *BTS2* in modulating Fe and Zn homeostasis in *Arabidopsis thaliana*. The identification of interaction partners, e.g. by yeast-two hybrid analysis, is one of the most important remaining questions. This could indicate whether *BTS2* and *BTS* have common interacting proteins, such as *ILR3* or *bHLH115*.

Furthermore, *BTS* and *BTS2* share common features, such as a 2.0-fold higher expression under Fe deficiency. This raises the question whether the two proteins may have some overlapping function or act with the same molecular mechanism under different conditions and/or in different tissues. However, the lack of information related to transcript and elemental profile in *bts-1* precludes a satisfactory comparison between these mutants. Crosses between *bts2* and *bts-1* (and possibly a loss-of-function allele for *BTS3*) may partly answer this question. In addition, analysis of *IRT1* and *FRO2* transcript levels and ferric chelate reductase activity under several growth conditions in roots may provide some information concerning the aberrant accumulation of Fe in the roots of *bts2-1*. Generation of translational fusions of a *BTS2* cDNA fused to GFP would be a powerful tool to investigate *BTS2* localization at the cellular level and address its regulation.

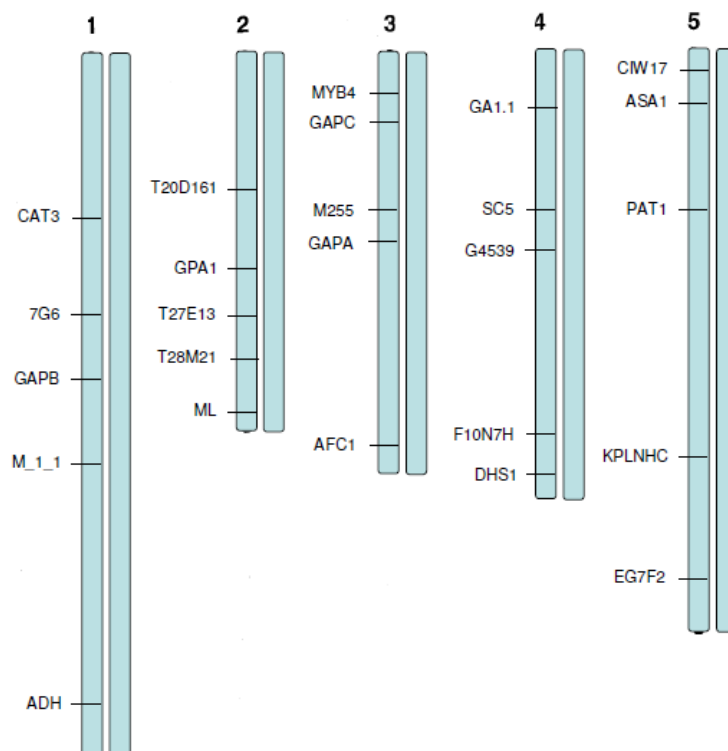
6. SUPPLEMENTAL DATA

6.1 SUPPLEMENTAL FIGURES



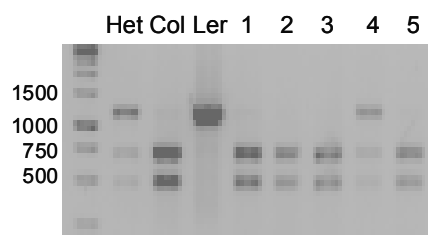
Supplemental Figure 1. Schematic representation of the pSP-eGFP vector.

ORI, origin; P35S, Promoter 35S; MCS, Multi Cloning Site; ter, terminator; AMP, Ampicillin.



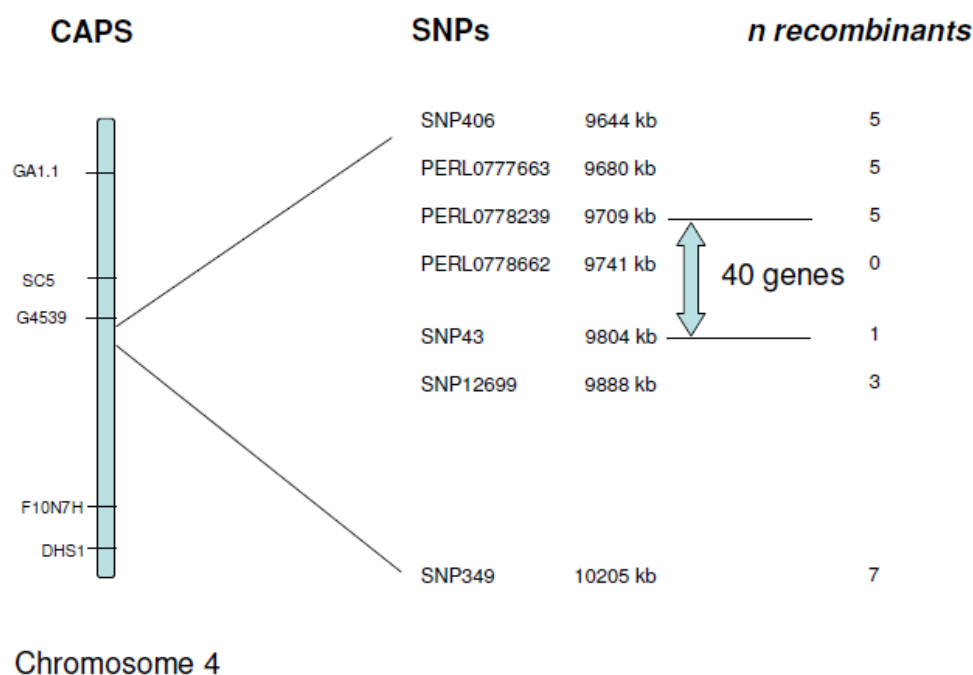
Supplemental Figure 2. CAPS markers used for mapping.

Shown is the chromosomal localization of all CAPS markers used for mapping the mutation in DK9. The chromosomes are depicted by vertical bars.



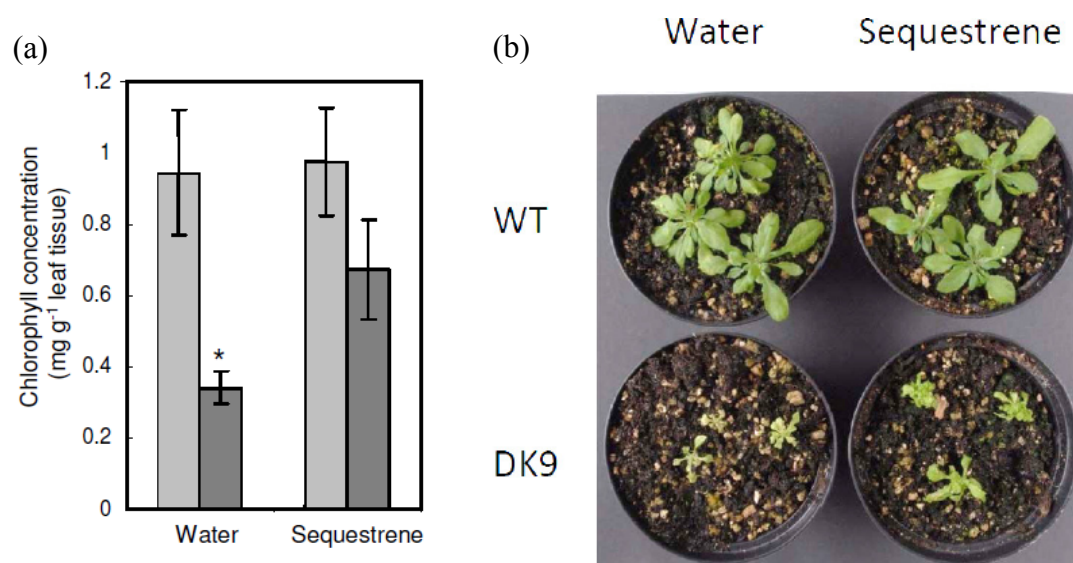
Supplemental Figure 3. Example of CAPS analysis.

Analysis of the restriction pattern of the CAPS marker GA1.1. DNA extracted from 10-d-old F2 seedlings was amplified with the primers corresponding to GA1.1 (Supplemental Table 5). A volume of 8 μ l from the total PCR product (50 μ l) was subjected to restriction (see paragraph 3.3.4) (Sambrook et al., 2001), and 10 μ l of the restriction volume was loaded on a 1% (w/v) agarose gel. The run was carried out for 20 min. DNA from homozygous Col (Col), homozygous Ler (Ler) and heterozygous Col/Ler seedlings (Het) were used as controls. The restriction pattern of five F2 seedlings is shown in the gel.



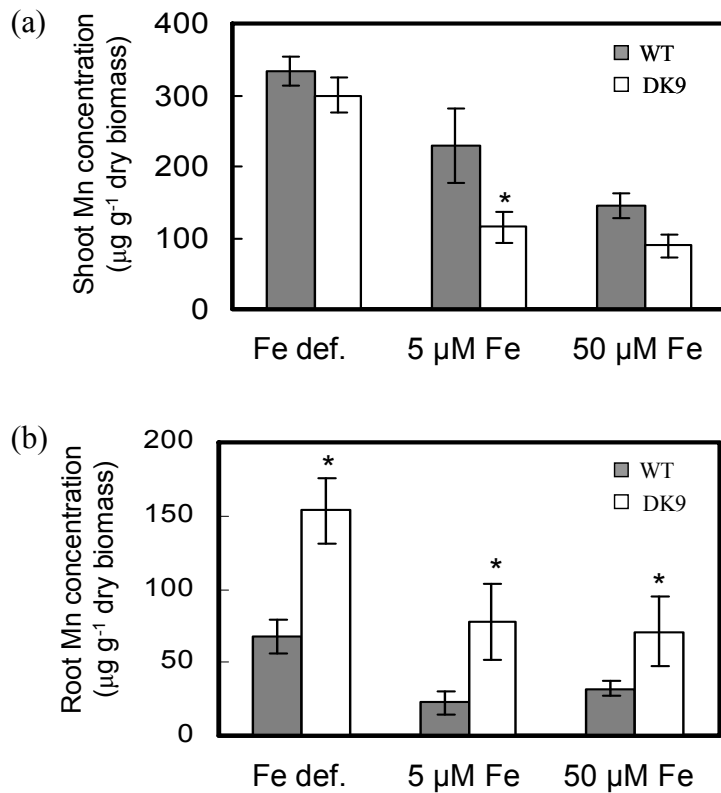
Supplemental Figure 4. Fine mapping of the region with the DK9 mutation.

Shown is the region of chromosome 4 containing the mutation. The chromosome is depicted by the vertical bar on the left, and a closer zoom of the segment carrying the mutation is shown on the right. The names and the physical position of the markers used for mapping the mutation are also indicated. For each SNP, the number of heterozygous recombinants is reported. DNA from a total of 656 chlorotic F2 seedlings was tested CAPS, Cleavage Amplification Polymorphism Sequence; SNPs, Single Nucleotide Polymorphisms.



Supplemental Figure 5. Phenotypic complementation of *rail-1* by FeEDDHA supplementation.

WT and homozygous *rail-1* mutant seedlings were grown on control Hoagland medium (5 μ M FeHBED) for 14 days before transfer onto soil. Plants were grown on soil for another 14 days and watered with sequestrene or tap water every three days before photographs were taken and leaves were harvested. (a) Chlorophyll concentrations in leaves of WT and *rail-1*. Data were analysed by two-way-ANOVA ($P < 0.05$ for interaction between treatment and genotype). Asterisks indicate significant differences between mutant and WT seedlings ($P < 0.05$, Student's *T*-test, Bonferroni corrections). Bars represent means \pm SD of 8 replicate plants per genotype. (b) Photographs showing WT and *rail-1* plants cultivated under the tested Fe conditions.



Supplemental Figure 6. Mn accumulation in *rail-1* and wild type seedlings grown under different Fe conditions.

Shown are Mn concentrations detected in (a) shoots and (b) roots of WT and *rail-1* seedlings grown on vertical plates containing Hoagland medium (5 μM FeHBED), Fe deficiency and Fe excess conditions for 14 days. Roots and shoots were harvested separately, and Mn concentrations were quantified by ICP-AES. Bars represent arithmetic means \pm SD of $n = 4$ replicate plates, for each of which material was pooled from 12 seedlings per genotype for analysis. An asterisk above a bar indicates that the corresponding value for *rail-1* is significantly different ($P < 0.05$) from the value determined for the WT for the respective organ according to a Student's *t*-test with no corrections.

- (a) W-X12-D-X2-H-K-X-L-F/V-<variable>-L-X6-H-F-X2-E-X2-L-M-<variable>-H/K
-X2-H-F-I/L/V-<variable>-W/L/V-X-H-I-X3-D-X2-Y-X3-L/V
- (b) C-X2-C-X(9-39)-C-X(1-3)-H-X(2-3)-C-X2-C-X(4-48)-C-X2-C
- (c) C-X-H-Y-X9-C2-X5-C-X2-C-H-X5-H-X11-C-X2-C-X9-C-X2-C

Supplemental Figure 7. Domains found in the putative E3 ubiquitin ligase BTS2

Consensus pattern of the (a) hemerythrin (b) zinc finger CHY-type and (c) zinc finger C3HC4-type domains. X is any amino acid. A number after X denotes the number of residues.

6.2 SUPPLEMENTAL TABLES

Supplemental Table 1. Treatments carried out to correct the *rail-1* mutant phenotype on soil

rail-1 and control plants were watered and sprayed every two days with FeEDDHA or hormones until siliques opened. Hormones were sprayed on plants every two days until siliques opened. Inflorescences were covered with a film of the applied solution. IAA, NAA and ACC were dissolved in ultrapure H₂O and 0.025% (v/v) Triton X-100, whereas 2,4-D was dissolved in 99% (v/v) ethanol.

Compound	Concentration	Administration
Sequestrene	0.5 mM	Watering solution and spray
IAA	1 mM	Spray
2,4-D	1 mM	Spray
NAA	50 μM	spray
ACC	1 mM	spray

Supplemental Table 2. Oligonucleotides used in PCR experiments.

Name	Primer Sequence (5'-3' direction)	Description
LBb	GCGTGGACCGCTTGCTGCAACT	Genomic characterisation T-DNA lines
LBa	TGGTTCACGTAGTGGGCCATCG	
RBb	ATTTATGGAACGTCAGTGGAGC	
RBa	CTGAGTGGCTCCTTCAACG	
FWg	ATGGATTCACCGCCGAAG	Genomic characterisation <i>rail-2</i>
REVg	ACTGCCAAGAAGGTCACCAA	
FWseq	TGAAGAGATTGGAGCGGATT	Sequencing of the region around substitution (<i>rail-1</i>)
REVseq	TAAGTCACTCTGCGGCCTTT	
FWtra	ATGGATTCACCGCCGAAG	Transcript characterisation <i>RAII</i> -RNAi
REVtra	ACTGCCAAGAAGGTCACCAA	
F	GAGCCTTCACCGAGAATTT	Genomic characterisation <i>bts2-1</i>
R	TGGTGTGTAGGAGGCACAA	
a1	TATTGCGTCGACTTCCTCCT	Transcript characterisation <i>bts2-1</i> , <i>BTS2</i> -RNAi
a2	GCAAAAGGTTTGTGGGAAA	
b1	GGTTTCGCTTCGGTTATTCA	
b2	TCATCAGCAGCTCCTTCAAA	
c1	TCGAGGAGGAAACAGAGGAA	
c2	TGGTGTGTAGGAGGCACAA	
At4g17620_p SPeGFP_fw	CGCTAGGTACCATGGATTCACCGCCGAA G	Cloning of <i>RAII</i> cDNA in pSP-eGFP
At4g17620_p SPeGFP_rev	GGGAACTGCAGTCCCTGAGGTGGTGGTGG TG	

Supplemental Table 3. Oligonucleotides used to determine mature miRNAs levels *via* real-time RT-PCR.

Name	Sequence (5' to 3' direction)	Description
miR159-RT	GTCGTATCCAGTGCAGGGTCCGAGGTGTTTCGCACTGG ATACGACTAGAGC	cDNA synthesis
miR169-RT	GTCGTATCCAGTGCAGGGTCCGAGGTATTCGCACTGG ATACGACCCGGCA	
miR172-RT	GTCGTATCCAGTGCAGGGTCCGAGGTATTCGCACTGG ATACGACCTGCAG	
miR173-RT	GTCGTATCCAGTGCAGGGTCCGAGGTATTCGCACTGG ATACGACGTGATT	
miR394-RT	GTCGTATCCAGTGCAGGGTCCGAGGTATTCGCACTGG ATACGACGGAGGT	
<i>TUB3</i> -RT	GTGCAGGGTCCGAGGTCCTCAGACAGCAAGTCACAC	
Universal reverse primer	GTGCAGGGTCCGAGGT	Determination of miRNA levels by real-time RT-PCR
miR159 forward	CGGCGGTTTGGATTGAAGGGA	
miR169 forward	CGGCGCAGCCAAGGATGATG	
miR172 forward	CGGCGAGAATCTTGATGATG	
miR173 forward	CGGCGTTCGCTTGCAGAGAGA	
miR394 forward	CGGCGTTGGCATTCTGTCC	
<i>TUB3</i> forward	TACCCCAGCTTTGGTGATTG	

Supplemental Table 4. Oligonucleotides used for quantitative real-time RT-PCR.

Name	Primer Sequence (5'-3' direction)	Description
<i>EF1a</i> forward	TGAGCACGCTCTTCTTGCTTTCA	Constitutively expressed genes used for normalisation of target gene expression
<i>EF1a</i> reverse	GGTGGTGGCATCCATCTTGTTACA	
<i>HEL</i> forward	CCATTCTACTTTTTGGCGGCT	
<i>HEL</i> reverse	TCAATGGTAACTGATCCACTCTGATG	
<i>UBQ10</i> forward	GGCCTTGATAATCCCTGATGAATAAG	
<i>UBQ10</i> reverse	AAAGAGATAACAGGAACGGAAACATAGT	
<i>FER1</i> forward	GGCTACGGTGGACACAAACAA	Genes with role in Fe homeostasis
<i>FER1</i> forward	TTCACCTCTTCGAAAGGCTGG	
<i>FRO2</i> forward	ATTTACCCGATCGACCACAACA	
<i>FRO2</i> reverse	TGCTCACGGAGATGACCAAGA	
<i>FRO3</i> forward	TCCTCAATCACTTCCAACCGA	
<i>FRO3</i> reverse	TGCTATTGAATCCAGCCTTGC	
<i>IRT1</i> forward	CCCCGCAAATGATGTTACCTT	
<i>IRT1</i> reverse	GGTATCGCAAGAGCTGTGCAT	
<i>ZIF1</i> forward	AAGTGTGTCTGCCATAACCGG	
<i>ZIF1</i> reverse	TTGGCTCTGATCCACTGCTCT	
<i>IAR3</i> forward	TGTTGGAAGTGGTCATGCTCC	Genes with role in auxin conjugation
<i>IAR3</i> reverse	TCCTGCATAGCAAGTGCATCC	
<i>ILR1</i> forward	GATCGGATCCTGTTCGAAACC	
<i>ILR1</i> reverse	TAACGGAAGTGCCTCCATGTC	
<i>ILR3</i> forward	TCCTCTGCCACTAGCTCGAAA	
<i>ILR3</i> reverse	TGTCATTCAACCTGTCCCGTC	

Supplemental Table 5. CAPS markers used for mapping.

Name	Chr.	Location (AGI)	Primer Forward (5' to 3' direction)	Primer Reverse (5' to 3' direction)	Ampl icon (bp)	Restr. Enz.	Col-0 fragments	Ler fragments
7G6	1	12285372 - 12285812 bp	GTTTTACTTAGTC CAATGGTAG	GGGCTCGTTATGC CGTGAAG	450	<i>AccI</i>	220, 230	450
ADH	1	28975141 - 28976432 bp	AAAAATGGCAAC ACTTTGAC	GCGTGACCATCAAG ACTAAT	1291	<i>XbaI</i>	1291	1097, 194
CAT3	1	7144251 - 7145224 bp	CAGATGCAATGG CATCGTGGAG	CGGTGGTGCTCCAG TCTCCAAC	973	<i>HincII</i>	973	790, 183
GAPB	1	16127765 - 16129246 bp	TCTGATCAGTTGC AGCTATG	GGCACTATGTTTCAG TGCTG	1481	<i>DdeI</i>	605, 284, 225, 174	350, 284, 255, 225, 174
M_1_1	1	18495618 - 18496158 bp	TCAAAATGTATG GTTTGCCGTCAC	TTTTCATCCGCAAT GCTTCACAGG	540	<i>SexAI</i>	335, 205	540
GPA1	2	11196996 - 11198590 bp	GGGATTTGATGA AGGAGAAC	ATTCCTTGGTCTCC ATCATC	1594	<i>AflIII</i>	705, 680, 209	1385, 209
ML	2	18640043 - 18640843 bp	CGGAAACACGAA GCTGATGAGTTG GG	CGAGAACAAAATG TGTACGGGTGTG	800	<i>SnaBI</i>	400, 400	800
T20D161	2	9949768 - 9951428 bp	CGTATTTGCTGAT TCATGAGC	ATGGTTTACACTTG ACAGAGC	1700	<i>PstI</i>	1400, 300	1700
T27E13	2	12821867 - 12822767 bp	GGAATCATCGCTT GACGACTCC	GGACTTTTCGCCGT GAAGTCG	900	<i>NlaIII</i>	400, 310, 180, 10	710, 180, 10
T28M21	2	16734859 - 16737859 bp	TCGTCCTCGCGTT CCTCTTC	AGTCATCCAAGGCA ACAAAG	3000	<i>DraI</i>	2500, 500	3000
AFC1	3	19864096 - 19865496 bp	AGCTTTATCACGA TACACACTGC	GGAACCTCAAGTC TAAACAG	1400	<i>PvuII</i>	800, 600	1400
GapA	3	9795219 - 9795372 bp	TGTGCTCAACCAA ACTTAGCC	CACCGTGATCTAAG GAGAGCAAG	698	<i>DdeI</i>	420,178,1 00	240,180,1 78,100
GapC	3	1081292 - 1082735 bp	ACGGAAAGACAT TCCAGTC	CTGTTATCGTTAGG ATTCGG	1443	<i>EcoRV</i>	730, 713	713, 390, 340
M255	3	8335084 - 8336084 bp	AAGGGAAGTGGA TTGGCTCCATGGC	GTGTTTAGTAATGA ATAATCATCAATC	1000	<i>ScrFI</i>	500, 500	1000
MYB4	3	46335 - 47735 bp	CCAAATGACAAC GACGTTATC	GCCGGTTGAAGA AAGGGCC	1400	<i>HaeIII</i>	1000, 400	1200, 200
DHS1	4	18537948 - 18539613 bp	AGAGAGAATGAG AAATGGAGG	CAAGTGACCTGAAG AGTATCG	1668	<i>BsaAI</i>	1188, 480	1668
F10N7H	4	15498955 - 15500152 bp	CCTGCCCAATATG CCAAAGC	GTGTATACATGCGT GTCAGC	1200	<i>HaeII</i>	1000, 200	1200
G4539	4	9631247 - 9631811 bp	GGACGTAGAATC TGAGAGCTC	GGTCATCCGTTCCC AGGTAAAG	600	<i>HindIII</i>	600	480, 120
GA1.1	4	1242594 - 1243791 bp	CCGGAGAATCGT ACGGTAC	AAGCTTCGAACTCA AGGTTC	1234	<i>BsaBI</i>	707, 527	1196, 38
SC5	4	9165026 - 9165690 bp	CACAAGCTATAC GATGCTCACC	TCGACGACTCTCAA GAACCC	550	<i>AccI</i>	550	300, 250
ASA1	5	1720605 - 1722305 bp	CCTCTAGCCTGAA TAACAGAAC	CTTACTCTGTCTT GCTTAC	1700	<i>BclI</i>	1042, 686	686, 553, 489
CIW17	5	1437930 - 1439963 bp	GATTTCCCAGAC GATTT	AGTTTATTGTGTC GGTTTT	2033	<i>AccI</i>	2033	1228, 805
EG7F2	5	24626811 - 24628211 bp	GCATAGAATTTG ACGATAACGAGC	GATCTGTGATAGGAC TACGAGAC	1200	<i>XbaI</i>	1200	700, 500
KLPNHC	5	17614421 - 17615331 bp	CGTTGCTCGTGGG TTTTGTAA	CTTGATAAGTTCT TGCTGTGA	910	<i>EcoRI</i>	910	655, 255
PAT1.1	5	5956164 - 5958064 bp	GTATGAGAACAT AGTAACCCCATG	GTCGACGTGGTGCG GTGGGTTG	1900	<i>DdeI</i>	1000, 600, 300	1000, 900

Supplemental Table 6. Distances between the DK9 mutation and the closest CAPS markers

Name	Position in Chr. 4	% heterozygous recombinants	Distance (cM)
FCA3b	8665865 - 8666762 bp	9	4.5
SC5	9165026 - 9165690 bp	6.9	3.45
G4539	9631247 - 9631811 bp	1.1	0.55

Supplemental Table 7. SNP markers used for mapping.

Name	Position in Chr. 4 (bp)	Primer forward (5' to 3' direction)	Primer reverse (5' to 3' direction)
sgcsnp406	9644726	ATGCAAATGGGCTACATTCC	GTTGTTTTGGAACGGTTTG
PERL0777663	9680418	TGGGGTTAGCTTIGTTGGTT	AACAGCAAAAAGATATTAGCAAGG
PERL0778239	9709410	GAAACATCCATTGATCCCTGT	TTCTGCTGCCAAGTTTTGTA
PERL0778662	9741507	AACAAAAGTTGAACCGTCAGG	TCAAGATTCTCGCTCGCTTA
sgcsnp43	9804448	TCTCTCAAAAAGATCAAACACATACA	TCGACAAAGTAAGCCATAAAGAA
sgcsnp12699	9888876	TCCCCAAATTCTTGACCAAA	TGGATAGCTTATACGTCGATCTTG
sgcsnp349	10205248	TCCATTTGCCTTCTCTTACG	AACCTGCTTGCAGAAAAACA

6.3 LIST OF ABBREVIATIONS

Abbreviation	Full name
2,4-D	2,4-dichlorophenoxyacetic acid
ACC	1-aminocyclopropane-1-carboxylic acid
ARE	AU-rich element
bp	base pairs
CaMV	cauliflower mosaic virus
CAPS	Cleaved Amplified Polymorphic Sequences
DNA	deoxyribonucleic acid
EDDHA	ethylene-diamine-N,N'-bis(2-hydroxyphenylacetic acid)
EDTA	ethylene-diamine-tetraacetate
electron	e ⁻
EMS	Ethyl methanesulfonate
Ethanol	EtOH
<i>g</i>	standard gravity, 9.80665 m s ⁻²
GFP	Green fluorescent protein
GUS	Glucuronidase
h	hour
HBED	N,N'-bis(2-hydroxybenzyl)-ethylene-diamine-N,N'-diacetic acid
IAA	indolic 3-acetic acid
ICP-AES	inductively-coupled plasma atomic emission spectrometry
kb	kilobases
KO	knockout
LacZ	β-galactosidase
MES	2-(N-morpholino)ethanesulfonic acid
min	minute
miRNA	microRNA
MS	Murashige and Skoog
NAA	1-naphthaleneacetic acid
O/N	overnight (12-16 h)
OD	optical density
PCR	polymerase chain reaction

Supplemental data

Abbreviation	Full name
PEG	polyethylene glycol
Pho	alkaline phosphatase
ppm	parts per million
relA1	relaxedA1
RNA	ribonucleic acid
ROS	reactive oxygen species
rpm	revolutions per minute
RT	room temperature (25 °C)
RTL	relative transcript level
RT-PCR	Reverse Transcription-PCR
s	second
SD	standard deviation
SE	standard error
SNP	Single Nucleotide Polymorphism
supE	ochre suppressor
TAE	Tris-acetate EDTA
T-DNA	transfer DNA
Tris	2-amino-2-hydroxymethyl-propane-1,3-diol
UTR	untranslated region
v/v	volume per volume
w/v	weight per volume
WT	wild-type
X-Gluc	5-Bromo-4-chloro-3-indolyl- β -D-glucuronide

7. LITERATURE

- Aebi H.** (1983). Catalase. In *Methods of enzymatic analysis*. B. HU ed., Weinheim, Germany: Verlage Chemie, 273-286.
- Alexander M.** (1969). Differential staining of aborted and nonaborted pollen. *Stain technology* **44**, 117-122.
- Anderson G. and Vulpe C.** (2009). Mammalian iron transport. *Cell Mol Life Sci* **66**, 3241-3261.
- Anderson P. and Kedersha N.** (2006). RNA granules. *J Cell Biol* **172**, 803-808.
- Arava Y.** (2009). Compaction of polyribosomal mRNA. *RNA Biol* **6**, 399-401.
- Arrivault S., Senger T. and Krämer U.** (2006). The Arabidopsis metal tolerance protein AtMTP3 maintains metal homeostasis by mediating Zn exclusion from the shoot under Fe deficiency and Zn oversupply. *Plant J* **46**, 861-879.
- Azevedo J., Garcia D., Pontier D., Ohnesorge S., Yu A., Garcia S., Braun L., Bergdoll M., Hakimi M. and Lagrange T.** (2010). Argonaute quenching and global changes in Dicer homeostasis caused by a pathogen-encoded GW repeat protein. *Genes & Dev* **24**, 904-915.
- Balagopal V. and Parker R.** (2009). Polysomes, P bodies and stress granules: states and fates of eukaryotic mRNAs. *Curr Opin Cell Biol* **21**, 403-408.
- Baralle D. and Baralle M.** (2005). Splicing in action: assessing disease causing sequence changes. *J Med Genet* **42**, 737-748.
- Bartel, B. and Fink G.** (1995). ILR1, an amidohydrolase that releases active indole-3-acetic acid from conjugates. *Science* **268**, 1745-1748.
- Beard J. and Connor J.** (2003). Iron status and neural functioning. *Annual Review of Nutrition* **23**, 41-58.
- Beauchamp C. and Fridovich I.** (1971). Superoxide dismutase: improved assays and an assay applicable to acrylamide gels. *Anal Biochem* **44**, 276-287.
- Beelman C., Stevens A., Caponigro G., LaGrandeur T., Hatfield L., Fortner D. and Parker R.** (1996). An essential component of the decapping enzyme required for normal rates of mRNA turnover. *Nature* **382**.

- Bertani G.** (1951). Studies on lysogenesis I. The mode of phage liberation by lysogenic *Escherichia coli*. *J Bacteriol* **62**, 293-300.
- Bienfait H.F. and Van Der Mark S.** (1983). Phytoferritin and its role in iron metabolism. In *Metals and Micronutrients: Uptake and Utilization by Plants* D.A.a.W.S.P.e. Robb ed., Academic Press. N.Y. U.S.A., 111-123.
- Bousquet-Antonelli C., Presutti C. and Tollervey D.** (2000). Identification of a regulated pathway for nuclear pre-mRNA turnover. *Cell Research* **102**, 765-775.
- Bradford M.** (1976). A rapid and sensitive method for the quantitation of microgram quantities of protein utilizing the principle of protein-dye binding. *Anal Biochem* **72**, 248-256.
- Brown J., Bharathi A., Ghosh, A., Whalen W., Fitzgerald E. and Dhar R.** (1995). A mutation in the *Schizosaccharomyces pombe* rael1 gene causes defects in poly(A)1 RNA export and in the cytoskeleton. *J Biol Chem* **270**, 7411-7419.
- Byrne M.** (2005). Networks in leaf development. *Curr Opin Plant Biol* **8**, 59-66.
- Cailliatte R., Schikora A., Briat JF., Mari S., Curie C.** (2010). High-affinity manganese uptake by the metal transporter NRAMP1 is essential for Arabidopsis growth in low manganese conditions. *Plant Cell* **22**, 904-917.
- Campbell F.** (2008). *Elements of Metallurgy and Engineering Alloys* (ASM International).
- Campbell M.** (1999). *Biochemistry*. (Harcourt).
- Carthew R. and Rubin G.** (1990). seven in absentia, a gene required for specification of R7 cell fate in the *Drosophila* eye. *Cell* **63**, 561-577.
- Chekanova J., Gregory B., Reverdatto S., Chen H., Kumar R., Hooker T., Yazaki J., Li P., Skiba N. and Peng Q.** (2007). Genome-wide high resolution mapping of exosome substrates reveals hidden features in the Arabidopsis transcriptome. *Cell* **131**, 1340-1353.
- Chen M.** (2005). MicroRNA biogenesis and function in plants. *FEBS Lett.* **579**, 5923-5931.
- Cheng Y., Dai X. and Zhao Y.** (2006). Auxin biosynthesis by the YUCCA flavin monooxygenases controls the formation of floral organs and vascular tissues in Arabidopsis. *Genes & Dev* **20**, 1790-1799.
- Colangelo E.P. and Guerinot M.L.** (2004). The essential basic helix-loop-helix protein FIT1 is required for the iron deficiency response. *Plant Cell* **16**, 3400-3412.

- Connolly E., Fett J. and Guerinot M.L.** (2002). Expression of the IRT1 Metal Transporter Is Controlled by Metals at the Levels of Transcript and Protein Accumulation. *Plant Cell* **14**, 1347-1357.
- Corcoran C., Huang Y. and Sheikh M.** (2004). The p53 paddy wagon: COP1, Pirh2 and MDM2 are found resisting apoptosis and growth arrest. *Cancer Biol Ther* **3**, 721-725.
- Cowling V.** (2009). Regulation of mRNA cap methylation. *Biochem J* **425**, 295-302.
- Demuyneck S., Li K., van der Schors R. and Dhainaut-Courtois N.** (1993). Amino acid sequence of the small cadmium-binding protein (MP II) from *Nereis diversicolor* (annelida, polychaeta). Evidence for a myohemerythrin structure. *Eur J Biochem* **217**, 151-156.
- Dharmasiri N. and Estelle M.** (2004). Auxin signaling and regulated protein degradation. *Trends Plant Sci* **9**, 302-308.
- Durrett T., Gassmann W. and Rogers E.** (2007). The FRD3-mediated efflux of citrate into the root vasculature is necessary for efficient iron translocation. *Plant Physiol* **144**, 197-205.
- Duy D., Wanner G., Meda A., von Wiren N., Soll J. and Philippar K.** (2007). PIC1, an ancient permease in *Arabidopsis* chloroplasts, mediates iron transport. *Plant Cell* **19**, 986-1006.
- Dybczyński R., Polkowska-Motrenko H., Samczyński Z. and Szopa Z.** (1998). Virginia Tobacco Leaves (CTA-VTL-2) – new Polish CRM for inorganic trace analysis including microanalysis. *Fresenius J. Anal. Chem.* **360**, 384-387.
- FAO/WHO.** (2002). Human vitamin and mineral requirements R. FAO/WHO ed. (Bangkok, Thailand).
- Fenton H.** (1894). *J Chem Soc Proc* **10**.
- Fleming A.** (2005). The control of leaf development. *New phytologist* **166**, 9-20.
- Freemont P.** (2000). RING for destruction? *Curr Biol* **10**, 84-87.
- Ghosh, A. and Lima C.** (2010). Enzymology of RNA cap synthesis. *Wiley Interdiscip Rev RNA* **1**, 152-172.
- Goeres D., Van Norman J., Zhang W., Fauver N., Spencer M. and Sieburth E.** (2007). Components of the *Arabidopsis* mRNA Decapping Complex Are Required for Early Seedling Development. *Plant Cell* **19**, 1549-1564.

- Govindjee, Kern J., Messinger J. and Whitmarsh J.** (2010). Photosystem II. eLS. John Wiley & Sons, Ltd: Chichester, 188-197.
- Graham R., Welch R. and Saunders D.** (2007). Nutritious subsistence food systems. *Advances in Agronomy* **92**, 1-74.
- Guerinot M. and Yi Y.** (1994). Iron: Nutritious, noxious, and not readily available. *Plant Physiol* **104**, 815-820.
- Gy I., Gascioli V., Laressergues D., Morel J., Gombert J., Proux F., Proux C., Vaucheret H. and Mallory, A.** (2007). Arabidopsis FIERY1, XRN2, and XRN3 are endogenous RNA silencing suppressors. *Plant Cell* **19**, 3451-3461.
- Harper R., Stowe-Evans E., Luesse D., Muto H., Tatematsu K., Watahiki M., Yamamoto K. and Liscum E.** (2000). The NPH4 locus encodes the auxin response factor ARF7, a conditional regulator of differential growth in aerial Arabidopsis tissue. *Plant Cell* **12**, 757-770.
- Harris D. and Aisen P.** (1989). Physical biochemistry of the transferrins. In *Iron Carriers and Iron Proteins*. T. Loehr, H. Gray and A. Lever eds (Weinheim: VCH Publishers), 239-351.
- Haydon M.J. and Cobbett C.S.** (2007). A novel major facilitator superfamily protein at the tonoplast influences zinc tolerance and accumulation in Arabidopsis. *Plant Physiol* **143**, 1705-1719.
- Haydon M.J., Kawachi M., Wirtz M., Hillmer S., Hell R. and Kraemer U.** (2012). Vacuolar nicotianamine has critical and distinct roles under iron deficiency and for zinc sequestration in Arabidopsis. *Plant Cell* **24**, 724-737.
- Hilson P., Allemeersch J., Altmann T., Aubourg S., Avon A., Beynon J., Bhalerao R., Bitton F., Caboche M., Cannoot B., Chardakov V., Cognet-Holliger C., Colot V., Crowe M., Darimont C., Durinck S., Eickhoff H., Falcon de Longevialle A., Farmer E., Grant M., Kuiper M., Lehrach H., Leon C., levyva A., Lundeberg J., Lurin C., Moreau Y., Nietfeld W., Paz-Ares J., Reymond P., Rouzé P., Sandberg G., Dolores Segura M., Serizet C., Tabrett A., Tacconnat L., Thareau V., Van Hummelen P., Vercruyse S., Vuylsteke M., Weingartner M., Weisbeek P., Wirta V., Wittinik F., Zabeau M. and Small I.** (2004). Versatile gene-specific sequence tags for Arabidopsis functional genomics: transcript profiling and reverse genetics applications. *Genome Research* **14**, 2176-2189.

- Hoagland D.** (1948). Lectures on the inorganic nutrition of plants. (MA, USA: Chronica Botanica Company).
- Holmes M., Le Trong I., Turley S., Sieker L. and Stenkamp R.** (1991). Structures of deoxy and oxy hemerythrin at 2.0 Å resolution. *J Mol Biol* **218**, 583-593.
- Hu Y., Xie Q. and Chua N.** (2003). The Arabidopsis auxin-inducible gene ARGOS controls lateral organ size. *Plant Cell* **15**, 1951-1961.
- Jander G., Norris S.R., Rounsley S.D., Bush D.F., Levin I.M. and Last R.L.** (2002). Arabidopsis map-based cloning in the post-genome era. *Plant Physiol* **129**, 440-450.
- Johnson D., Dean D., Smith A. and Johnson M.** (2005). Structure, function and formation of biological iron-sulfur clusters. *Ann Rev Biochem* **74**, 247-281.
- Kampfenkel K., Van Montagu M. and Inzé M.** (1995). Effects of Iron Excess on *Nicotiana plumbagnifolia* Plants. *Plant Physiol* **107**, 725-735.
- Kerkeb L., Mukherjee I., Chatterjee I., Lahner B., Salt D. and Connolly E.** (2008). Iron-induced turnover of the Arabidopsis IRON-REGULATED TRANSPORTER1 metal transporter requires lysine residues. *Plant Physiol* **146**, 1964-1973.
- Kim S., Punshon T., Lanzirotti, A., Li L. Alonso J., Ecker J., Kaplan J. and Guerinot M.** (2006). Localization of Iron in Arabidopsis Seed Requires the Vacuolar Membrane Transporter VIT1. *Science* **314**, 1295-1298.
- Kobayashi T., Ogo Y., Itai R., Nakanishi H., Takahashi M., Mori S. and Nishizawa N.** (2007). The rice transcription factor IDEF1 is essential for the early response to iron deficiency, and induces vegetative expression of late embryogenesis abundant genes. *Plant J* **60**, 948-961.
- Kong W. and Yang Z.** (2010). Identification of iron-deficiency responsive microRNA genes and cis-elements in Arabidopsis. *Plant Physiol Biochem* **48**, 153-159.
- Kovalchuk I., Kovalchuk O. and Hohn B.** (2000). Genome-wide variation of the somatic mutation frequency in transgenic plants. *EMBO J* **19**, 4431-4438.
- Krieg D.** (1963). Ethyl methanesulfonate-induced reversion of bacteriophage T4rII mutants. *Genetics* **48**, 561-580.
- Lahner B., Gong J., Mahmoudian M., Smith E. Abid K., Rogers E., Guerinot M., Harper J., Ward J., McIntyre L., Schroeder J. and Salt D.** (2003). Genomic

- scale profiling of nutrient and trace elements in *Arabidopsis thaliana*. *Nat Biotech* **21**, 1215-1221.
- Laity J., Lee B. and Wright P.** (2001). Zinc finger proteins: new insights into structural and functional diversity. *Curr Opin Struct Biol* **11**, 39-46.
- Lanquar V., Lelièvre F., Bolte S., Hamès C. Alcon C., Neumann D., Vansuyt G., Curie C., Schroeder A., Kraemer U., Barbier-Brygoo H. and Thomine S.** (2005). Mobilization of vacuolar iron by *AtNRAMP3* and *AtNRAMP4* is essential for seed germination on low iron. *EMBO J* **24**, 4041-4051.
- Lewin B.** (2004). *Genes VIII*. (Prentice Hall International).
- Lingam S., Mohrbacher J., Brumbarova T., Potuschak T., Fink-Straube C., Blondet E., Genschik P. and Bauer P.** (2011). Interaction between the bHLH transcription factor FIT and ETHYLENE INSENSITIVE3/ETHYLENE INSENSITIVE3-LIKE1 reveals molecular linkage between the regulation of Iron acquisition and ethylene signaling in *Arabidopsis*. *The Plant Cell* **23**, 1815-1829.
- Liu K., Kang B.-C., Jiang H., Moore S., Li H., Watkins C., Setter T. and Jahn M.** (2005). A GH3-like gene, *CcGH3*, isolated from *Capsicum chinense* L fruit is regulated by auxin and ethylene. *Plant Mol Biol* **58**.
- Long T., Tsukagoshi H., Busch W., Lahner B., Salt D. and Benfey P.** (2010). The bHLH transcription factor POPEYE regulates response to iron deficiency in *Arabidopsis* roots. *Plant Cell* **22**, 2219-2236.
- Lorick K., Jensen J., Fang S., Ong A., Hatakeyama S. and Weissman A.** (1999). RING fingers mediate ubiquitin-conjugating enzyme (E2)-dependent ubiquitination. *Proc Natl Acad Sci U S A* **96**, 11364-11369.
- Lykke-Andersen S., Brodersen D. and Jensen T.** (2009). Origins and activities of the eukaryotic exosome. *J Cell Sci* **15**, 1487-1494.
- Marshak S.** (2007). *Essentials of geology*. (W. W. Norton).
- McElver J.** (2001). Insertional mutagenesis of genes required for seed development in *Arabidopsis thaliana*. *Genetics* **159**, 1751-1763.
- McKie A., Marciani P., Rolfs A., Brennan K. and Wehr K.** (2000). A novel duodenal iron-regulated transporter, *IREG1*, implicated in the basolateral transfer of iron to the circulation. *Mol Cell* **5**, 299-309.
- Meier I.** (2012). mRNA export and sumoylation-Lessons from plants. *Biochim Biophys Acta* **1819**, 531-517.

- Millevoi S. and Vagner S.** (2010). Molecular mechanisms of eukaryotic pre-mRNA 3' end processing regulation. *Nucleic Acids Research* **38**, 2757-2759.
- Moon J., Parry G. and Estelle M.** (2004). The ubiquitin-proteasome pathway and plant development. *Plant Cell* **16**, 3181-3195.
- Morrissey J., Baxter I., Lee J., Li L., Lahner B., Grotz N., Kaplan J., DE S. and ML G.** (2009). The ferroportin metal efflux proteins function in iron and cobalt homeostasis in Arabidopsis. *The Plant Cell* **21**, 3326-3338.
- Mukherjee I., Campbell N. Ash J. and Connolly E.** (2006). Expression profiling of the Arabidopsis ferric chelate reductase (FRO) gene family reveals differential regulation by iron and copper. *Planta* **223**, 1178-1190.
- Murashige T. and Skoog F.** (1962). A revised medium for rapid growth and bio assays with tobacco tissue cultures. *Physiologia Plantarum* **15**, 473-497.
- Neugebauer K.** (2002). On the importance of being co-transcriptional. *J Cell Science* **15**, 3865-3871.
- Newman T., Ohme-Takagi M., Taylor C. and Green P.** (1993). DST sequences, highly conserved among plant SAUR genes, target reporter transcripts for rapid decay in tobacco. *Plant Cell*. *Plant Cell* **5**, 701-714.
- Nozoye T., Nagasaka S., Kobayashi T., Takahashi M., Sato Y., Sato N., Uozumi H., Nakanishi H. and Nishizawa N.** (2011). Phytosiderophore efflux transporters are crucial for iron acquisition in graminaceous plants. *J Biol Chem* **286**, 5446-5454.
- Ogo Y., Itai R., Nakanishi H., Inoue H., Kobayashi T., Suzuki M., Takahashi M., Mori S. and Nishizawa N.** (2006). Isolation and characterization of IRO2, a novel iron regulated bHLH transcription factor in graminaceous plants. *Journal of Experimental Botany* **57**, 2867-2878.
- Okada M. and Ye K.** (2009). Nuclear phosphoinositide signaling regulates messenger RNA export. *RNA Biol* **6**, 12-16.
- Palatnik J., Wollmann H., Schommer C., Schwab R., Boisbouvier J., Rodriguez R., Warthmann N. Allen E., Dezulian T., Huson D., Carrington J. and Weigel D.** (2007). Sequence and expression differences underlie functional specialization of arabidopsis microRNAs miR159 and miR319. *Dev Cell* **13**, 115-125.
- Pant B., Buhtz A., Kehr J. and Scheible W.-R.** (2008). MicroRNA399 is a long-distance signal for the regulation of plant phosphate homeostasis. *Plant J* **53**, 731-738.

- Perez-Quintero A., Neme R., Zapata A. and Lopez C.** (2010). Plant microRNAs and their role in defense against viruses: a bioinformatics approach. *BMC Plant Biol* **10**, 138.
- Petit J., Briat J. and Lobréaux S.** (2001). Structure and differential expression of the four members of the *Arabidopsis thaliana* ferritin gene family. *Biochem J* **359**, 575-582.
- Pollmann S., Neu D., Lehmann T., Berkowitz O., Schaefer T. and Weiler E.** (2006). Subcellular localisation and tissue specific expression of amidase 1 from *Arabidopsis thaliana*. *Planta* **224**, 1241-1253.
- Porra R., Thompson W. and Kriedemann P.** (1989). Determination of accurate extinction coefficients and simultaneous equations for assaying chlorophylls a and b extracted with four different solvents: verification of the concentration of chlorophyll standards by atomic absorption spectroscopy. *Biochim. Biophys. Acta.* **975**, 384-394.
- Potuschak T., Vansiri A., Binder B., Lechner E., Vierstra R. and Genschik P.** (2006). The exoribonuclease XRN4 is a component of the ethylene response pathway in *Arabidopsis*. *Plant Cell* **18**, 3047-3057.
- Pugh D., Faro A., Lutya P., Hoffmann E. and Rees D.** (2006). WNN, a novel ubiquitin-like domain, implicates RBBP6 in mRNA processing and ubiquitin-like pathways. *BMC Struct Biol* **6**, 1-15.
- Qin G., Gu H., Zhao Y., Ma Z., Shi G., Yang Y., Pichersky E., Chen H., Liu M., Chen Z. and Qu L.-J.** (2005). An Indole-3-Acetic Acid Carboxyl Methyltransferase Regulates *Arabidopsis* Leaf Development. *Plant Cell* **17**, 2693-2704.
- Rampey R., Woodward A., Hobbs B., Tierney M., Lahner B., Salt D. and Bartel B.** (2006). An *Arabidopsis* basic helix-loop-helix leucine zipper protein modulates metal homeostasis and auxin conjugate responsiveness. *Genetics* **174**, 1841-1857.
- Ravet K., Reyt G., Arnaud R., Krouk G., Djouani E., Boucherez J., Briat J. and Gaymard F.** (2012). Iron and ROS control of the DownStream mRNA decay pathway is essential for plant fitness. *EMBO J* **31**, 175-186.
- Robinson N.J., Procter C.M., Connolly E.L. and Guerinot M.L.** (1999). A ferric-chelate reductase for iron uptake from soils. *Nature* **397**, 694-697.

- Roschttardt H., Seguela-Arnaud M., Briat J., Vert G. and Curie C.** (2011). The FRD3 citrate effluxer promotes iron nutrition between symplastically disconnected tissues throughout Arabidopsis development. *The Plant Cell* **23**, 2725-2737.
- Ruzicka K., Ljung K., Vanneste S., Podhorska' R., Beeckman T., Friml J. and Benkova' E.** (2007). Ethylene regulates root growth through effects on auxin biosynthesis and transport-dependent auxin distribution. *Plant Cell* **19**, 2197-2212.
- Rymarquis L., Souret F. and Green P.** (2011). Evidence that XRN4, an Arabidopsis homolog of exoribonuclease XRN1, preferentially impacts transcripts with certain sequences or in particular functional categories. *RNA* **17**, 501-511.
- Salahudeen A., Thompson J., Ruiz J., Ma H., Kinch L., Li Q., Grishin N. and Bruick R.** (2009). An E3 ligase possessing an iron-responsive hemerythrin domain is a regulator of iron homeostasis. *Science* **Oct 30**, 722-726.
- Samaniego F., Chin J., Iwai K., Rouault T. and Klausner R.** (1994). Molecular characterization of a second iron-responsive element binding protein, iron regulatory protein 2. Structure, function, and post-translational regulation. *J Biol Chem* **269**, 30904-30910.
- Sambrook J., Fritsch E. and Maniatis T.** (2001). *Molecular cloning: a laboratory manual*. (NY: Cold Spring Harbour Laboratory Press).
- Santi S. and Schmidt W.** (2008). Dissecting iron deficiency-induced proton extrusion in Arabidopsis roots. *New Phytol* **183**, 1072-1084.
- Schoenberg D.** (2011). *Mechanisms of endonuclease-mediated mRNA decay*. Wiley Interdiscip Rev RNA **2**, 582-600.
- Schuler M., Rellan.Alvarez R., Fink-Straubec C. Abadia J. and Bauer P.** (2012). Nicotianamine Functions in the Phloem-Based Transport of Iron to Sink Organs, in Pollen Development and Pollen Tube Growth in Arabidopsis. *Plant Cell* **24**, 2380-2400.
- Shanmugam V., Tsednee M. and Yeh K.** (2012). ZINC TOLERANCE INDUCED BY IRON 1 reveals the importance of glutathione in the cross-homeostasis between zinc and iron in Arabidopsis thaliana. *Plant Journal* **69**, 1006-1017.
- Simon E., Camier S. and Séraphin B.** (2006). New insights into the control of mRNA decapping. *Trends Biochem Science* **31**, 241-243.

- Sinclair S. and Kraemer U.** (2012). The zinc homeostasis network of land plants. *Biochim Biophys Acta*.
- Sivitz A., Grinvalds C., Barberon M., Curie C. and Vert G.** (2011). Proteasome-mediated turnover of the transcriptional activator FIT is required for plant iron-deficiency responses. *Plant Journal* **66**, 1044-1052.
- Slomovic S. and Schuster G.** (2011). Exonucleases and endonucleases involved in polyadenylation-assisted RNA decay. *Wiley Interdiscip Rev RNA* **2**, 106-123.
- Smalle J. and Vierstra R.** (2004). The ubiquitin 26S proteasome proteolytic pathway. *Annu Rev Plant Biol* **55**, 555-590.
- Solomon E., Decker A. and Lehnert N.** (2003). Non-heme iron enzymes: contrasts to heme catalysis. *Proc Natl Acad Sci U S A* **100**, 3589-3594.
- Song J., Huang S., Dalmay T. and Yang Z.** (2012). Regulation of leaf morphology by microRNA394 and its target *LEAF CURLING RESPONSIVENESS*. *Plant Cell and Physiology* **53**, 1283-1294.
- Souret F., Kastenmeyer J. and Green P.** (2004). *AtXRN4* degrades mRNA in *Arabidopsis* and its substrates include selected miRNA targets. *Mol Cell* **15**.
- Stacey M.** (2008). The *Arabidopsis AtOPT3* protein functions in metal homeostasis and movement of iron to developing seeds. *Plant Physiol* **146**, 589-601.
- Stein A.** (2010). Global impacts of human mineral nutrition. *Plant and Soil*.
- Stenkamp R.** (1994). Dioxygen and Hemerythrin. *Chem Rev* **94**, 715-726.
- Stepanova A., Hoyt J., Hamilton A. and JM, a.A.** (2005). A link between ethylene and auxin uncovered by the characterization of two root-specific ethylene-insensitive mutants in *Arabidopsis*. *Plant Cell* **17**, 2230-2242.
- Tam Y., Epstein E. and Normanly J.** (2000). Characterization of Auxin Conjugates in *Arabidopsis*. Low Steady-State Levels of Indole-3-Acetyl-Aspartate, Indole-3-Acetyl-Glutamate, and Indole-3-Acetyl-Glucose1. *Plant Physiol* **123**, 589-596.
- Trumbo P., Yates A., Schlicker S. and Poos M.** (2001). Dietary reference intakes: vitamin A, vitamin K, arsenic, boron, chromium, copper, iodine, iron, manganese, molybdenum, nickel, silicon, vanadium, and zinc. *J Am Diet Assoc* **101**, 294-301.
- U.S. Geological Survey.** (2003). *Mineral Commodity Summaries*, G.S. United States ed, 202.

- Ulmasov T., Murfett J., Hagen G. and Guilfoyle T.** (1997). Aux/IAA proteins repress expression of reporter genes containing natural and highly active synthetic auxin response elements. *Plant Cell* **9**, 1963-1971.
- United States Department of Agriculture, a.r.s.** (2003). USDA table of nutrient retention factors, a.r.s. United States Department of Agriculture ed.
- van de Mortel J., Villanueva L., Schat H., Kwekkeboom J., Coughlan S., Moerland P., van Themaat E., Koornneef M. and Aarts M.** (2006). Large expression differences in genes for iron and zinc homeostasis, stress response, and lignin biosynthesis distinguish roots of *Arabidopsis thaliana* and the related metal hyperaccumulator *Thlaspi caerulescens*. *Plant Physiol* **142**, 1127-1147.
- Vanacova S. and Stefl R.** (2007). The exosome and RNA quality control in the nucleus. *EMBO Rep* **8**, 651-617.
- Varkonyi-Gasic E., Wu R., Wood M., Walton E. and Hellens R.** (2007). A highly sensitive RT-PCR method for detection and quantification of microRNAs. *Plant methods* **3**.
- Varotto C., Maiwald D., Pesaresi P., Jahns P., Salamini F. and Leister D.** (2002). The metal ion transporter IRT1 is necessary for iron homeostasis and efficient photosynthesis in *Arabidopsis thaliana*. *Plant J* **31**, 589-599.
- Vashisht A., Zumbrennen K., Huang X., Powers D., Durazo A., Sun D., Bhaskaran N., Persson A., Uhlen M., Sangfelt O., Spruck E., Leibold J. and Wohlschlegel J.** (2009). Control of iron homeostasis by an iron-regulated ubiquitin ligase. *Science* **326**, 718-721.
- Vert G., Grotz N., Dédaldéchamp F., Gaymard F., Guerinot M.L., Briat J. and Curie C.** (2002). IRT1, an *Arabidopsis* transporter essential for iron uptake from soil and plant growth. *Plant Cell* **14**, 1223-1233.
- von Wiren N., Klair S., Bansal S., Briat J., Khodr H. and Shioiri T.** (2009). Nicotianamine chelates both FeIII and FeII: implications for metal transport in plants. *Plant Physiol* **119**, 1107-1114.
- Waters B., Blevins D. and Eide D.** (2002). Characterization of FRO1, a pea ferric-chelate reductase involved in root iron acquisition. *Plant Physiol* **129**, 85-94.
- Weber C., Nover L. and Fauth M.** (2008). Plant stress granules and mRNA processing bodies are distinct from heat stress granules. *Plant J* **56**, 517-530.

- Wei P.-C., Lo W.-T., Su M.-I., Shew J.-Y. and Lee W.-H.** (2012). Non-targeting siRNA induces NPGPx expression to cooperate with exoribonuclease XRN2 for releasing the stress. *Nucl Acids Res* **40**, 323-332.
- White P. and Brown P.** (2010). Plant nutrition for sustainable development and global health. *Annals of Botany* **105**, 1073-1080.
- Wilson D. and Doudna Cate J.** (2012). The structure and function of the eukaryotic ribosome. *Cold Spring Harb Perspect Biol* **4**.
- Xiang S., Cooper-Morgan A., Jiao X., Kiledjian M., Manley J. and Tong L.** (2009). Structure and function of the 5'→3' exoribonuclease Rat1 and its activating partner Rai1. *Nature* **458**, 784-788.
- Xu W. and Chua N.-H.** (2009). *Arabidopsis* Decapping 5 Is Required for mRNA Decapping, P-Body Formation, and Translational Repression during Postembryonic Development. *Plant Cell* **21**, 2270-2279.
- Xue Y., Bai X., Lee I., Kallstrom G., Ho J., Brown J., Stevens, A. and Johnson, A.** (2000). *Saccharomyces cerevisiae* *RAI1* (YGL246c) is homologous to human *DOM3Z* and encodes a protein that binds the nuclear exoribonuclease Rat1p. *Mol and Cell Biol* **20**, 4006-4015.
- Yuan Y., Wu H., Wang N., Kli J., Zhao W., Du J., Wang D. and Ling H.** (2008). FIT interacts with AtbHLH38 and AtbHLH39 in regulating iron uptake gene expression for iron homeostasis in *Arabidopsis*. *Cell Research* **18**, 385-397.
- Zakrzewska-Placzec M., Souret F., Sobczyk G., Green P. and Kufel J.** (2010). *Arabidopsis thaliana* XRN2 is required for primary cleavage in the pre-ribosomal RNA. *Nucleic Acids Research* **38**, 4487-4502.
- Zhang M.** (1998). Statistical features of human exons and their flanking regions. *Hum Mol Genet* **7**, 919-932.
- Zhao L., Kim Y., Dinh T. and Chen X.** (2007). miR172 regulates stem cell fate and defines the inner boundary of APETALA3 and PISTILLATA expression domain in *Arabidopsis* floral meristems. *Plant J* **51**, 840-849.
- Zheng D., Chen C. and Shyu, A.** (2011a). Unraveling regulation and new components of human P-bodies through a protein interaction framework and experimental validation. *RNA* **17**, 1-15.

- Zheng L., Ying Y., Wang L., Wang F., Whelan J. and Shou H.** (2011b). Identification of a novel iron regulated basic helix-loop-helix protein involved in Fe homeostasis in *Oryza sativa*. *BMC Plant Biol* **10**, 166.
- Zhou J. and Erdman J.** (1995). Phytic acid in health and disease. *Crit Rev Food Sci Nutr* **35**, 495-508.
- Zuo Y. and Deutscher M.** (2001). Exoribonuclease superfamilies: structural analysis and phylogenetic distribution. *Nucleic Acids Research* **29**, 1017-1026.

ACKNOWLEDGMENTS

I would like to thank Prof. Dr. Ute Krämer for giving me the possibility to work in her group and for helping me to achieve the goal of the PhD degree. Prof. Dr. Karin Schumacher and Prof. Dr. Rüdiger Hell are acknowledged for the stimulating discussions during our regular meetings.

Special thanks go to Dr. Michael J Haydon for the precious inputs and the bright ideas. In addition, I express my gratitude to Dr. Stefan Reuscher with whom I shared many nice moments inside and outside the laboratory, and Dr. Scott Sinclair with whom I had many coffees and discussions about science. I want to acknowledge Vasantika Singh for her positive aura, Dr. Maria Bernal for her kindness and friendship, and Romario Melo for his lovely attitude towards life.

The following people are acknowledged for their advices during several phases of my research project: Dr. Ines Kubigsteltig, Dr. Justyna Cebula, Dr. Ricardo Stein, Kai-Uwe Best. Thanks to Jochen Schab and Klaus Hagemann for the great atmosphere in the office and to the groups led by Dr. Heike Holländer-Czytko, Dr. Markus Piotrowski, Prof. Dr. Thomas Höfer and Dr. Karsten Rippe for the nice time passed together.

Last but not least, I thank Sarah and my family for the continuous and incomparable support throughout these years.

